Université de Montréal

Solid-state NMR and Electrochemical Dilatometry Study of Charge Storage in Supercapacitor with Redox-active Ionic Liquid Electrolyte

par Yanyu Wang

Départment de chimie
Faculté des arts et des sciences

Mémoire présentée à la Faculté des études supérieures et postdoctorales
en vue de l'obtention du grade de Maîtrise ès sciences (M.Sc.) en chimie

en chimie

Octobre, 2018

Résumé

Les liquides ioniques électroactifs se distinguent comme nouveaux électrolytes prometteurs pour les supercapacités électrochimiques en permettant notamment d'atteindre des densités énergétiques plus élevées qu'en milieux organiques ou avec des liquides ioniques traditionnels. Cet accroissement est dû aux réactions de transfert électronique (faradiques) qui y prennent place en plus de ceux dans la double-couche qui sont purement capacitifs. Les études fondamentales sur les mécanismes menant au stockage d'énergie dans des supercapacités à base de liquides ioniques électroactifs sont, bien qu'essentielles, peu nombreuses en comparaison avec les systèmes classiques. Le développement d'approches basées sur la spectroscopie de résonance magnétique nucléaire à l'état solide (SS-NMR) permet l'obtention d'information sur l'environnement local au sein des matériaux d'électrodes qui est nécessaire pour comprendre les mécanismes de stockage dans les supercapacités. Elle permet notamment de suivre l'adsorption et la désorption des ions dans la microstructure du carbone activé utilisé pour les électrodes. Ces approches ont jusqu'à maintenant été utilisées uniquement pour l'étude de systèmes classiques où le stockage n'est effectué que par les mécanismes non-faradiques (double-couche électrigue). Dans ce mémoire je présenterai l'utilisation de la SS-NMR en combinaison avec la dilatométrie électrochimique pour l'étude approfondie des mécanismes de stockage dans des supercapacités constituées d'électrodes à base de carbone activé et utilisant un électrolyte à base de liquide ionique électroactif. La capacité de cette approche pour la détermination de la contribution faradique à la charge emmagasinée a été démontrée pour la première fois. Cette étude a permis de démontrer que le mécanisme de stockage avec un électrolyte électroactif diffère en fonction du voltage appliqué aux électrodes. À l'électrode positive, la désorption des co-ions dans les micropores du carbone activé domine à bas voltage alors que l'adsorption des contre-ions devient importante à haut voltage où elle est accompagnée de l'oxydation du groupement électroactif présent sur le liquide ionique. À l'électrode négative, l'adsorption du contre-ion est le mécanisme principal peu importe le voltage appliqué. L'utilisation de la dilatométrie électrochimique qui permet de mesurer le changement d'épaisseur d'une électrode en fonction du potentiel appliqué a confirmé ces observations. Les résultats de ce mémoire ont permis de mieux

comprendre le stockage d'énergie par les supercapacités électrochimiques et l'approche développée pourra être appliquée aux systèmes d'électrolytes électroactifs afin d'en améliorer les performances.

Mots-clés : Liquide ionique électroactif; Supercapacité électrochimique; Réaction faradique; Spectroscopie de résonance magnétique nucléaire; Dilatométrie électrochimique.

Abstract

Redox-active ionic liquids are emerging as promising new electrolytes for supercapacitors, providing higher capacitance and energy density than organic or ionic liquid electrolytes. Fundamental studies of the charge storage mechanism in supercapacitors are of critical importance for the development and application of devices. Solid-state NMR (SS-NMR) methodology having the ability to provide local environment information within electrodes at the molecular level has been recently developed to study the mechanism of charge storage in supercapacitors. The charge storage in supercapacitors with organic or ionic liquid electrolytes has been studied by SS-NMR. The charge storage in supercapacitors with redox-active species that involves faradaic processes is different from those of electrochemical double-layer capacitors comprising organic solvents or ionic liquids as electrolytes. However, there are until now no published findings on charge storage mechanisms in supercapacitors with redox-active electrolytes. Therefore, fundamental studies of the charge storage mechanism in supercapacitors with redox-active ionic liquid electrolytes are needed. In this thesis, SS-NMR techniques combined with electrochemical dilatometry were used to investigate in depth the charge storage in supercapacitors comprising redox-active ionic liquid electrolytes. The charge contributed from the faradaic reaction of the redox-active species is determined for the first time by the NMR measurements. Moreover, it is revealed that the charge storage mechanism of supercapacitors with the redox-active ionic liquid electrolyte EMIm FcNTf/ACN (1-ethyl-3-methylimidazolium ferrocenylsulfonyl (trifluoromethylsulfonyl) imide/acetonitrile) is driven by different charge regimes for different voltages. More specifically, charge storage on the positive electrode occurs via co-ion desorption in the low voltage range and subsequently counter-ion adsorption in the high voltage range, whereas charging on the negative electrode occurs exclusively by counter-ion adsorption over the studied voltage range. The electrochemical dilatometry measurements show macroscopic dimensional changes of the electrodes during charging, further confirming the proposed mechanism suggested by SS-NMR. The results give a detailed picture of the charge storage of supercapacitors with a redox-active ionic liquid electrolyte, providing new insights on the charge storage in supercapacitors.

Keywords : Redox-active ionic liquid; Supercapacitors; Faradaic reaction; Solid-state NMR, Electrochemical dilatometry.

Table of Contents

List of tables

Chapter 1

List of figures

Figure 2-2. Dilatometer in the full cell configuration Figure 2-2. Dilatometer in the full cell configuration.

Figure 2-3. (a) A cartoon showing in-pore ions located close to carbon surfaces in carbon micropores. (b) SEM image showing voids and large spaces between carbon particles where ex-pore ions reside. Reprinted from Ref. 2. (c) ^{19}F MAS NMR (7.1 T) spectra of YP-50F carbon film soaked with $Pyr_{13}TFSI$ ionic liquid. Reprinted from Ref. 3. (d) Schematic illustration of the ring current-induced magnetic field, B_{ind}, associated with delocalized π-electrons in a six-membered carbon ring within an applied magnetic field B_0. Reprinted from Ref. 2.

Figure 2-4. Schematic illustrations of possible charge storage mechanisms within a micropore that contains anions and cations prior to charging. If the electrode surface is positively polarized, an equal negative ionic charge can arise through either (a) adsorption of ex-pore anions into the micropores, (b) exchange of ex-pore cations for in-pore anions or (c) the expulsion of cations from the micropores. Reprinted from Ref. 5.

Chapter 3

Figure 3-1. ^{19}F NMR spectra recorded at MAS (8 kHz, top) and in static mode (bottom) shows the necessity of spinning to obtain a sufficient resolution to isolate the in-pore ion contribution. The signals came only from the F atoms on the FcNTf anion. The peaks at about -35, -55 and -100 ppm are spinning sidebands. The measurements were done on the YP-50F carbon electrodes (95 wt % activated carbon and 5 wt % PTFE) soaked overnight in a solution of 50 wt % of the ionic liquid EMIm FcNTf in acetonitrile. The excess of electrolyte was removed prior to the measurements.

Figure 3-2. ^{19}F NMR spectra of YP-50F carbon electrodes after contacting an excess of three different EMIm FcNTf/ACN electrolytes overnight and removing the excess solution. The electrolytes contained (a) 30 wt %, (b) 50 wt % and (c) 80 wt % of the redox-active ionic liquid. The ex-pore peak (δ = -78 ppm) intensity reflects the increasing quantity of FcNTf in the interparticle spaces of the porous electrode. The deconvolution of the spectra was used to evaluate the relative surface area of both peaks (ex-pore and in-pore) and the concentration of in-pore anions (presented in the d) panel).

Figure 3-3. ^{19}F NMR spectra of the positive and negative YP-50F activated electrodes of a supercapacitor cell that was charged at different voltages. All cells used a 50 wt % EMIm

FcNTf redox-active ionic liquid in acetonitrile electrolyte and were charged using a 1 h potentiostatic step at the given voltage for 1 h (after equilibrating the cell with 5 GCD cycles, see Material and methods section for conditions). An increase in the relative proportion of in-pore FcNTf anions is observed at higher voltage values only at the positive electrode, as expected for double-layer charging. The quantity of anions in the carbon of the negative electrode remained constant.

Figure 3-4. Effect of the voltage on the ^{19}F chemical shift of in-pore (red triangle and blue diamond for negative and positive electrode, respectively) and ex-pore (black cross) anions. This variation of the peak resonance suggest a modification of the immediate anion environment during the charging process, an effect commonly seen with ionic liquids in activated carbon electrodes. The chemical shift of anions outside of the pores (bulk and interparticle spacing) is not affected by the voltage. Before recording the NMR spectra, the supercapacitor cells were poised to a voltage between 0 and 2 V for a duration of 1 h.

Figure 3-5. In-pore FcNTf anion population found in the positive (a) and negative electrode (b) of a supercapacitor after applying different voltage between 0.0 and 2.0 V for 1 h. Values are given as millimoles per gram of YP-50F carbon in each electrode and were calculated from the relative peak surface area after deconvolution of the NMR spectra. The increase at the positive electrode between 1.0 and 2.0 V is indicative of significant amounts of anion into pores during charging of the supercapacitor.

Figure 3-6. Comparison of ionic and total electronic charge stored in the supercapacitor at different voltages. The ionic charge is calculated from the increase in the quantity of in-pore FcNTf anions relative to the amount found in the carbon after soaking (unbiased electrodes, Figure 3-2d). The total charge represents the amount of coulomb that was accumulated over the potentiostatic step. For an applied voltage of 1.0 V and above, the oxidation of ferrocene to ferrocenium becomes a significant contribution to the charging mechanism.

Figure 3-7. Results from the in situ electrochemical dilatometry measurements on a supercapacitors cell with 50 wt % EMIm FcNTf acetonitrile solution as electrolyte. The measurements were done on the positive (a and b) and on the negative electrode (c), separately. Panel (b) shows an enlargement of the second cycle at the positive electrode. At low voltage, a contraction of the electrode is noted which is attributed to the expulsion of

List of abbreviations

SCs: supercapacitors

EDLCs: electrochemical double-layer capacitors

EDL: electrical double layer

C: capacitance

A: surface area of the electrode

ε: dielectric constant of the electrolyte

d: effective thickness of the EDL

IHP: inner Helmholtz plane

OHP: outer Helmholtz plane

C_T: total capacitance

C_p: capacitance of positive electrode

C_n: capacitance of negative electrode

C_s: mass specific capacitance

C_v: the volumetric capacitance

V: cell voltage

E: energy density

P: power density

R: equivalent series resistance of SC

ESPW: electrochemical stability potential window

ESR: equivalent series resistance

IL: ionic liquid

SSA: specific surface area

PSD: pore-size distribution

ACs: activated carbons

CDCs: carbide-derived carbons

PANI: polyaniline

PPy: polypyrrole

CNTs: carbon nanotubes

ACNTs: aligned CNTs

LBL: layer-by-layer

EPD: electrophoretic deposition

CVD: chemical vapor deposition

rGO: reduced graphene oxide

PANI: polyaniline

PTh: polythiophene

ACN: acetonitrile

PC: propylene carbonate

$TEABF_4$: tetraethylammonium tetrafluoroborate

MD: molecular dynamics

DFT: density functional theory

MC: Monte Carlo

NMR: nuclear magnetic resonance

EQCM: electrochemical quartz-crystal microbalance

SANS: small angle neutron scattering

IM: imidazolium

EMIM: 1-ethyl-3-methylimidazolium

BMIM: 1-butyl-3-methylimidazolium

BF_4^-: tetrafluoroborate

PF_6^-: hexafluorophosphate

TFSI or NTf_2: bis(trifluoromethanesulfonyl)imide

FSI: bis(fluorosulfonyl)imide

DCA: dicyanamide

OTf: trifluoromethanesulfonate

$[Pyr_{14}][TFSI]$: N-butyl-N-methylpyrrolidinium bis(trifluoromethanesulfonyl)imide

$[Me_3S][TFSI]$: trimethylsulfonium bis(trifluorosulfonyl)imide

$[PIP_{13}][FSI]$: propylpiperidinium bis[fluorosulfonyl]imide

EC: ethylene carbonate

DMC: dimethyl carbonate

DAIM: diallylimidazolium

DMF: dimethylformamide

SPE: solid polymer electrolyte

GPE: gel polymer electrolyte

PEO: poly ethylene oxide

PVA: poly vinyl alcohol

HQ: hydroquinone

MB: methylene blue

PPD: p-phenylenediamine

[FcMIM][NTf_2]: 1-(methylferrocenyl)-3-ethylimidazolium bis(trifluoromethanesulfonyl)imide

[EMIM][FcNTf]: 1-ethyl-3-methylimidazolium ferrocenylsulfonyl-(trifluoromethylsulfonyl)-imide

AQ: anthraquinone

TEMPO: 2,2,6,6-tetramethylpiperidinyl-1-oxyl

DMSO: dimethyl sulfoxide

DSC: differential scanning calorimetry

TGA: thermal gravimetric analysis

PTFE: polytetrafluoroethylene

PVDF: polyvinylidene fluoride

WE: working electrode

CE: counter electrode

MAS: magic-angle spinning

Pyr_{13}TFSI: 1-methyl-1-propylpyrrolidinium bis(trifluoromethanesulfonyl)imide

SS-NMR: solid-state NMR

RILs: redox-active ionic liquids

IR: infrared spectroscopy

GCD: galvanostatic charge–discharge

Acknowledgements

First of all, I would like to express my sincere gratitude to my supervisor, Prof. Dominic Rochefort, for the tremendous support of my Master's study and research, for the patient guidance, encouragement and advice throughout my study time. I have been extremely lucky to have him as supervisor for my Master's study.

I would also like to thank all professors and staff at Department of Chemistry who ever helped me in any aspects. In particular I would like to thank Cedric Malveau and other staff in the NMR laboratory, who trained me how to use the solid-state NMR and gave lots of helpful suggestions for the NMR measurements.

All members in Prof. Dominic Rochefort's group helped me a lot in both study and personal time. I appreciate the friendships we constructed and good advice and collaboration they generously provided. I had a good time to work with all of them.

In regards to financial support, I would like to thank the Natural Sciences and Engineering Research Council of Canada (NSERC), for providing the funding which allowed the completion of this work.

Finally, I must express my gratitude to my family, for their continued support and encouragement. I am grateful for the patience of my parents who experienced all of the ups and downs of my research.

Chapter 1 Introduction

The need to develop and scale up sustainable, clean and efficient energy sources as well as new technologies associated with energy conversion and storage is being given worldwide urgent priority due to the accelerating depletion of existing fossil fuel reserves and the affiliated environmental problems, e.g., increased greenhouse gas emissions and general air and water pollution. Among various areas of application, lithium-ion batteries, fuel cells and supercapacitors (SCs) are at the forefront as the most effective and practical energy conversion and storage devices.

SCs, also known as ultracapacitors or electrochemical capacitors, have drawn great attentions as promising next-generation power sources to fill the gap between electrolytic capacitors and batteries. They offer advantages such as a higher energy density than electrolytic capacitors, a higher power density induced by a fast charge/discharge rate (within several seconds or several minutes) and a longer cycle life (>100 000 cycles) when compared to batteries and fuel cells. Figure 1-1 illustrates a Ragone plot for the most important energy storage systems.[1] Currently, SCs have attracted considerable interest in a wide variety of applications such as portable electronics, electric or hybrid electric vehicles, aircrafts and smart grids. For example, in the case of both electric and hybrid vehicles including fuel cell ones, SCs could serve as an intermediate power source for short-term acceleration and recovery of energy during breaking, thus saving energy and protecting the battery from the high-frequency rapid discharging and charging process.[2]

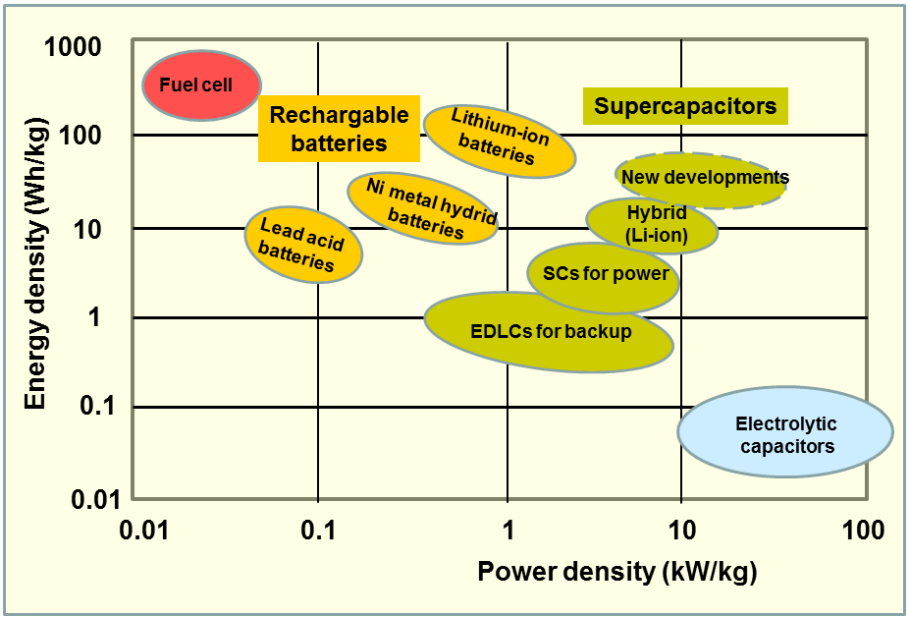

Figure 1-1. Ragone chart showing specific power vs. specific energy of various energy storage systems. Reprinted from Wikipedia (https://en.wikipedia.org/wiki/Supercapacitor).

1.1 Fundamentals of supercapacitors

A SC consists of two electrodes in contact with an electrolyte solution isolated by a separator. According to the charge storage mechanism, SCs can be briefly classified as electrochemical double-layer capacitors (EDLCs), pseudocapacitors or hybrid-capacitors.[3] (see Figure 1-2)

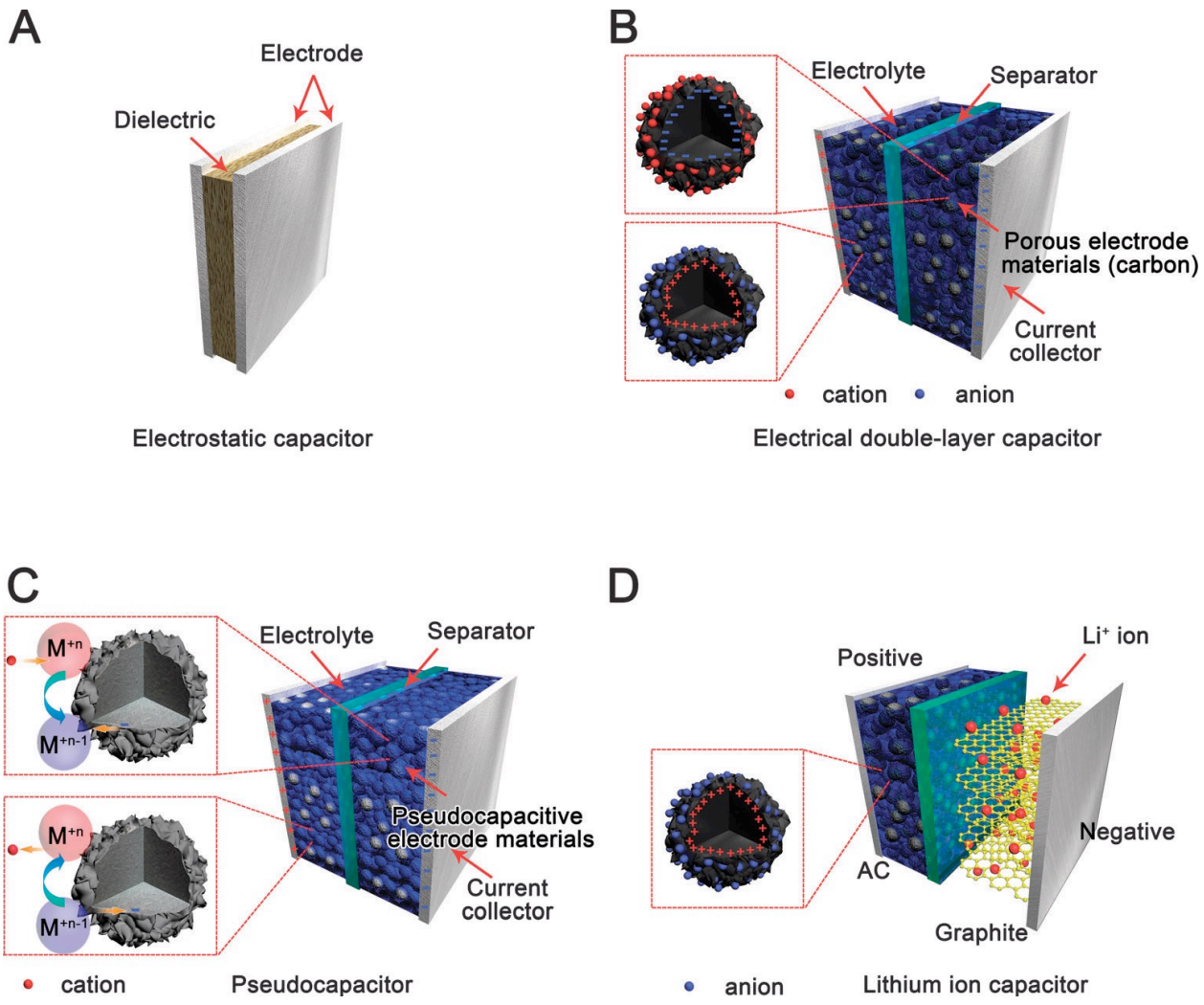

Figure 1-2. Schematic diagram of (A) an electrostatic capacitor, (B) an electrical double-layer capacitor, (C) a pseudocapacitor, and (D) a hybrid-capacitor. Reprinted from ref. 3.

1.1.1 Electrical double-layer capacitors (EDLCs)

In general, the electrodes of EDLCs are fabricated from nanoscale materials that have a high surface area and a high porosity. Currently, carbon materials that have high surface area are the most popular materials for the electrode of SCs. The energy storage mechanism in EDLCs arises from the electrostatic charge accumulated at the interface between the electrode and the electrolyte. The concept of the electrical double layer (EDL) was first described and modeled by von Helmholtz in the 19th century.[4] As schematically illustrated in Figure 1-3a,

the Helmholtz model describes the separation of charge and the formation of two layers of opposite charge at the electrode/electrolyte interface when an electrode is polarized. Under this condition, ions of opposite sign diffuse through the electrolyte to form a condensed layer with a thickness of a few nanometers in a plane parallel to the electrode surface, ensuring charge neutrality. This accumulation of charge is referred to as the electrical double layer. The potential in the vicinity of the electrode decreases when the distance between the ions and the electrode increases. The capacitance of this simplified Helmholtz double layer through reversible ion adsorption on the carbon surface is defined by equation (1):

$$C = \frac{A\varepsilon}{4\pi d} \tag{1}$$

where A is the surface area of the electrode; ε is the dielectric constant of the electrolyte; and d is the effective thickness of the EDL. Since the simple Helmholtz model does not take into account several factors such as the diffusion of ions in the solution and the interaction between the dipole moment of the solvent and the electrode, Gouy and Chapman[5,6] proposed a diffuse layer model to consider a continuous distribution of electrolyte ions (both cations and anions) in the electrolyte solution driven by thermal motion, in which the potential decreases exponentially from the electrode surface to the bulk solution (see Fig. 1-3b). However, a serious problem with the Gouy–Chapman model is the overestimation of the EDL capacitance. The capacitance of two separated arrays of charges increases inversely with their separation distance, hence a very large capacitance value would arise in the case of point charge ions very closely approaching the electrode surface. In 1924, Stern[7] suggested a model combining the Helmholtz and Gouy–Chapman model by accounting for the hydrodynamic motion of the ionic species in the diffuse layer and the accumulation of ions close to the electrode surface. The Stern model explicitly states two regions of ion distribution—the compact Helmholtz layer (Stern layer) and the diffuse layer (see Fig. 1-3c). By introducing the compact layer closest to the electrode, the problem of a far too high capacitance that arises in the Gouy–Chapman treatment is automatically avoided. In the compact layer, ions are strongly adsorbed by the electrode and Grahame made an important distinction between an inner and an outer Helmholtz layer in the interphase which corresponds to different distances of closest approach to the electrode surface. The inner Helmholtz plane (IHP) refers to the distance of closest approach of specifically adsorbed ions and the outer Helmholtz plane (OHP) refers to that of

the non-specifically adsorbed ions. The OHP is also the plane where the diffuse layer begins. The diffuse layer is what the Gouy–Chapman model defines, where the non-specifically adsorbed ions are distributed in a three-dimensional region because of thermal agitation in the solution.

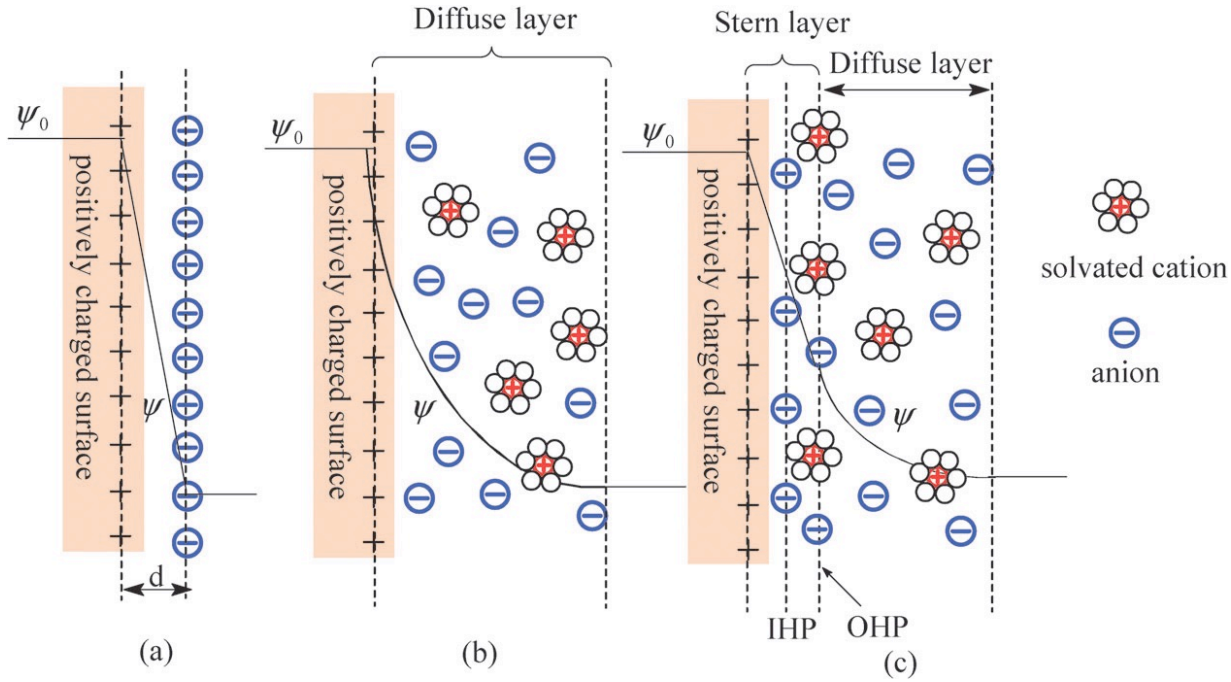

Figure 1-3. Models of the electrical double layer at a positively charged surface: (a) the Helmholtz model, (b) the Gouy–Chapman model, and (c) the Stern model, showing the inner Helmholtz plane (IHP) and the outer Helmholtz plane (OHP). d is the double layer distance described by the Helmholtz model. ψ_0 and ψ are the potentials at the electrode surface and the electrode/electrolyte interface, respectively. Reprinted from ref. 16.

1.1.2 Pseudocapacitors

The charge physically stored in a porous electrode by the accumulation of electrostatic charge at the electrode/electrolyte interface is unfortunately limited and therefore EDLCs have a limited specific capacitance and a low energy density. Advanced approaches to increase the energy density of SCs are to hybridize the electrode materials by adding electrochemically active materials to the carbon materials or to completely replace the carbon materials with

electrochemical-active materials. Alternatively, the introduction of redox-active electrolyte by dissolving electroactive species in the electrolyte or using electroactive species solely as the electrolyte is also a means to increase the energy density. SCs with electrochemical-active materials as the electrodes or electrolyte are called faradaic supercapacitors or pseudocapacitors. Pseudocapacitors not only store charges in the EDL, but also undergo fast and reversible redox reactions (faradaic reactions) on the electrode surfaces. Pseudocapacitors generally providing greater pseudocapacitances (10–100 times the capacitance in conventional EDLCs) are highly desirable as the next generation of SCs. The most commonly known redox-active species for the electrodes of pseudocapacitors are several transition metal oxides, including RuO_2, MnO_2, Co_3O_4,[8-10] conducting polymers such as polyaniline[11], and carbon materials functionalized with oxygen or nitrogen heteroatoms[12]. The redox-active electrolytes include electrolytes mixed with redox-active species such as iodine, bromine, hydroquinones.[13-15]

1.1.3 Hybrid supercapacitors

Hybrid SCs refer to the one using both the electrical double-layer (EDL) and faradaic mechanisms to store charges. There are two different types of hybrid supercapacitor systems, which can be distinguished by their electrode configurations: asymmetric (e.g. one electrode consists of electrostatic carbon material while the other consists of pseudocapacitive material) and battery-type (e.g. combination of a supercapacitor electrode with a lithium-ion battery electrode). With a correct electrode combination it is possible to increase the cell voltage, which in turn leads to an improvement in the energy density of SCs.

1.2 Technical specifications of supercapacitors

In this section, I will introduce briefly several parameters such as capacitance, energy density, power density, etc., which are very important factors for discussing and evaluating the supercapacitors.

1.2.1 Capacitance

As shown in Fig. 1-2b, the entire SC can be treated as two capacitors in series since both electrode/electrolyte interfaces represent a capacitor. Hence the total capacitance (C_T) can be expressed as:

$$\frac{1}{C_T} = \frac{1}{C_p} + \frac{1}{C_n} \tag{2}$$

where C_p and C_n are the capacitances of the positive and negative electrodes, respectively. For a symmetric SC, since $C_p = C_n$, the total capacitance (C_T) would be half of either electrode's capacitance. In the case of the asymmetric SC, C_T is mainly dominated by the electrode with the smaller capacitance. To evaluate the capacitance of an electrode material, a specific capacitance is often used, which can be expressed either as the mass specific capacitance (also called gravimetric specific capacitance) (C_s), or the volumetric capacitance (C_v). Generally, C_s is the most frequently used one to characterize an electrode material, with units of Faraday per gram ($F \cdot g^{-1}$). A comparison between different electrode materials can be made based on their values of C_s.

1.2.2 Energy density and power density

When a SC is charged, a cell voltage V builts up across the two electrodes. The stored energy E (Wh), also called the energy density, in a supercapacitor is given by equation (3):[16]

$$E = \frac{1}{2} C_T V^2 \tag{3}$$

in which C_T is the total capacitance of the cell. The maximum power density P (W) is given by equation (4): [16]

$$P = \frac{1}{4R} V^2 \tag{4}$$

where R is the equivalent series resistance of the SC. The energy and power densities normalized by the weight of the device or the electrode provide a basis for comparison between devices, especially from an application point of view. As the two equations show, V,

C_T and R are three important variables determining the performance of a SC. In order to improve both the energy density and power density of a SC, increasing the values of both V and C_T and simultaneously reducing the value of R are desirable. Since both the energy density and power density are proportional to the square of the operating voltage, an increase of cell voltage would have a greater contribution to the improvement of the energy density and power density of a SC than increasing the capacitance or reducing the resistance. Generally, the maximum operating voltage of a SC is strongly dependent on the electrochemical stability potential window (ESPW) or the potential window of the electrolyte. Alternatively, the normalization of energy density and power density can also be carried out by the device volume (m^3) rather than the mass (kg) to provide a comparison for the compact devices.

1.2.3 Equivalent series resistance (ESR)

The ESR (Ω) is composed of the intrinsic resistance of the electroactive materials, contact resistance between the electroactive materials and the current collector, diffusion resistance of ions in the electrode materials and through the separator, and ionic resistance of electrolytes. It is an important parameter for determining the SC's power density as indicated by equation (4), which indicates that the power density increases with a decreasing ESR value. Similar to other electrochemical energy storage devices, a high ESR limits the charging/discharging rate, leading to a low power density. Therefore, for some pulse power applications, the ESR value of a SC is even more important than the capacitance value. Normally, ESR is the sum of resistances including the intrinsic resistance of the electrode material, the ionic resistance of the electrolyte and contact resistance between the current collector and the electrode.[16] As identified, the resistances of the bulk electrolyte solution and the electrolyte inside the electrode pores tend to dominate the ESR, especially when non-aqueous electrolytes such as organic, ionic liquid (IL) and solid-state electrolytes are used in the SCs. Therefore, in order to achieve a high power density for a SC, it is necessary to use an electrolyte with high ionic conductivity. However, there is often a trade-off between the ionic conductivity and the operating potential window of the electrolyte. In general, aqueous electrolytes, such as H_2SO_4 and KOH, have high ionic conductivities, but low operating

potential windows. In contrast, although non-aqueous electrolytes such as organic and IL can offer high operating voltages, their ionic conductivities are generally at least one order of magnitude lower than those of the aqueous electrolytes,[17] leading to a higher ESR, and thereby limiting the power density. Therefore, to achieve both high energy and power densities for SCs, it is essential to develop electrolytes with a wide operating voltage and a small ESR (or high ion conductivity).

1.2.4 Cycle-life

Cycle-life, an indicator of the stability of SC, is also one of the important parameters for evaluating the overall SC performance. General test procedures for stability analysis involve the electrode undergoing charge and discharge cycling in a certain electrolyte to compare the initial and final capacitance. EDLCs using carbon electrodes generally have a very high cycling stability.[18] However, when pseudocapacitive reactions are introduced, the cyclic stability is generally reduced due to the non-ideal electrochemical reversibility resulting from the interactions between the electrolyte ions and the electrode materials. Actually, the cycle-life of SCs depends on many factors such as the cell type, the electrode material, the electrolyte, the charge/discharge rate, the operating voltage and the temperature.

1.2.5 Self-discharge rate

Another issue concerning the SC performance is the self-discharge rate, which is related to the potential losses of a charged electrode over a period of storage time.[19] During the self-discharge process, current leakage leads to a decrease of the cell voltage, which may limit the use of SCs for some applications requiring a fixed amount of energy retention. The SC self-discharge rate and its mechanism are dependent on the type of electrolyte, impurities and residual gases.

1.2.6 Thermal stability

Currently most applications of SCs are achieved in the temperature range of -30 to 70 °C.[20] Expanding the working temperature range of SCs can further widen the scope of the applications of SCs. For example, most space avionics applications are required to operate at temperatures as low as -55 °C.[20] Fuel cell vehicles, on the other hand, may require a higher working temperature. In addition, the working temperature can affect several properties of SCs such as the energy and power densities, ESR, cycle life and self-discharge rate. The performance of temperature-dependent SCs is strongly dependent on the nature of the electrolyte, e.g. the concentration, the type of conducting salt and the property of solvent.

1.3 Electrodes of supercapacitors

The capacitance and charge storage of SCs intimately depend on the electrode materials used. Therefore, further developing new materials with high capacitance and improved performance relative to existing electrode materials is one of the most critical aspects in the development of SCs. In general, the electrode materials of SCs can be categorized into three types: (1) carbon materials with high specific surface area, (2) conducting polymers, and (3) transition metal oxides and hydroxides.[3]

1.3.1 Carbon-based materials

Carbon materials store charges mainly in an electrochemical double layer formed at the interface between the electrode and the electrolyte. Therefore, the capacitance predominantly depends on the surface area accessible to the electrolyte ions. The important factors influencing their electrochemical performance are the specific surface area (SSA), pore size distribution (PSD), pore structure and electrical conductivity.[1,21] The general rule for selecting carbon materials as the SC electrode is to obtain a high accessible specific surface area with good electrical conductivity. Table 1-1 shows examples of different carbon structures that have high SSA and high conductivity and can be used as SC electrodes.[215]

Table 1-1. Different carbon structures used in EDLCs with onion-like carbon, carbon nanotubes, graphene, activated carbon, carbide-derived carbon and templated carbon. Reprinted from ref.215.

Material	Carbon onions	Carbon nanotubes	Graphene	Activated carbon	Carbide derived carbon	Templated carbon
Dimensionality	0-D	1-D	2-D	3-D	3-D	3-D
Conductivity	High	High	High	Low	Moderate	Low
Volumetric Capacitance	Low	Low	Moderate	High	High	Low
Cost	High	High	Moderate	Low	Moderate	High
Structure		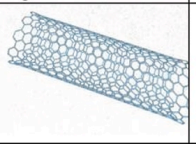	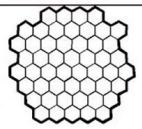	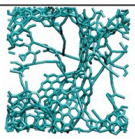	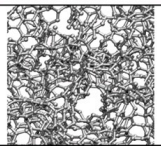	

Based on equation (1), it is usually anticipated that the larger the SSA, the higher the capacitance. Initial research on carbon materials was directed towards significantly increasing the pore volume by developing materials with large SSA. However, the increase in capacitance is relatively limited because not all micropores of the carbon material are electrochemically accessible to form an electrical double layer when they are immersed in electrolyte. It has been demonstrated that there is no linear relationship between the SSA and the capacitance, i.e., the capacitance of various carbon materials does not increase linearly with SSA. Despite the SSA of activated carbons (ACs) being as high as 2500–3000 $m^2 \cdot g^{-1}$, only a relatively small $C_s < 10$ $\mu F \cdot cm^{-2}$ was obtained compared to the theoretical value (15–25 $\mu F \cdot cm^{-2}$).[22] On the contrary, activated carbon fibers with a SSA of only 1000 $m^2 \cdot g^{-1}$ exhibit an extremely high capacitance corresponding to that of the conventional ACs with a SSA of 3000 $m^2 \cdot g^{-1}$. [23]

Efforts have been made to study the relationship between the pore size of porous carbon materials and their capacitance performance. An adequate pore size is more important than a high surface area for achieving high values of capacitance, and the optimal pore sizes are found to be 0.7 and 0.8 nm in aqueous and organic media, respectively.[24] Moreover, J. Chmiola et al. demonstrated that carbide-derived carbons (CDCs) with a pore size of 0.8–1.0 nm exhibit an anomalous increase in capacitance due to the desolvation of ions upon entering the micropores (Figure 1-4a).[25,26] These observations indicate that the micropores

electrochemically accessible to the electrolyte ions to form an electrical double layer have a significant effect on the capacitance value. Largeot et al. have experimentally determined the relationship between the electrolyte ion size and the pore size of CDCs when no solvent is present in the system and concluded that the maximum EDL capacitance is achieved when the pore size is very close to the electrolyte ion size (Figure 1-4b).[21] Both larger and smaller pores lead to a significant decrease in capacitance. This phenomenon was also verified in aqueous electrolyte in a recent study conducted by the same group.[27] These interesting findings challenged the conventional view that only those pores larger than the size of solvated electrolyte ions are capable of forming a double layer and contributing to the charge storage due to the ion sieving effect. The above observations have only been reported for special carbon materials. Thus, the relationship between pore size and capacitance should be thoroughly investigated both theoretically and experimentally, which is beneficial for designing advanced carbon materials with optimal pore structure and maximized electrochemical performance.

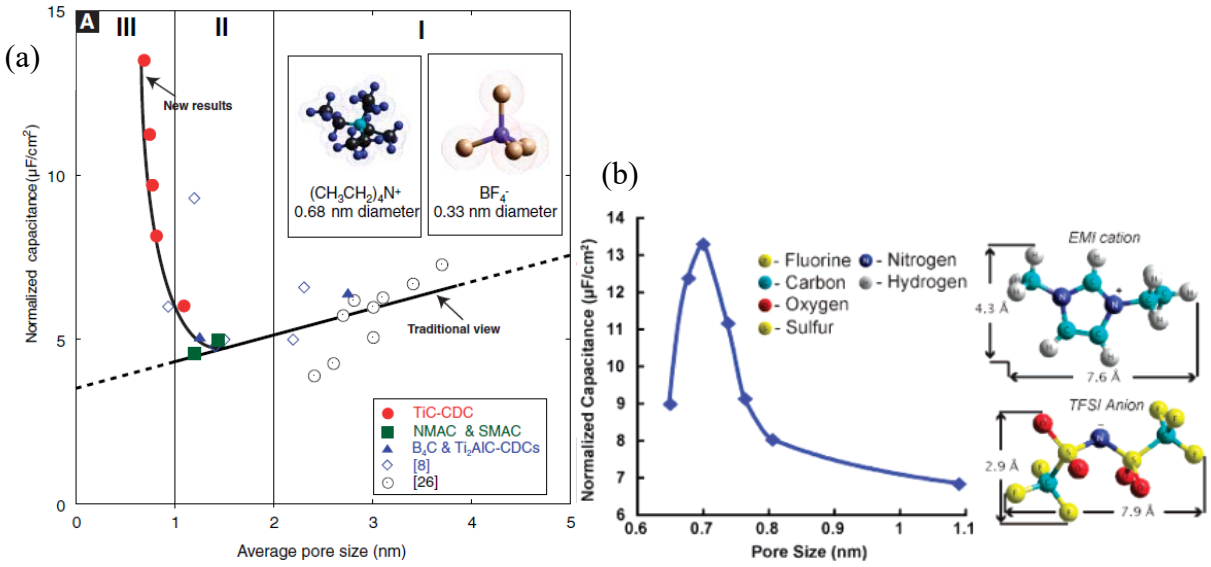

Figure 1-4. (a) Plot of normalized specific capacitance versus average pore size shows that capacitance decreases with decreasing pore size until a critical value was reached, unlike the traditional view which assumed that capacitance continually decreased. Reprinted from ref. 25. (b) Normalized capacitance change versus the pore size of the CDC samples; inset shows HyperChem models of the structure of EMIM and TFSI ions. Reprinted from ref. 27.

1.3.1.1 Activated carbons (ACs)

ACs are the most widely used electrode materials due to their large surface area, relatively good electrical properties and low cost. ACs are generally produced by creating a three-dimensional porous network through either physical (thermal) or chemical activation of various types of carbonaceous materials (e.g. coal, wood, nutshell, etc.). Physical activation usually refers to the treatment of carbon precursors at high temperature (from 700 to 1200 °C) in the presence of oxidizing gases such as steam, CO_2 and air. Chemical activation is usually carried out at lower temperature (from 400 to 700 °C) with activating agents like phosphoric acid, potassium hydroxide, sodium hydroxide and zinc chloride. Depending on the activation methods as well as the carbon precursors used, ACs possessing various physicochemical properties with well-developed SSA as high as 3000 $m^2 \cdot g^{-1}$ have been produced.[22,24,28,29,31-33]

In addition to SSA, pore-size distribution (PSD) is also an important parameter affecting the electrochemical performance of ACs. In general, a narrow PSD gives an increase in surface area of regular pore distributions compared with a broad PSD, leading to an increase in capacitance and energy density,[35] which means that monodispersed pores and elaborately optimized PSD would be an ideal choice for the electrode material of SCs.[36] In addition, Kondrat et al. demonstrated that the optimal pore size that provides the maximal energy density increases with increasing operating voltage and saturates at high voltages.[36]

The initial carbon precursors have an important impact on the SSA and the electrochemical performance. The most commonly used precursors for commercial AC production include petroleum coke, pitch and coal.[37-40] Depending on different activation conditions, a variety of ACs with different SSAs of 900–3500 $m^2 \cdot g^{-1}$ and C_s of 200–350 $F \cdot g^{-1}$ in aqueous electrolytes and 130–220 $F \cdot g^{-1}$ in non-aqueous electrolytes have been produced. Given the limitation of fossil fuel resources, plenty of biomass-derived ACs have attracted attention during the past few years. ACs are widely prepared from various natural precursors, such as nutshells[41-43], seaweeds[44-45], woods[41,46], corn grains[47], saccharides[48,49], etc. Unfortunately, ACs derived from natural precursors usually have significant difference in terms of their properties, which is seriously detrimental for the use of SCs especially in the automotive field. Thus, various synthetic polymers such as phenol formaldehyde resins[50], polystyrene-based resins[51], polyfurfuryl alcohols[52], polyaniline (PANI)[53] and polypyrrole (PPy)[54] have generated considerable interest and explored as promising alternative precursors in recent years due to their low cost, commercial availability, uniform structure and high purity. Yan et al. synthesized an AC by the carbonization of rod-shaped PANI and subsequent KOH activation, showing a high C_s of 455 $F \cdot g^{-1}$ and a remarkable rate capability due to its high SSA of 1976 $m^2 \cdot g^{-1}$, narrow PSD (<3 nm) and short diffusion length.[53] Wei et al. prepared an AC from PPy using a one-step KOH activation process.[54] The as-produced AC possesses 0.5–4 nm pores with a pore volume of 2.39 $cm^3 \cdot g^{-1}$ and ultrahigh SSA up to 3432 $m^2 \cdot g^{-1}$, leading to a high C_s of 300 $F \cdot g^{-1}$ in ionic liquid at 60 °C, which is more than a two-fold improvement compared to commercial ACs and other reported novel carbon materials.

Moreover, activation methods and conditions also play significant roles in the porosity and electrochemical performance of ACs. Due to lesser extent of carbon etching than chemical

activation, ACs prepared by physical activation processes usually have relative low SSA (680–2420 $m^2 \cdot g^{-1}$) and pore volume, and low C_s (33.7–206 and 56–172 $F \cdot g^{-1}$ in aqueous and non-aqueous electrolytes, respectively).[41,42,55] With regards to the chemical activation, activation conditions such as the activation temperature, activation time and mass ratio of activation agent and precursor are key factors affecting the yield, SSA and pore structure of ACs, which accordingly affect their capacitive performances.[54,56-58] Typically, a high activation temperature, long activation time and large mass ratio of activation agent and precursor lead to enhanced SSA, pore volume and average pore size.[54,59] However, excessive activation will result in large pore volume, low electrical conductivity and corresponding loss of power delivery and low volumetric energy density.

Furthermore, surface functionalities also have an important influence on the electrode performance. The surface functionalities may induce faradaic reactions, contributing some additional capacitance to the total capacitance.[45,57,60,61] Carbon with high oxygen content prepared by the pyrolysis of seaweed for supercapacitors exhibited a C_s of 125 $F \cdot g^{-1}$ and a high energy density of 10.7 $Wh \cdot kg^{-1}$ with a cell voltage of 1.6 V.[62] However, the presence of surface functionalities or moisture generally gives rise to a poor electrode stability during cycling, an increase in the series resistance, an increase in the leakage current, the decomposition of the organic electrolyte and the deterioration of capacitance.[63] Thus, surface chemistry of ACs should be elaborately optimized to enhance the long-term cycling stability.

Nowadays, a variety of ACs produced through physical or chemical activation from various precursors are the most extensively used electrode materials for commercial supercapacitors. Nevertheless, their practical applications are still limited to some extent as the energy density is still relative low and the control of PSD and pore structure is still challenging. Therefore, it is of great importance to design and produce ACs with elaborately designed PSD, minimized pore tortuosity, interconnected pore structure, short pore length and controlled surface chemistry in order to facilitate the ion transport and enhance the energy storage without sacrificing their power capability and cycle life.

1.3.1.2 Carbide-derived carbons (CDCs)

CDCs are produced by the extraction of non-carbon atoms from carbides (TiC, B_4C, ZrC, Ti_3SiC_2, Ti_2AlC and SiC) by the reaction:

$$MC + nCl_2 \rightarrow MCl_{2n} + C(s) \quad (5)$$

This method allows the synthesis of micro- and mesoporous carbons with SSA of 1000-3000 $m^2 \cdot g^{-1}$ and controlled pore size, since porosity is formed by leaching out non-carbon atoms M from the crystal structure of the carbide precursor.[64-68] For example, V. Presser et al. reported the synthesis of TiC-CDC with a narrow PSD having a mean value that is tunable between 0.6 and 1.1 nm by changing the synthesis temperature.[64]

The adverse effect of the micropores in CDCs is the relatively slow ion transport in small pores and thus a moderate rate of charge and discharge, seriously limiting their power storage. One strategy to mediate this limitation is to develop hierarchical porous CDCs with straight ordered mesopores.[67,69] Ordered mesoporous channels are favorable for the insertion and retention of the electrolyte ions, and can serve as highways for fast ionic transport. Meanwhile, the micropores on the mesopore walls can increase the SSA, providing more sites for charge storage. M. Rose et al. demonstrated a SC with CDC electrode exhibiting not only a very high C_s of ≈ 202 $F \cdot g^{-1}$ in aqueous electrolyte, but also an exceptionally high power performance with up to 90% of the capacitance retained when the current density was increased from 0.1 to over 20 $A \cdot g^{-1}$ due to the presence of straight mesoporous channels combined with a high micropore content in CDC.[69]

From an academic point of view, CDCs are very important material for study as they can provide valuable information about the effect of pore size, channel structure, and other parameters on ion diffusion and charge storage in carbon nanomaterials. However, CDCs still have very limited commercial potential due to their high cost, serious safety and environmental concerns associated with their production.

1.3.1.3 Carbon nanotubes (CNTs)

CNTs that are one-dimensional carbon materials, have been extensively studied for EDLC applications due to their excellent electrical conductivity, unique pore structure, exceptional mechanical, chemical and thermal stability.[34,35] However, the C_s of CNTs is generally low due to the limitation of their SSA (less than 600 $m^2 \cdot g^{-1}$).[30] Intriguingly, although the surface area of CNTs is relatively moderate, their area C_s can reach up to 50.4 $\mu F \cdot cm^{-2}$, which is higher than those of ACs (20–50 $\mu F \cdot cm^{-2}$) owing to the low density and the perfect electrolyte accessibility by the entanglement of CNTs.[30] On the other hand, carbon nanotubes can serve as excellent substrates for electrode composites by decorating or coating the CNT surface with a thin film of redox materials for improvement of conductivity and cell performance.[70]

Over the past decade, there are considerably increasing interests in flexible and lightweight energy-storage systems to meet the demands for portable electronic devices. Recently, CNTs have been printed on plastics, papers or coated on textiles to fabricate thin and flexible SCs.[71-73] In the electrodes of these SCs, CNTs not only act as highly conductive and flexible active materials, but also play a role in increasing the effective surface area of the films to maximize the efficiency of thin film SCs. Z. Q. Niu et al. reported a compact-designed SC fabricated using large-scale, free-standing and flexible single-walled CNT films as both the anode and cathode, which exhibited a high energy density (≈43.7 $Wh \cdot kg^{-1}$) and a power density (≈193.7 $kW \cdot kg^{-1}$) due to small internal resistance.[71] K.-H. Choi et al. have demonstrated a stretchable and wearable SC using SWNTs coated textiles as electrode, exhibiting a high C_s of 140 $F \cdot g^{-1}$and an extraordinary energy density of 20 $Wh \cdot kg^{-1}$ at a specific power of 10 $kW \cdot kg^{-1}$ in 1 $mol \cdot L^{-1}$ $LiPF_6$ electrolyte, and showing an extremely good cycling stability with only 2 % variation in capacitance over 130 000 cycles.[73]

Moreover, aligned CNTs (ACNTs) have aroused particular interests in SC applications due to their advantages over randomly entangled CNTs.[74-76] ACNTs have relatively regular pore structures and conductive channels, leading to higher effective SSA, facilitating fast ion and electron transportation and providing improved charge storage abilities, which is highly desirable in high power required applications. A. Izadi-Najafabadi et al. fabricated electrodes for SCs from vertically ACNTs with near-ideal SSA (1300 $m^2 \cdot g^{-1}$), which could operate at a

high voltage (4 V) while maintaining durable full charge-discharge cyclability with an energy density (94 $Wh \cdot kg^{-1}$, 47 $Wh \cdot L^{-1}$) and power density (210 $kW \cdot kg^{-1}$, 105 $kW \cdot L^{-1}$), far exceeding those of AC SCs both gravimetrically and volumetrically.[74] The ordered pore structure of SWNT electrodes have a lower tortuosity, facilitating fast ion transport and thus higher power capability.

Due to the fact that the power performance would be seriously limited by the large contact resistance between active materials and current collector, various methods have been employed to reduce the internal resistance of CNT electrodes in order to obtain high power capabilities. An effective approach is to assemble binder-free CNT films, which can be realized through layer-by-layer (LBL) assembly[77,78] and electrophoretic deposition (EPD)[79]. LBL CNT electrodes were demonstrated ultrahigh capacitance of 160 $F \cdot g^{-1}$ in 1 M H_2SO_4, which is extremely higher than those of ACNTs and conventional CNTs.[78] Compared to LBL assembly methode, EPD is a relatively quick means to fabricate CNT films, which usually uses an oppositely charged metal current collector to attract CNTs in CNT suspension by the effect of electrostatic attraction.[79] This method has several advantages including short assembly time, simple equipments and applicability for large-scale production. Another promising approach to reduce the internal resistance of CNT electrodes is direct growth of CNTs on conductive substrates, such as graphite foil[80], aluminum[81], Au[82] and metallic alloy[83]. This approach minimizes the contact resistance between the active material and the current collector and greatly simplifies the electrode fabrication process.

Despite of these tremendous achievements, a number of issues in CNTs including limited SSA, unnegligible impurities and high production cost still need to be addressed in order to further promote the industrial application of CNTs.

1.3.1.4 Graphene

Graphene is one-atom-thick two-dimensional layer of sp^2-bonded carbon. Because of high SSA of 2,630 $m^2 \cdot g^{-1}$ and extraordinary theoretical capacitance of 550 $F \cdot g^{-1}$, graphene has great opportunity to replace the traditional carbon materials such as ACs in SCs.[34] Various methods have been developed to effectively synthesize graphene via top-down or bottom-up

strategies. In general, top-down strategy is mainly based on the exfoliation of graphite, including micromechanical cleavage, oxidation-exfoliation-reduction, intercalation exfoliation and solid exfoliation (e.g., ball milling).[84] Bottom-up strategy includes organic synthesis from small structurally-defined molecules (e.g., polyphenylene[85]) and chemical vapor deposition (CVD)[86]. Notably, the graphene products vary distinctly in terms of number of layers, sizes, functional groups, wrinkles, defects (inplane holes or heteroatom doping) and shapes (e.g., graphene nanoribbons) depending on synthesis methods, which could be remarkably reflected by huge differences in apparent properties (e.g., SSA and density) and electrochemical performance of electrochemical energy storage devices. For instance, mechanically exfoliated graphene sheets possess perfect crystallinity but void of abundant defects. The as-produced graphene exhibits a low sheet resistance of around 400 $\Omega \cdot sq^{-1}$ at room temperature[87], much higher than that of reduced graphene oxide (rGO) sheets produced by wet chemical routes, in which many defects and oxygen containing functional groups are left in the graphene sheets, therefore resulting in low conductivity[88].

Restacking of graphene sheets during preparation that causes substantial ionic resistance for the electrode is a crucial issue to avoid. To minimize the aggregation, a number of efforts have been made, including incorporating spacers (e.g., metal nanoparticles[91,92], oxide/hydroxide nanoparticles[93-96], water molecule[97], conducting polymers[98,99], carbon nanomaterials[100-102]), preparation of porous or crumpled graphene sheets[103-105] and activation of graphene[106,107]. These attempts not only greatly enhance the electrochemical utilization of graphene layers but also facilitate the diffusion and migration of electrolyte ions.

Because of the fluffy state of the graphene sheets, the packing density of common graphene electrodes is rather low (from 0.05 to 0.75 $g \cdot cm^{-3}$), which would result in low volumetric energy density.[89] By simply compressing graphene sheets electrode material, volumetric capacitance and energy density would be enhanced.[214] Notably, ion diffusion could be not efficiently achieved in most compact graphene materials due to limited channels for efficient diffusion and transport of electrolyte ions, leading to a low volumetric capacitance. Therefore, rational design of porous structures in compact graphene-based film electrode is of importance for achieving high volumetric capacitance. Taking advantage of intrinsic microcorrugated 2D configuration and self-assembly behavior of rGO, Yang et al.[89]

demonstrated the fabrication of rGO electrodes by capillary compression of adaptive graphene gel films in the presence of a nonvolatile liquid electrolyte. This soft approach enables subnanometer scale integration of graphene sheets with electrolytes to form highly compact carbon electrodes with a continuous ion transport network. The SCs based on the resulting liquid electrolyte-mediated rGO film electrode can achieve a high volumetric energy density of 60 $Wh \cdot L^{-1}$. Tao et al.[90] developed a highly dense but porous graphene-based monolithic carbon by adding zinc chloride during capillary drying of graphene hydrogel, the SSA of the monolithic graphene was tuned from 370 to over 1,000 $m^2 \cdot g^{-1}$, while the monoliths still maintained high density from 1.6 to 0.6 $g \cdot cm^{-3}$. Having a good balance of porosity and density, the directly sliced graphene pellet electrode with a thickness up to 400 μm delivered a capacitance of 150 $F \cdot cm^3$ in an ionic liquid electrolyte, corresponding to a volumetric energy density of ~65 $Wh \cdot L^{-1}$ in a symmetric SC, which was among the highest value reported to date for SCs.

1.3.2 Pseudocapacitive materials

As mentioned above, materials based on EDL mechanism have limited specific capacitance. SCs made of redox-active materials bearing greater pseudocapacitance are highly desirable as the next generation of SCs.[108] They not only store charges in the double layer as a conventional supercapacitor electrode does, but also undergo fast and reversible surface redox reactions (faradaic reactions). Therefore, considerable efforts have been devoted in recent years to develop electrode materials with pseudocapacitance. This kind of material is generally classified into two types: conducting polymers and electroactive metal oxides/hydroxides.

1.3.2.1 Metal oxides/hydroxides

In general, metal oxides/hydroxides can provide a higher energy density in SCs than conventional carbon materials and a better electrochemical stability than polymer materials. To date, the investigated metal oxides/hydroxides include RuO_2, MnO_2, Co_3O_4, $Co(OH)_2$,NiO, $Ni(OH)_2$ and V_2O_5, etc.

1.3.2.1.1 RuO_2

Among various transition metal oxides, RuO_x is the most extensively studied candidate due to its wide potential window, highly reversible redox reactions, three distinct oxidation states accessible within a 1.2 V voltage window, high proton conductivity, extraordinary high specific capacitance, good thermal stability, long cycle life, metallic-type conductivity and high rate capability.[109-110] With RuO_2 electrodes, EDL charging only contributes to about 10% of the accumulated charge, in the meantime with the occurance of redox pseudocapacitance mechanism. The pseudocapacitive behaviors of RuO_2 in acidic and alkaline media involve different reactions, which accordingly present different sensitivities toward crystallinity. For example, amorphous RuO_2 materials in the H_2SO_4 electrolyte showed a maximum C_s of 720 $F \cdot g^{-1}$ upon calcination at 150 °C.[111] For a crystalline state of RuO_2 in a KOH electrolyte, a maximum capacitance of 710 $F \cdot g^{-1}$ was achieved by calcinating at 200 °C.[112] (6) corresponding mechanisms have been demonstrated to be as follow. In an acidic solution, rapid reversible electron transfer is accompanied by the electroadsorption of protons on the surface of RuO_2 particles, where Ru oxidation states can change from Ru (II) to Ru (IV).[3,113] However, in an alkaline solution, the changes in the valency state of RuO_2 are quite different. The ruthenium is oxidized to RuO_4^{2-}, RuO_4^- and RuO_4 on charging and these high valency state compounds are reduced to RuO_2 upon discharging.[199]

It has been demonstrated that the C_s of RuO_2 strongly depends on several factors, including the SSA, the crystallinity, the combined water in RuO_2 as well as the electrolyte. Owing to the pseudocapacitance of RuO_2 arising mainly from the surface reaction, high SSA can provide more active sites to participate in redox reactions, resulting in high C_s. Thus, several approaches such as depositing RuO_2 films on various substrates with rough surface, coating thin RuO_2 films on high SSA materials and synthesizing nanoscaled RuO_2 particles, have been explored toward enhancing the SSA of RuO_2.[114-116] Amorphous RuO_2 thin films deposited on stainless steel substrates by anodic deposition showed stable electrochemical performance with a maximum C_s of 1190 $F \cdot g^{-1}$ in H_2SO_4 electrolyte.[116] An amorphous RuO_2 usually exhibits remarkable electrochemical performance as the redox reaction takes place

both on the surface and in the bulk. RuO_2 with high crystallinity is unfavorable for the transport and diffusion of protons, resulting in large diffusion resistance.[108] Moreover, the combined water in RuO_2 allows the diffusion of cations inside the electrode layer by hopping of alkaline and H^+ ions between H_2O and OH^- sites.[108] Hydrous RuO_2 ($RuO_2 \cdot 0.5H_2O$) showed a C_s as high as ≈900 $F \cdot g^{-1}$, which was more than 1000 times greater than that of anhydrous RuO_2 (0.75 $F \cdot g^{-1}$).[117] Furthermore, the used electrolyte (acid/base and concentration) also has a significant impact on the electrochemical performance of RuO_2.[3]

Despite the high C_s and excellent rate capability of amorphous hydrous RuO_2, the relatively high cost, low abundance and environmental concerns seriously prohibit its further commercialization for SCs. Recent years, considerable efforts have been devoted to exploit relative cheap and environmentally benign materials that exhibit similar electrochemical behavior to that of RuO_2 as alternative candidates to RuO_2, such as MnO_2, NiO, Co_3O_4, V_2O_5, etc.[118-121]

1.3.2.1.2 MnO_2

MnO_2 as a highly promising alternative to RuO_2 has attracted enormous attentions as electrode materials for SCs due to its high theoretical C_s (≈1100 $F \cdot g^{-1}$), low cost, abundance and environmentally friendly nature. In general, pseudocapacitive charge storage of MnO_2 in an aqueous electrolyte takes place via the redox of Mn between the +4 and +3 oxidation states at the surface or in the bulk.[122] Nevertheless, MnO_2 does not possess the high electronic conductivity as that of RuO_2 (10^4 $S \cdot cm^{-1}$ for bulk single crystal). Depending on the crystal structure, the conductivity of MnO_2 ranges from 10^{-7} to 10^{-3} $S \cdot cm^{-1}$.[123] As a result, charge storage in MnO_2 occurs within a thin layer of the surface.[122] This corresponds to a significantly lower capacitance values than the theoretical value for thick composite electrodes, where typical C_s ranges between 200 and 250 $F \cdot g^{-1}$. On the other hand, it has been shown that ultrathin films of MnO_2 can achieve a C_s of >1000 $F \cdot g^{-1}$ [122], indicating that nanostructuring is a highly effective method for accessing all of the MnO_2 storage sites. To overcome the poor electrical conductivity, several advanced methods have been widely explored, such as incorporating metal with excellent conductivity into MnO_2 or hybridizing

MnO_2 with excellent electrically conductive components including carbon materials and conducting polymers.[124-127]

1.3.2.2 Conductive polymers

Conductive polymers are another attractive pseudocapacitive material for SCs as they possess many advantages, such as low cost, low environmental impact, high conductivity, high storage capability and adjustable redox activity through chemical modification.[108,128] The pseudocapacitance of conducting polymers is generally attributed to the reversible oxidation and reduction of the π-conjugated double bonds in polymer networks. The most often studied conductive polymers in SC applications are polyaniline (PANI), polypyrrole (PPy), polythiophene (PTh) and their corresponding derivatives. Due to the relative poor conductivity, C_s of around 150–190, 80–100, and 78–117 $F \cdot g^{-1}$ are generally obtained for PANI, PPy or PTh in both aqueous and non-aqueous electrolytes, which correspondingly results in a poor power density and may not meet the practical requirements. Additionally, another obstacle inhibiting the application of conductive polymers is their poor cyclability due to structural degradation of electrode caused by swelling and shrinking during the charge/discharge process. As a consequence, the electrochemical performance is extremely compromised. Therefore, rational structure design is highly desirable to obtain an electrochemically stable conductive polymer electrode. Incorporating conductive polymers with porous rigid backbones seems to be an effective method. It has been demonstrated that the electrochemical performance of conductive polymers could be considerably enhanced when hybridized with various materials such as carbon, metal and metal oxide materials.[129,130] To date, although considerable achievements have been made in synthesizing various conductive polymers with nanostructure and binary nanostructured composites over the past several years, some issues still exist, such as complicated procedures, low loading of active materials, moderate C_s and rate capability as well as poor cycling stability. Therefore, efforts still need to be devoted to address these issues and synthesize novel, low cost and environmentally benign multivariate composite to achieve optimum electrochemical performances for the applications of SCs.

1.4 Electrolytes of supercapacitors

The electrolyte consisting of the electrolyte salt and solvent is one of the key components of SCs, providing ionic conductivity and thus enabling charge compensation on each electrode in the cell. The electrolyte within a SC not only plays a fundamental role in the EDL formation (in EDLCs) and the reversible redox process for the charge storage (in pseudocapacitors), but also determines the electrochemical performance of SCs. Currently, the majority of commercial SCs use organic electrolytes with a cell voltage of 2.5–2.8 V. Most organic electrolyte-based SCs employ acetonitrile (ACN) or propylene carbonate (PC) solvent.[131]

The electrolyte nature, including the ion type and size, the concentration and solvent, the interaction between the ion and the solvent, the interaction between the electrolyte and the electrode materials and the potential window, all play roles in the EDL capacitance and pseudocapacitance, the energy and power densities as well as the SC cycle-life. For example, the electrochemical stability potential window (ESPW) of the electrolyte directly determines the SC's operational cell voltage, affecting both the energy and power densities. The ESR of an SC is directly related to the electrolyte's ion conductivity and can have a strong effect on the power density. Furthermore, the interactions between the ion and the solvent as well as between the electrolyte and the electrode material can affect the life-time and self-discharge of SCs.

To date, various types of electrolytes for SCs have been developed and reported. They can be mainly classified as liquid electrolytes and solid/quasi-solid-state electrolytes. Generally, liquid electrolytes can be further grouped into aqueous electrolytes, organic electrolytes and ionic liquids (ILs), while solid or quasi-solid state electrolytes can be divided into organic solid electrolytes and inorganic solid electrolytes. There has been no perfect electrolyte developed that meets all the requirements until now and each electrolyte has its own advantages and disadvantages. For example, SCs using aqueous electrolytes possess both high conductivity and capacitance, yet their operating voltage is limited due to the narrow decomposition voltage of aqueous electrolytes. Although organic electrolytes and ILs can be

operated at higher voltages, they normally suffer from much lower ionic conductivity. Solid-state electrolytes may avoid the potential leakage problem that the liquid electrolytes have, but they also suffer from low conductivity. To overcome the drawbacks of targeted electrolytes, extensive efforts have been made to develop new electrolyte materials so as to improve the overall SC's performance. In this regard, several approaches have been developed, including (1) developing new electrolytes with wider operating potential window, higher ionic conductivity (lower viscosity) and wider working temperature range, (2) taking full advantage of the positive effects of given electrolytes on the SC's properties such as capacitance, energy and power densities, thermal stability and self-discharge process and (3) constructing fundamental understandings of the effect of the electrolyte on the SC's performance through advanced experimental, modeling and simulation methods.

1.4.1 Aqueous electrolyte

Aqueous electrolytes usually provide high conductivity (e.g., about 0.8 $S \cdot cm^2$ for 1 M H_2SO_4 at 25 °C), which is at least one order of magnitude higher than that of organic and IL electrolytes.[132] This is beneficial for lowering the ESR, leading to a better power delivery of SCs. The selection criteria for aqueous electrolytes generally takes in consideration the sizes of the bare and hydrated ions and the mobility of the ions, which influence not only the ionic conductivity but also the specific capacitance value. In addition, the ESPW of electrolytes and the corrosive degree should also be taken into account.

Generally, aqueous electrolytes can be grouped into acid, alkaline and neutral solutions in which H_2SO_4, KOH and Na_2SO_4 are representatives and also the most frequently used electrolytes. As previously mentioned, the main disadvantage of aqueous electrolytes is their relatively narrow ESPW, restricted by the decomposition of water. For example, hydrogen evolution occurs at a negative electrode potential of around 0 V vs. SHE, and oxygen evolution at a positive electrode potential of around 1.23 V, leading to the SC with cell voltage of about 1.23 V.[134] The gas evolution would potentially give rise to the rupture of the SC cells, triggering the safety concern and reducing their performance. To avoid the gas evolution, the cell voltage of SCs with aqueous electrolytes is commonly restricted to about 1.0 V. However,

by elaborately taking advantage of the strong solvation effects between ions, ions and solvent, or solvent-solvent molecules, it is possible to reach the operating voltage rang of 2.2 V without any significant capacitance fade.[133] In addition, the operating temperature range of SCs with aqueous electrolytes has also to be limited to the freezing point and the boiling point of water.

1.4.2 Organic electrolyte

Although extensive studies have focused on aqueous electrolyte-based SCs in academia, organic electrolyte-based SCs are currently predominating the commercial market because of their high operational potential window typically in the range of 2.5 to 2.8 V. The increased operational cell voltage can provide a significant improvement in both the energy and power densities. Furthermore, using organic electrolytes allows the use of cheaper materials (e.g., Al) for the current collectors and packages. Typical organic electrolytes for the commercial EDLCs consist of the conductive salts (e.g., tetraethylammonium tetrafluoroborate ($TEABF_4$)) dissolved in organic solvents such as ACN or PC. However, there are some issues that should be considered when using the organic electrolytes for SCs. Compared to SCs using aqueous electrolytes, SCs with organic electrolytes usually have a higher cost, a smaller C_s, a lower conductivity and safety concerns related to the flammability, volatility and toxicity. In addition, an organic electrolyte requires high purity and assembling in a strictly-controlled environment in order to avoid any impurities (e.g., water) that can result in large degradation in performance and serious self-discharge issues.[3] Similar with aqueous electrolyte-based SCs, the nature of salts and solvents such as ion size, the interaction between ion and solvent, conductivity, viscosity and ESPW has profound impacts on the performance of organic electrolyte-based SCs.

The C_s of an EDLC depends not only on the SSA but also on the pore size and size distribution of the carbon materials.[25] The accessibility of pores is intimately related to the properties of an organic electrolyte, such as the sizes of cation and anion species and the interaction between ion and solvent. The carbon materials with very small pore size may increase the SSA, but can also restrict the accessibility of electrolyte ions. In particular, the

larger organic ions cannot easily get access into the small pores, resulting in a detrimental effect on the C_s. Therefore, it is important to figure out the relationship between the pore size of carbon materials and the size of electrolyte ions to obtain maximized C_s. With respect to this, considerable efforts have been devoted to understand the relationship between ion size and the capacitive behaviour of carbons with different pore size distributions, and then optimize the matching between pore size and electrolyte ion size.[25,135,136] In addition, both the sizes of solvated ions and bare (desolvated) ions should also be taken into consideration. It has been demonstrated that when the ions enter into the pores with the size close to the size of desolvated ions, the desolvation or distortion of the solvated ions could lead to an anomalous increase in the C_s.[25] Besides the C_s, other properties such as the ESR, charge-discharge rate and power density should also be considered when optimizing the pore structures and designing the electrolytes.

Recently, theoretical modeling and simulations of EDL in organic electrolytes have received increasing attention, which may provide useful guidances for EDLC design from a microscopic point of view.[137] These theoretical approaches including molecular dynamics (MD) simulation, density functional theory (DFT) calculations and Monte Carlo (MC) simulation give insights into the solvation of ions in organic solvents and the EDL structure, and the effect of carbon pore size and morphologies on the capacitance.[138-140] In parallel, a number of experimental approaches on the electrolyte–electrode interactions have also been explored in order to gain a deeper understanding of the electrolyte behaviour in working SCs.[141-150] In this regard, various experimental methodologies, including nuclear magnetic resonance (NMR)[142–145,150], electrochemical quartz-crystal microbalance (EQCM)[145], in situ infrared spectroelectrochemistry[147], and in situ small angle neutron scattering (SANS)[146] were employed. With the help of these useful analysis methods, fundamental understandings of ion dynamics during the charging–discharging process, local ion structures at the electrolyte/electrode interface, ion electroadsorption and the pore size effect have been greatly advanced.

The ESPW of an organic electrolyte is an important property determining the SC operational cell voltage and correspondingly the energy and power densities. Generally, the ESPW of an organic electrolyte depends on several factors, including the type of conducting

salts (i.e., cation and anion), solvent and impurities especially the trace amount of water.[17,151] Moreover, aging and the related deterioration of organic electrolyte-based EDLCs are also important issues needing to be addressed. The degradation is mainly caused by factors including wide operation cell voltage that may result in gas evolution due to the electrolyte decomposition and the oxidation of electrode materials[152], the intercalation of electrolyte ion or the electrochemical reaction of the organic electrolytes[153,154] and harsh working conditions such as high peak temperature. Therefore, understanding the aging and deterioration mechanisms will be beneficial for the development of SCs. In addition, from the safety issue concerns, it is also important to have a better understanding for the aging behavior of SCs. Regarding the self-discharge of the SCs, the presence of trace amount of water in the organic electrolyte was identified to be major reason and the self-discharge mechanism was found to be dependent on the type of organic electrolyte.[155,156]

Conductive salts in organic electrolyte provide charge carriers (i.e., cations and anions) for the operation of SCs. In this respect, the ion concentration and mobility should play important roles in the ionic conductivity. The conductive salts have a profound influence on the ESPW, the thermal stability of the electrolytes and the specific capacitance of SCs. Thus, the selection and development of conductive salts for certain organic solvents should consider several factors such as solubility, conductivity, stability, safety and cost. Because of good overall properties, $TEABF_4$ is currently the most commonly used salt and has been widely applied in commercial SCs. Besides $TEABF_4$, several other salts including symmetric and asymmetric tetraalkylammonium slats, tetraalkylphosphonium salts, etc. have also been studied or developed to gain further improvements of their properties (e.g. solubility, conductivity, stability and temperature performance) for the organic electrolytes in SCs. In addition to the organic cations, organic salts based on the inorganic cations, such as Li^{+}[157,158], Na^{+}[159] and Mg^{2+}[160] have also attracted lots of attention. In particular, organic electrolytes based on the lithium salts have been widely used in the pseudocapacitors and hybrid SCs due to the small ionic size of Li^{+}. The use of lithium salts for SCs is largely inspired by the development of lithium ion batteries.

1.4.3 Ionic liquids

1.4.3.1 General compositions, properties and supercapacitor performances

Ionic liquids (ILs) are generally defined as molten salts composed of cations and anions with melting points below 100 °C.[161] An IL usually consists of a large asymmetric organic cation and an inorganic or organic anion, and this special combination of certain cation and anion contributes to a low melting point.[162] Due to almost unlimited structural variations and unique properties, ILs span a wide range of applications and thereinto as alternative electrolytes for energy storage devices such as SCs. The key properties of ILs includes high thermal, chemical and electrochemical stability, nonvolatility and nonflammability.[162] Moreover, the physical and chemical properties of ILs can be tunable because of the large variety of cation-anion combinations.[163] Hence, ILs are also called task-specific ILs. This property is very attractive for the applications of ILs as electrolytes in SCs since the IL electrolytes can be optimized or customized to meet certain requirements of SCs such as the operative cell voltage, the working temperature range, ESR (related to the ionic conductivity), etc. Based on their composition, ILs can be basically classified into aprotic, protic and zwitterionic types (Figure 1-5).[162]

The ILs used in SCs so far account for only a very small segment of the large family of ILs. In the published literature, the common employed ILs in SCs are based on imidazolium, pyrrolidinium, ammonium, sulfonium, phosphonium cations, etc. and the typical anions are tetrafluoroborate (BF_4^-), hexafluorophosphate (PF_6^-), bis(trifluoromethanesulfonyl)imide (TFSI or NTf_2), bis(fluorosulfonyl)imide (FSI), dicyanamide (DCA), etc. (Figure 1-6). Generally, the imidazolium-based ILs can provide higher ionic conductivity while the pyrrolidinium-based ILs have larger ESPW.[164] In fact, there is a tradeoff between the ionic conductivity and ESPW of ILs. As mentioned previously, the operative cell voltages of commercial organic electrolyte (e.g., ACN and PC) based EDLCs are generally limited to 2.5–2.8 V. However, the SCs using IL electrolytes could offer higher operative cell voltages above 3 V.[164] On the other hand, organic solvents such as ACN also face safety issues due to their volatile and flammable nature especially when used at high temperatures. In this regard, the solvent-free ILs are advantageous in solving the safety problems associated with organic solvents and also favorable for the application of SCs operating at high temperatures.

Unfortunately, there are some disadvantages for most ILs, including high viscosity, low ionic conductivity and high cost, which highly limit their practical use in SCs. For example, the ionic conductivity of [EMIM][BF_4] that is relatively high (14 $mS \cdot cm^{-1}$ at 25 °C) among the common ILs, is still much lower than that of $TEABF_4$/ACN (59.9 $mS \cdot cm^{-1}$ at 25 °C). With respect to the conductivity of ILs, some cations of ILs for SCs such as pyrrolidinium cations that have a structure similar to that of surfactants tend to aggregate in ILs like surfactants, which would affect both the ion mobility and thus the ionic conductivity of ILs.[169,170] Moreover, the viscosities of ILs such as [EMIM][BF_4] and [BMIM][BF_4] are 41 cp and 219 cp[165], respectively, which are much higher than that of organic electrolyte (e.g., 0.3 cp for the ACN organic electrolytes). Both the low conductivity and high viscosity of IL-based electrolytes can significantly increase the ESR of IL-based SCs, weakening both the rate and power performance if the loss in power density cannot be compensated by an increase of the cell voltage. This issue tends to be more serious at room temperature and low temperature as demonstrated by some comparative studies between organic and IL electrolytes.[164] In addition, the C_s of IL electrolyte-based EDLCs is often lower than that of both aqueous and organic electrolyte-based ones especially at high scan rates or high charge-discharge rates, probably due to the high viscosity of ILs.[166] To improve the performance of IL-based SCs, optimization in the selection of IL composition and cell design has been conducted by both experimental and theoretical means, providing fundamental insights into the EDL at the interface of IL and electrode as well as the molecular mechanism in IL-based SCs.[166-168] Therefore, research in the IL-based SCs field is mainly focused on the following aspects: (1) fundamentally understanding of the EDL structure and capacitance; (2) improvement of the properties related to electrochemical performances of ILs (e.g., ionic conductivity, viscosity and ESPW) by modifying the cations or anions of ILs; (3) employment of a mixture of ILs or introduction of organic solvents to improve the overall performance of IL-based electrolytes SCs.

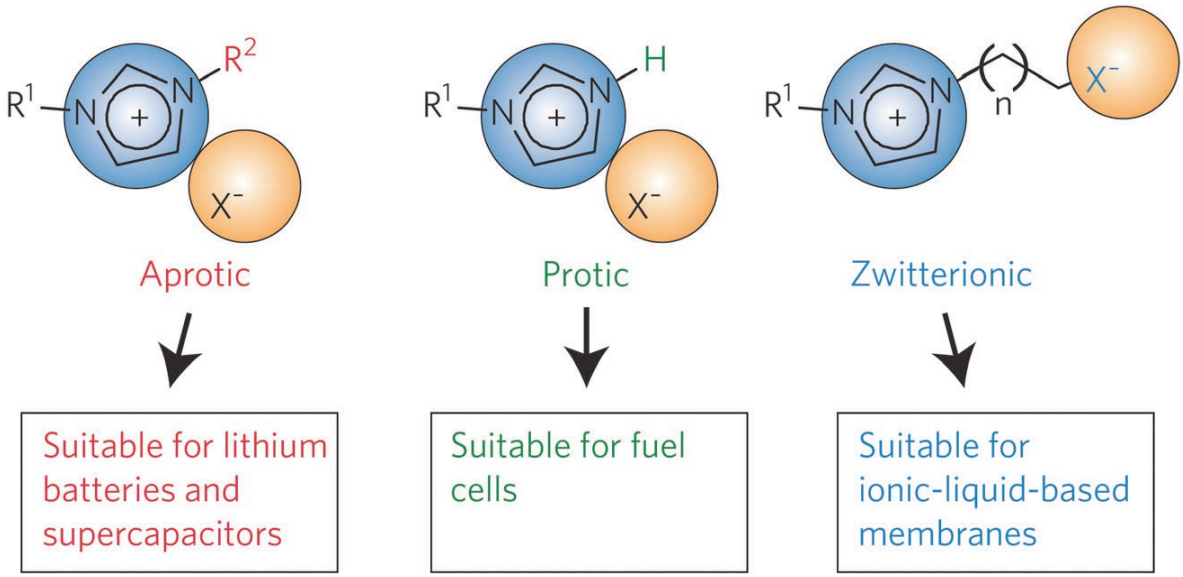

Figure 1-5. Basic types of ionic liquids: aprotic, protic and zwitterionic types. Reprinted from ref. 162.

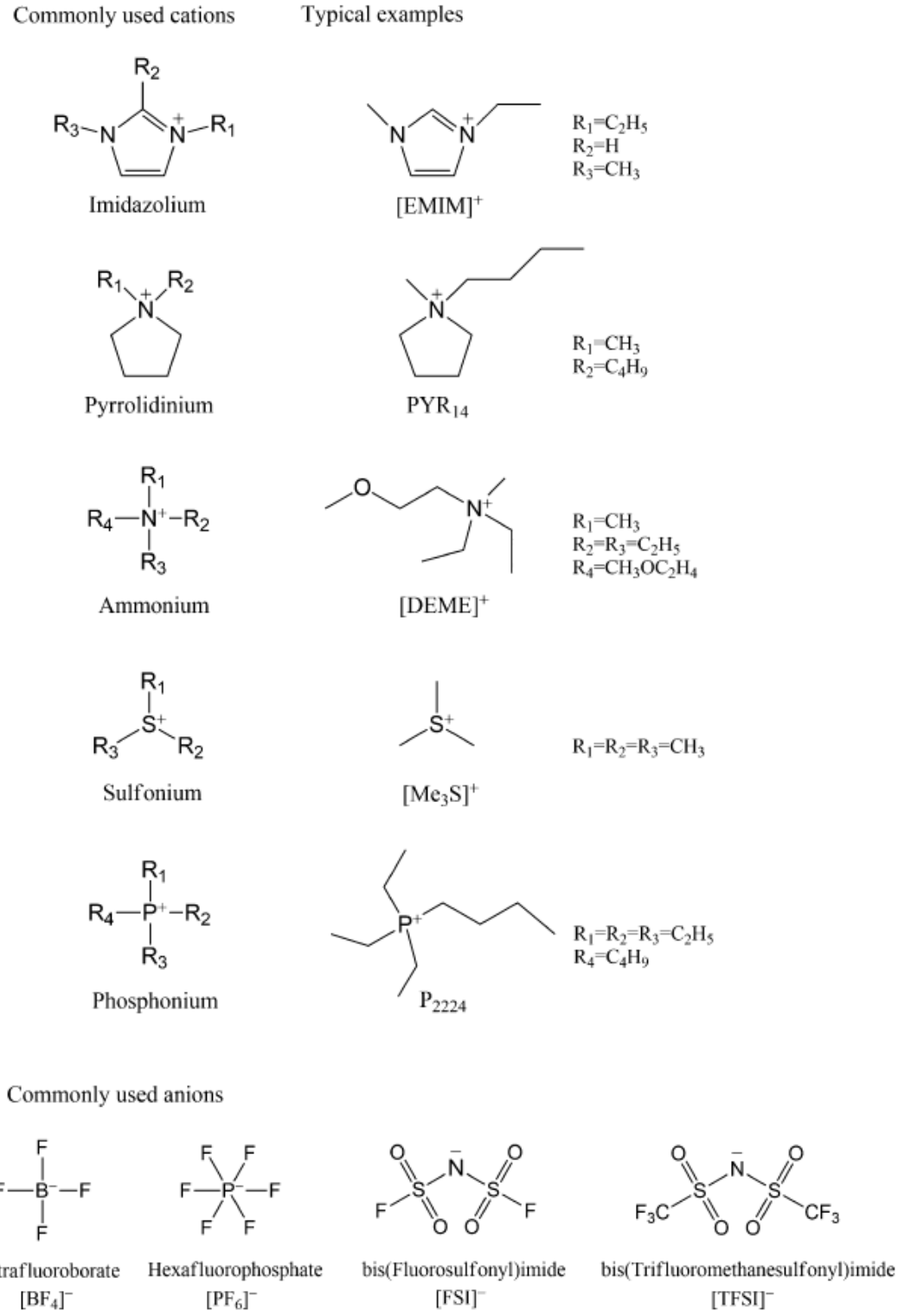

Figure 1-6. Commonly used cations, anions of ILs for SCs, and some typical examples of ILs. Reprinted from ref. 131.

1.4.3.2 Pure ionic liquid electrolyte

Regarding 1-ethyl-3-methylimidazolium ([EMIM])-based ILs, Kurig et al.[175] studied various IL electrolytes featuring $[EMIM]^+$ cations and different anions for EDLCs based on carbon cloth electrodes. It was found that the adsorption capacitance and adsorption kinetics of ions onto the electrode surface depend strongly on the electrode potential and chemical composition and polarity of the ionic liquid and therefore influence noticeably the power density of SC test cells. The power density and relaxation time constant are also strongly influenced by the viscosity and conductivity of ILs. $[EMIM][BF_4]$ and $[EMIM][B(CN)_4]$ ILs demonstrate the best overall performance among the studied ILs (Figure 1-7a). Shi et al.[171] studied the performance of graphene-based EDLCs with a series of ILs composed of $[EMIM]^+$ cations and different anions including BF_4^-, NTF_2^-, DCA^-, $EtSO_4^-$ and OAc^-. It was found that EDLC with the [EMIM][DCA] IL electrolyte had the highest specific capacitance and rate capability as well as the smallest resistance due to the lowest viscosity, ion size and molecular weight among the studied ILs. However, [EMIM][DCA] IL-based EDLC had a much smaller ESPW (2.3 V) which was much narrower than that of the $[EMIM][BF_4]$ IL-based EDLC (～4 V). As a result, the latter delivered the highest specific energy density (67 W h·kg^{-1} at 1 A·g^{-1}), which was the highest value among the EDLCs with the studied ILs (Figure 1-7b). Imidazolium-based ILs with different alkyl chain lengths have also been studied.[172,173] Mousavi et al.[172] provided a systematic study of the influence of the physical properties of ionic liquid electrolytes on the electrochemical stability and electrochemical performance of EDLCs employing a 3-D ordered mesoporous carbon model. It has been shown that the specific capacitance of EDLCs decreases monotonically with increasing carbon chain length. Moreover, Mousavi et al.[172] also investigated several ILs with diverse cations (imidazolium with different alkyl chain length, ammonium, pyridinium, piperidinium and pyrrolidinium) and anions (BF_4^-, NTf_2^-, OTf^-). It has been shown that the cation size has a significant effect on the electrolyte viscosity and conductivity, as well as the capacitance of EDLCs. Imidazolium- and pyridinium-based ionic liquids provide the highest cell capacitance, and $[EMIM][NTf_2]$ offered the highest specific energy and is the best performing IL among the investigated ILs. (Figure 1-7c)

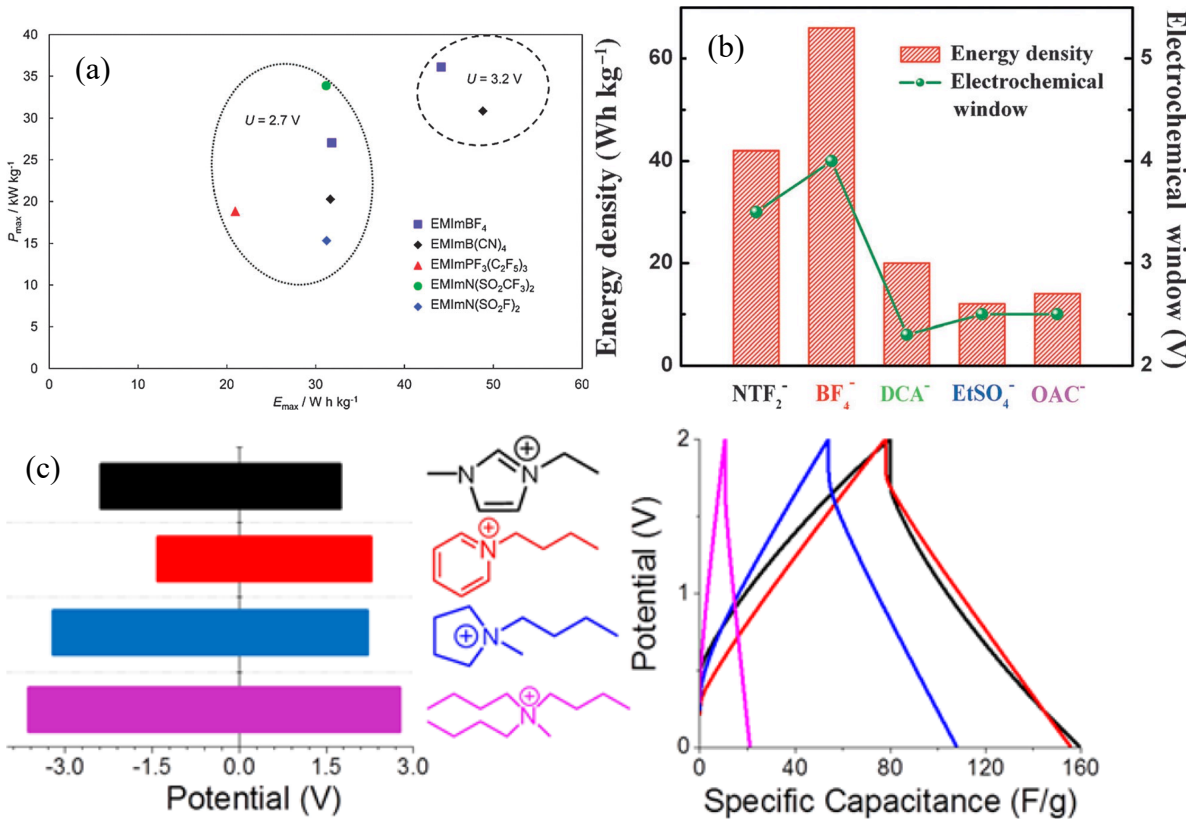

Figure 1-7. (a) Power density vs. energy density plots at 2.7 V and at 3.2 V for electrochemical supercapacitors with ILs studied. Reprinted from ref. 175. (b) Relationship between the electrochemical window and the energy density of graphene electrodes measured in different IL electrolytes. Reprinted from ref. 171. (c) The effect of cation size of ionic liquids on the capacitance of EDLCs. Reprinted from ref. 172.

In addition to imidazolium-based IL electrolytes, ILs with other cations (e.g., pyrrolidinium-based[174,179,180], ammonium-based[172,176,177], sulfonium-based[178], and fluorohydrogenate ILs[177]) have also been extensively studied as potential electrolytes for EDLCs. Regarding the ILs with pyrrolidinium cations, S. Pohlmann, et al.[179] investigated N-butyl-N-methylpyrrolidinium bis(trifluoromethanesulfonyl)imide ([Pyr_{14}][TFSI]) as the electrolyte for EDLCs with activated carbon composite electrodes. The EDLCs delivered a maximum specific energy of ~30 Wh·kg^{-1} at a cell voltage of 3.5 V at 60 °C. Furthermore, Wolff, C. et al.[180] investigated [Pyr][DCA] ILs including Pyr_{13}[DCA], Pyr_{14}[DCA] and Pyr_{12O1}[DCA] as electrolytes in EDLCs. At high current density (50 mA·cm^{-2}) the EDLCs

based on [DCA]-ILs delivered substantially higher energy than the TFSI-based one. In particular, the one employing Pyr_{13}[DCA] shows the highest power capability, owing to its high ionic conductivity, low viscosity and high molarity, which is until now among the highest reported values for solvent- and fluorine-free AC-based EDLCs at room temperature. Regarding the ILs with ammonium-based cations[172,176,177], ammonium-based ILs usually offer exceptionally wider ESPWs than those of imidazolium-based ILs and organic electrolyte such as $TEABF_4$/PC, but yield very low energy density and are a poor choice for EDLCs. Regarding the sulfonium-based cations, Anouti et al.[178] studied the trimethylsulfonium bis(trifluorosulfonimide) [Me_3S][TFSI] IL electrolyte for AC-based EDLCs. [Me_3S][TFSI] IL exhibited an ESPW of about 5 V on a Pt electrode and could operate at up to 3 V on AC electrode-based EDLCs. It was also observed the EDLC using this IL as electrolyte was suitable for high temperature operation, delivering a maximum energy density of 44.1 $Wh \cdot kg^{-1}$ at 80 °C. Anions of ILs also play an important role in their hydrophilic–hydrophobic properties. The hydrophobicity was found to increase in the following order: $CH_3CO_2^-$, NO_3^- < OTf^-, BF_4^- < PF_6^-, $TFSI^-$ (hydrophobic).[181] In addition, a small amount of water in ILs is often deleterious to their ESPW.[182] Therefore, hydrophobic anions such as $TFSI^-$ and FSI^- have received increasing attention for their usage in SCs.

The most commonly studied ILs have higher melting points above 0 °C, limiting their use as electrolytes of SCs for low temperature applications. To extend the operative temperature range to lower temperatures below 0 °C, the strategy of a mixture of IL mixtures has been explored.[184-186] For example, Lin et al.[185] developed a eutectic IL mixture of propylpiperidinium bis[fluorosulfonyl]imide ([PIP_{13}][FSI]) and [PYR_{14}][FSI] (1 : 1 by weight or molar ratio). This IL mixture had a liquid-state range as low as -80 °C. Using exohedral nanostructured carbon (nanotubes and onions) as electrodes, the EDLCs with this [PIP_{13}][FSI] + [PYR_{14}][FSI] IL mixture electrolyte could be operated within a significantly extended temperature range from -50 to 100 °C. Moreover, by employing high SSA and porous KOH-activated microwave exfoliated graphite oxide electrodes[184], the EDLCs with this IL mixture showed outstanding capacitive performance with high capacitance (up to 180 $F \cdot g^{-1}$) and wide electrochemical window (up to 3.5 V) over the wide temperature range from -50 °C to 80 °C. This is the first demonstration of a carbon–ionic liquid system capable of delivering capacitance in excess of 100 $F \cdot g^{-1}$ below room temperature.

1.4.3.3 Mixture of ionic liquid and organic solvent

In order to reduce the viscosity and increase the conductivity of ILs, especially at low temperatures, organic solvents added to ILs have been explored as electrolytes for SCs. Imidazolium-based ILs are the most extensively studied ones mixed with organic solvents due to their relatively high conductivity and good performances among commonly used ILs. In this aspect, McEwen et al.[188] found that the conductivities of IL/organic carbonates mixture electrolytes (ILs: [EMIM][PF_6] and [EMIM][BF_4]) were approximately 25 % greater than that based on the $TEABF_4$ organic electrolyte. A conductivity as high as 27 $mS \cdot cm^{-1}$ was observed in 2 M [EMIM][PF_6]/EC–DMC (EC: ethylene carbonate, DMC: dimethyl carbonate). In addition, a 2 M [EMIM][PF_6]/PC electrolyte could offer both a higher specific capacitance and better thermal stability than 1 M $TEABF_4$/PC. Orita et al.[189] studied a series of allyl functionalized ILs mixed with organic solvents (typically PC) as electrolytes for EDLCs. The EDLCs with [DAIM][TFSI] (DAIM: diallylimidazolium)/PC showed higher capacitance and lower resistance within a wider temperature range compared with [EMIM] based ones. However, the stability of the EDLC with [DAIM][BF_4]/PC was inferior, which could be improved by the addition of DMC to PC. Lin et al.[190] found that although the bare molecular sizes of $[EMIM]^+$ and $[TFSI]^-$were similar, they had different solvated ion sizes in the ACN solvent and they are in the order of: $[TFSI]^-$ in ACN > $[EMIM]^+$ in ACN >$[EMIM]^+ \approx [TFSI]^-$. Therefore, the optimization of the pore structure and size distribution of porous carbon with respect to IL size in an organic solvent should take the solvated ion size into account, which may be different from that in the pure IL electrolyte. In addition, imidazolium-based ILs mixed with organic solvents have also been explored as electrolytes for both pseudocapacitors and hybrid SCs. For example, Zhang et al.[187] found that the introduction of DMF to [BMIM][PF_6] increased the capacitance and meanwhile decreased the internal resistance of the asymmetric AC/MnO_2 SC. This improvement was attributed to the improved electrolyte penetration and ion mobility when compared to pure IL.

1.4.4 Solid electrolyte

With the rapid growing demand of powers for portable electronics, wearable electronics, micro-electronics, printable electronics and especially flexible electronic devices,

solid-state electrolyte-based electrochemical energy storage devices have attracted great attentions in recent years. The solid-state electrolytes serve as not only the ionic conducting media but also the separators in SCs. The major advantages of using solid-state electrolytes are the simplification of packaging and fabricating processes of SCs and liquid-leakage free. To date, major types of the solid-state electrolytes developed for SCs are basically polymer electrolytes and only very limited works on inorganic solid materials (e.g., ceramic electrolytes[191]). The polymer-based solid electrolytes for SCs can be further classified into three types: the solid polymer electrolyte (SPE, also known as dry polymer electrolytes), the gel polymer electrolyte (GPE) and the polyelectrolyte. Due to the presence of a liquid phase in GPE, it also be called as quasi-solid state electrolyte.[131] As shown in Figure 1-8, the SPE is composed of a polymer (e.g., PEO) and a salt (e.g., LiCl) without any solvents. The ionic conductivity of SPE is provided by the transportation of salt ions through the polymer. The GPE consists of a polymer host (e.g., PVA) and an aqueous electrolyte (e.g., H_2SO_4), a conducting salt dissolved in a solvent or an IL. In this case, the polymer serves as a matrix, which can be swollen by the solvent, and the ions transport in the solvent instead of in the polymer phase. In the polyelectrolyte, the ionic conductivity is contributed by the charged polymer chains. As identified, each type of these solid-state electrolytes has their own advantages and disadvantages. Generally, GPE has the highest ionic conductivity among these three types of solid-state electrolytes due to the presence of a liquid phase in the GPE. Therefore, GPE-based SCs currently dominate the solid electrolyte-based SC devices, and studies on SCs using SPE are very limited.[192] However, depending on their composition, GPE may suffer from relatively poor mechanical strength and narrow operative temperature range especially when water is used as the solvent. Furthermore, the weak mechanical strength of GPE may result in internal short circuits, causing safety issues.[9] Although SPEs generally have low ionic conductivity, they have relatively high mechanical strength when compared to GPE. These solid-state electrolytes for SCs have some common disadvantages such as the limited contact surface area between solid-state electrolytes and electrode materials especially in the case of nanoporous materials. This issue could lead to an increase in the ESR, limitation of the selection of active electrode materials and a reduced performance of SCs. Thus, when developing solid-state electrolytes for SCs, the key requirements such as high ionic conductivity, high chemical, electrochemical and thermal stability, and sufficient mechanical

strength and dimensional stability should be considered. In fact, it is difficult for a solid-sate electrolyte to meet all of these requirements. There are often some tradeoffs between ionic conductivity and mechanical strength.

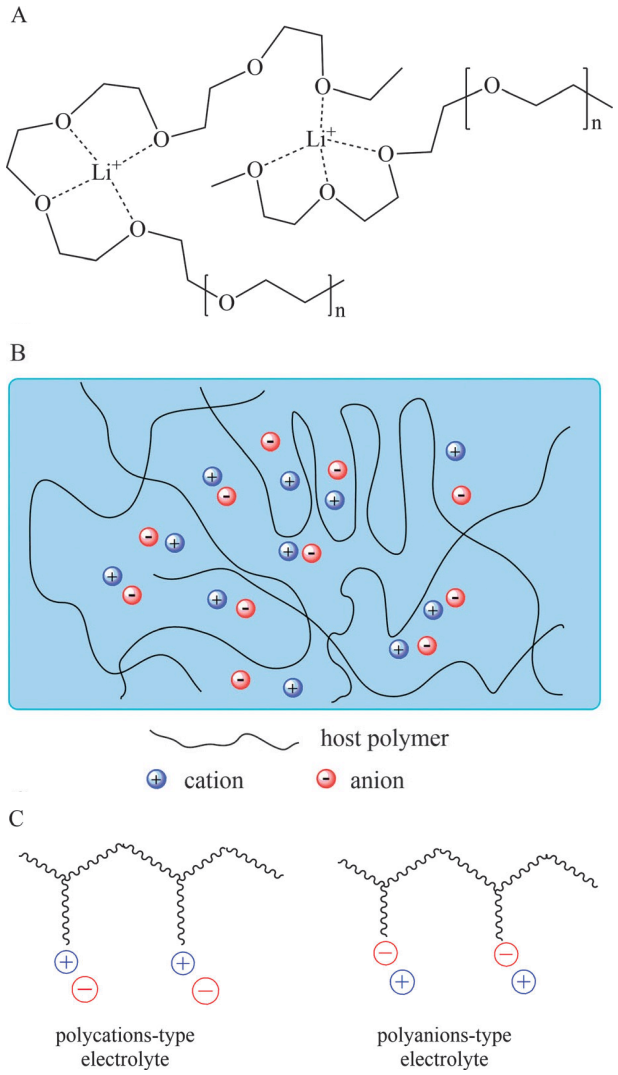

Figure 1-8. Schematic diagrams of (A) a dry solid-state polymer electrolyte (e.g., PEO/Li^+), (B) a gel polymer electrolyte, and (C) a polyelectrolyte. Reprinted from ref. 131.

1.4.5 Redox-active electrolyte

Recently, a new strategy has been explored to increase the capacitance of SCs by the introduction of a pseudocapacitance from a redox-active electrolyte. Fast and reversible faradaic reactions take place on the electrode surface, contributing extra capacitance to the total capacitance of SCs.[13,193,194]

1.4.5.1 Redox-active aqueous electrolyte

The commonly used electrochemical-active compounds are KI[13,194], hydroquinone (HQ)[193,199], methylene blue (MB)[195], p-phenylenediamine (PPD)[196], m-phenylenediamine[197], lignosulfonates[198], etc. A pioneering work reported a SC with KI electrolyte showing a maximum C_s of 1840 $F \cdot g^{-1}$ due to the dual roles of iodide ions, i.e., electrolyte with good ionic conductivity as well as a source of pseudocapacitive effects based on the occurance of the faradaic reactions.[13] Roldán and co-workers added hydroquinone to the supporting electrolyte for four different types of carbonbased SCs.[193] The addition of hydroquinone gave rise to a great increase in the capacitance values for all the tested SCs. The maximum C_s of 901 $F \cdot g^{-1}$ was obtained with an energy density of 31.3 $Wh \cdot kg^{-1}$, which is much higher than those previously reported carbon-based capacitors. The increase in capacitance was attributed to the additional pseudocapacitive contribution from the faradaic reactions of the hydroquinone/quinone system. However, further research is necessary to optimize the performance of the system due to the poor rate capability and cyclability with a decrease of 65 % in C_s after 4000 cycles. To surpress the faster self-discharge arised from the migration of redox-active electrolyte between two electrodes in the case of the SCs using a HQ-based redox-active electrolyte, two strategies were designed.[15] One was to use an ion-exchange membrane (e.g., Nafion) as a separator, and the other was to choose a redox-active electrolyte that could be reversibly converted into insoluble species during the charging–discharging process.

1.4.5.2 Redox-active ionic liquid electrolyte

To achieve a higher cell voltage and thus a higher energy density, a number of non-aqueous electrolytes especially IL-based electrolytes have been studied. Tooming et al.[183] demonstrated that the addition of 5 wt % 1-ethyl-3-methylimidazolium iodide ([EMIM][I]) into [EMIM][BF_4] could give a nearly 50 % increase in the SC's specific capacitance when compared to a bare [EMIM][BF_4] electrolyte and the SC using this ILs mixture electrolyte exhibited a high specific energy of 36.7 $Wh \cdot kg^{-1}$.

Beside conventional ILs bearing redox speices such as iodide, several novel redox ionic liquids functionalized with electroactive species on cations or/and anions of ILs have been designed and applied in SCs. For example, our group has reported two different ionic liquids by modifying either the imidazolium cation or the NTf_2 anion with ferrocene, namely, 1-(methylferrocenyl)-3-ethylimidazolium bis(trifluoromethanesulfonyl)imide ([FcMIM][NTf_2]) and 1-ethyl-3-methylimidazolium ferrocenylsulfonyl-(trifluoromethylsulfonyl)-imide ([EMIM][FcNTf]).[200-202] The SC employing the as-prepared redox IL [EMIM][FcNTf] as electrolyte offers an energy density of up to 13.2 $Wh \cdot kg^{-1}$, which represents an 83 % increase vs. the unmodified IL [EMIM][NTf_2].[202] In particular, when [EMIM][FcNTf] is employed in SC, the self-discharge at the positive electrode is fully suppressed due to the deposition of a film on the electrode. Very recently, E. Mourad et al.[203,204] demonstrated a biredox ionic liquid, where both anion and cation are functionalized with anthraquinone (AQ) and 2,2,6,6-tetramethylpiperidinyl-1-oxyl (TEMPO) moieties, respectively, and applied it as the electrolyte in SCs. The specific energy of SC with this biredox ionic liquid electrolyte could be doubled in comparison to those without redox-active active electrolyte and the enhanced capacitance is sustained for 2,000 cycles without deterioration. These novel redox-active ILs represent a means to overcome the major hurdle of self-discharge for high-energy SCs, opening up a new field in SCs using redox-active materials.

1.4.5.3 Redox-active solid electrolyte

The strategy of using a redox-mediator has also been tested in solid- or quasi-solid state electrolyte-based SCs and some enhanced performances have been observed. Typical redox additives in the solid-state electrolytes are iodides (e.g., KI[150] and NaI[205,206]),

$K_3Fe(CN)_6$[207], Na_2MoO_4[208], as well as organic redox compounds (e.g., hydroquinone[209], p-phenylenediamine[210] and methylene blue[211]), etc. Actually, these redox mediators are almost the same as those used in the liquid electrolytes. The solid-state electrolytes studied were mainly focused on the GPEs with polymer hosts such as PVA[150,208-211], PEO[206,207,212], and Nafions[205,213]. The redox mediators are usually dissolved in the liquid phase of the GPE. Thus, their effect and the working mechanism are basically similar to those in aqueous or organic electrolytes. In general, the redox-active GPEs show a much higher specific capacitance than those GPEs without redox mediators. For example, Fan et al.[150] demonstrated an AC-based SC using mixtures of redox KI and $VOSO_4$ PVA/H_2SO_4 GPE exhibiting a high C_s of 1232.8 $F \cdot g^{-1}$ and an energy density of 25.4 $Wh \cdot kg^{-1}$, which were nearly eight times higher than that of the SC without KI-$VOSO_4$. In addition, the SC using mixtures of redox mediators GPE presents higher energy densities than that using a single redox additive GPE. Zhou et al.[213] investigated the SCs using the PEO/$LiClO_4$–ACN organogel with two types of redox mediators – NaI/I_2 and $K_3Fe(CN)_6$/$K_4Fe(CN)_6$ as electrolytes. The SCs employing NaI/I_2 and $K_3Fe(CN)_6$/$K_4Fe(CN)_6$ deliver specific energy of 49.1 $Wh \cdot kg^{-1}$ at 1.6 $kW \cdot kg^{-1}$ and 33.6 $Wh \cdot kg^{-1}$ at 1.3 $kW \cdot kg^{-1}$, respectively, indicating the pseudocapacitive enhancement of the NaI/I_2 mediator is more pronounced than the $K_3Fe(CN)_6$/$K_4Fe(CN)_6$ mediator. Furthermore, the introduction of a redox mediator into GPE can also significantly increase the ionic conductivity, especially for the GPE with a conducting salt dissolved in an organic solvent.[205-207,211]

Despite the large pseudocapacitance contributed by the redox reaction of electrochemically active components, these redox active electrolytes also compromise the rate performance and cycling stability of SCs due to their intrinsic poor electrochemical stability. In addition, some electrolyte systems provide high C_s only at the positive electrode but low C_s at the negative electrode, which cannot be fully exploited for SCs. On the other hand, some aqueous redox electrolyte systems only provide high electrochemical activity in acidic solution, seriously preventing the commercialization due to the high cost of corrosion-resistant current collector and equipments. Therefore, numerous research efforts still need to be focused on scalable synthesis of redox electrolytes with good stability, high electrochemical performance as well as low cost.

1.5 Description of thesis and objectives

In the above text, different varieties of electrode materials were introduced. The aim of this thesis is to investigate the charge storage mechanism in SCs with redox-active electrolyte. The properties of the carbon-based material have strong correlations with the electrolyte used. Therefore, the carbon-based material, specifically the widely used activated carbon, rather than psudocapacitive materials such as conducting polymers and electroactive metal oxides, was chosen as the SC electrode material in this study.

Redox-active ionic liquids as electrolytes for supercapacitors provide a higher capacitance and energy density than organic or ionic liquid electrolytes. Fundamental studies of the charge storage mechanism in supercapacitors are of critical importance for the development and applications of devices. Solid-state NMR (SS-NMR) methodology that has the ability to provide atomic information on the local environments within electrodes has been recently developed to study the mechanism of charge storage in supercapacitors at the molecular level. The charge storage in supercapacitors with organic or ionic liquid electrolytes has been studied by SS-NMR. The charge storage in supercapacitors with redox-active species involving faradaic processes is different from those of electrochemical double-layer capacitors using organic solvents or ionic liquids as electrolytes. However, there is until now no research on charge storage mechanism in supercapacitors with redox-active electrolyte published. Therefore, the investigations of the charge storage mechanism in supercapacitors with redox ionic liquid electrolytes are highly required.

In this thesis, SS-NMR techniques combined with electrochemical dilatometry were used to investigate in depth the charge storage in supercapacitors comprising redox-active ionic liquid electrolytes. First, I will study the influence of the electrolyte concentration on the soaked electrode in the absence of an applied voltage. Then, I will investigate the charge storage mechanism and the faradaic contribution from the redox-active species for the supercapacitors with redox-active ionic liquid electrolyte. The charging process in the supercapacitor with redox-active ionic liquid electrolyte was also investigated by electrochemical dilatometry on the macroscopic scale. As a result, a full picture of the charge storage of supercapacitors with a redox-active ionic liquid electrolyte emerges, which will be helpful to better understand the charge storage of supercapacitors.

References

(1) P. Simon, Y. Gogotsi, Nat. Mater. 2008, 7, 845.

(2) R. Kötz, S. Müller, M. Bärtschi, B. Schnyder, P. Dietrich, F. N. Büchi, A. Tsukada, G. G. Scherer, P. Rodatz, O. Garcia, P. Barrade, V. Hermann, R. Gallay, Electrochem. Soc. Proc. 2001, 21, 564.

(3) B. E. Conway, Electrochemical supercapacitors: Scientific fundamentals and technological applications, Kluwer Academic/Plenum, New York, 1999.

(4) H. V. Helmholtz, Ann. Phys. (Leipzig) 1853, 89, 21.

(5) G. Gouy, J. Phys. 1910, 4, 457.

(6) D. L. Chapman, Philos. Mag. 1913, 6, 475.

(7) O. Stern, Z. Electrochem. 1924, 30, 508.

(8) M. S. Wu, P. C. Chiang, Electrochem. Solid-State Lett. 2004, 7, A123.

(9) W. Sugimoto, H. Iwata, Y. Murakami, Y. Takasu, J. Electrochem. Soc. 2004, 151, A1181.

(10) X. Dong, W. Shen, J. Gu, L. Xiong, Y. Zhu, H. Li, J. Shi, J. Phys. Chem. B 2006, 110, 6015.

(11) L. Z. Fan, Y. S. Hu, J. Maier, P. Adelhelm, B. Smarsly, M. Antonietti, Adv. Funct. Mater. 2007, 17, 3083.

(12) M. Seredych, D. Hulicova-Jurcakova, G. Q. Lu, T. J. Bandosz, Carbon 2008, 46, 1475.

(13) G. Lota and E. Frackowiak, Electrochem. Commun. 2009, 11, 87.

(14) S. Roldán, M. Granda, R. Menéndez, R. Santamaría, C. Blanco, J. Phys. Chem. C 2011, 115, 17606.

(15) L. B. Chen, H. Bai, Z. F. Huang, L. Li, Energy Environ. Sci. 2014, 7, 1750.

(16) L. L. Zhang, X. S. Zhao, Chem. Soc. Rev. 2009, 38, 2520.

(17) M. Ue, K. Ida, S. Mori, J. Electrochem. Soc. 1994, 141, 2989.

(18) A. Burke, J. Power Sources 2000, 91, 37.

(19) A. Davies, A. Yu, Can. J. Chem. Eng. 2011, 89, 1342.

(20) M. Lu, F. Beguin, E. Frackowiak, Supercapacitors: Materials, Systems and Applications, John Wiley & Sons, 2013.

(21) C. Largeot, C. Portet, J. Chmiola, P. L. Taberna, Y. Gogotsi, P. Simon, J. Am. Chem. Soc. 2008, 130, 2730.

(22) E. Raymundo-Pinero, F. Leroux, F. Beguin, Adv. Mater. 2006, 18, 1877.

(23) Y. J. Kim, C.-M. Yang, K. C. Park, K. Kaneko, Y. A. Kim, M. Noguchi, T. Fujino, S. Oyama, M. Endo, ChemSusChem 2012, 5, 535.

(24) E. Raymundo-Pinero, K. Kierzek, J. Machnikowski, F. Beguin, Carbon 2006, 44, 2498.

(25) J. Chmiola, G. Yushin, Y. Gogotsi, C. Portet, P. Simon, P. L. Taberna, Science 2006, 313, 1760.

(26) J. Huang, B. G. Sumpter, V. Meunier, Angew. Chem. Int. Ed. 2008, 47, 520.

(27) J. Segalini, E. Iwama, P. L. Taberna, Y. Gogotsi, P. Simon, Electrochem. Commun. 2012, 15, 63.

(28) D. Qu, H. Shi, J. Power Sources 1998, 74, 99.

(29) M. Endo, T. Maeda, T. Takeda, Y. J. Kim, K. Koshiba, H. Hara and M. S. Dresselhaus, J. Electrochem. Soc. 2001, 148, A910.

(30) K. H. An, W. S. Kim, Y. S. Park, Y. C. Choi, S. M. Lee, D. C. Chung, D. J. Bae, S. C. Lim, Y. H. Lee, Adv. Mater. 2001, 13, 497.

(31) O. Barbieri, M. Hahn, A. Herzog, R. Kötz, Carbon 2005, 43, 1303.

(32) K. Kierzek, E. Frackowiak, G. Lota, G. Gryglewicz, J. Machnikowski, Electrochim. Acta 2004, 49, 515.

(33) G. Salitra, A. Soffer, L. Eliad, Y. Cohen, D. Aurbach, J. Electrochem. Soc. 2000, 147, 2486.

(34) L. L. Zhang, R. Zhou, X. S. Zhao, J. Mater. Chem. 2010, 20 (29), 5983.

(35) Y. Zhai, Y. Dou, D. Zhao, P. F. Fulvio, R. T. Mayes, S. Dai, Adv. Mater. 2011, 23, 4828.

(36) S. Kondrat, C. R. Perez, V. Presser, Y. Gogotsi, A. A. Kornyshev, Energy Environ. Sci. 2012, 5, 6474.

(37) X. He, R. Li, J. Qiu, K. Xie, P. Ling, M. Yu, X. Zhang, M. Zheng, Carbon 2012, 50, 4911.

(38) C.-W. Huang, C.-T. Hsieh, P.-L. Kuo, H. Teng, J. Mater. Chem. 2012, 22, 7314.

(39) D. Lozano-Castello, D. Cazorla-Amoros, A. Linares-Solano, S. Shiraishi, H. Kurihara, A. Oya, Carbon 2003, 41, 1765.

(40) X. J. He, Y. J. Geng, J. S. Qiu, M. D. Zheng, S. A. Long, X. Y. Zhang, Carbon 2010, 48, 1662.

(41) F. C. Wu, R. L. Tseng, C. C. Hu, C. C. Wang, J. Power Sources 2005, 144, 302.

(42) J. Mi, X.-R. Wang, R.-J. Fan, W.-H. Qu, W.-C. Li, Energy Fuels 2012, 26, 5321.

(43) W.-S. Choi, W.-G. Shim, D.-W. Ryu, M.-J. Hwang, H. Moon, Microporous Mesoporous Mater. 2012, 155, 274.

(44) M. P. Bichat, E. Raymundo-Pinero, F. Beguin, Carbon 2010, 48, 4351.

(45) E. Raymundo-Pinero, M. Cadek, F. Beguin, Adv. Funct. Mater. 2009, 19, 1032.

(46) G. Dobele, T. Dizhbite, M. V. Gil, A. Volperts, T. A. Centeno, Biomass Bioenergy 2012, 46, 145.

(47) M. S. Balathanigaimani, W. G. Shim, M. J. Lee, C. Kim, J. W. Lee, H. Moon, Electrochem. Commun. 2008, 10, 868.

(48) L. Wei, M. Sevill, A. B. Fuertes, R. Mokaya, G. Yushin, Adv. Energy Mater. 2011, 1, 356.

(49) L. Wei, G. Yushin, Carbon 2011, 49, 4830.

(50) Z. J. Zheng, Q. M. Gao, J. Power Sources 2011, 196, 1615.

(51) S.-J. Han, Y.-H. Kim, K.-S. Kim, S.-J. Park, Curr. Appl. Phys. 2012, 12, 1039.

(52) V. Ruiz, A. G. Pandolfo, J. Power Sources 2011, 196, 7816.

(53) J. Yan, T. Wei, W. M. Qiao, Z. J. Fan, L. J. Zhang, T. Y. Li, Q. K. Zhao, Electrochem. Commun. 2010, 12, 1279.

(54) L. Wei, M. Sevilla, A. B. Fuertes, R. Mokaya, G. Yushin, Adv. Funct. Mater. 2012, 22, 827.

(55) E. Taer, M. Deraman, I. A. Talib, A. A. Umar, M. Oyama, R. M. Yunus, Curr. Appl. Phys. 2010, 10, 1071.

(56) J. Wang, M. M. Chen, C. Y. Wang, J. Z. Wang, J. M. Zheng, J. Power Sources 2011, 196, 550.

(57) L. Zhao, L.-Z. Fan, M.-Q. Zhou, H. Guan, S. Qiao, M. Antonietti, M.-M. Titirici, Adv. Mater. 2010, 22, 5202.

(58) Y. Lv, F. Zhang, Y. Dou, Y. Zhai, J. Wang, H. Liu, Y. Xia, B. Tu, D. Zhao, J. Mater. Chem. 2012, 22, 93.

(59) K. Naoi, P. Simon, Interface 2008, 17, 34.

(60) N. Gavrilov, I. A. Pašti, M. Vujković, J. Travas-Sejdic, G. C´irić-Marjanović, S. V. Mentus, Carbon 2012, 50, 3915.

(61) D.-W. Wang, F. Li, L.-C. Yin, X. Lu, Z.-G. Chen, I. R. Gentle, G. Q. Lu, H.-M. Cheng, Chem. Eur. J. 2012, 18, 5345.

(62) M. P. Bichat, E. Raymundo-Pinero, F. Beguin, Carbon 2010, 48, 4351.

(63) A. G. Pandolfo, A. F. Hollenkamp, J. Power Sources 2006, 157, 11.

(64) V. Presser, M. Heon, Y. Gogotsi, Adv. Funct. Mater. 2011, 21, 810.

(65) V. Presser, L. F. Zhang, J. J. Niu, J. McDonough, C. Perez, H. Fong, Y. Gogotsi, Adv. Energy Mater. 2011, 1, 423.

(66) C. R. Pérez, S.-H. Yeon, J. Ségalini, V. Presser, P.-L. Taberna, P. Simon, Y. Gogotsi, Adv. Funct. Mater. 2013, 23, 108.

(67) H. J. Liu, J. Wang, C. X. Wang, Y. Y. Xia, Adv. Energy Mater. 2011, 1, 1101.

(68) M. Heon, S. Lofland, J. Applegate, R. Nolte, E. Cortes, J. D. Hettinger, P.-L. Taberna, P. Simon, P. Huang, M. Brunet, Y. Gogotsi, Energy Environ. Sci. 2011, 4, 135.

(69) M. Rose, Y. Korenblit, E. Kockrick, L. Borchardt, M. Oschatz, S. Kaskel, G. Yushin, Small 2011, 7, 1108.

(70) G. Lota, K. Fic, E. Frackowiak, Energy Environ. Sci. 2011, 4 (5), 1592.

(71) Z. Q. Niu, W. Y. Zhou, J. Chen, G. X. Feng, H. Li, W. J. Ma, J. Z. Li, H. B. Dong, Y. Ren, D. A. Zhao, S. S. Xie, Energy Environ. Sci. 2011, 4, 1440.

(72) K.-H. Choi, J. T. Yoo, C. K. Lee, S.-Y. Lee, Energy Environ. Sci. 2016, 9, 2812.

(73) L. B. Hu, M. Pasta, F. La Mantia, L. F. Cui, S. Jeong, H. D. Deshazer, J. W. Choi, S. M. Han, Y. Cui, Nano Lett. 2010, 10, 708.

(74) A. Izadi-Najafabadi, S. Yasuda, K. Kobashi, T. Yamada, D. N. Futaba, H. Hatori, M. Yumura, S. Iijima, K. Hata, Adv. Mater. 2010, 22, E235.

(75) A. Izadi-Najafabadi, T. Yamada, D. N. Futaba, M. Yudasaka, H. Takagi, H. Hatori, S. Iijima, K. Hata, ACS Nano 2011, 5, 811.

(76) Q. Liao, N. Li, S. Jin, G. Yang, C. Wang, ACS Nano 9, 5, 5310.

(77) S. W. Lee, N. Yabuuchi, B. M. Gallant, S. Chen, B.-S. Kim, P. T. Hammond, Y. Shao-Horn, Nat. Nanotechnol. 2010, 5, 531.

(78) S. W. Lee, B. S. Kim, S. Chen, Y. Shao-Horn, P. T. Hammond, J. Am. Chem. Soc. 2009, 131, 671.

(79) C. S. Du, N. Pan, J. Power Sources 2006, 160, 1487.

(80) J. H. Chen, W. Z. Li, D. Z. Wang, S. X. Yang, J. G. Wen, Z. F. Ren, Carbon 2002, 40, 1193.

(81) C. Emmenegger, P. Mauron, P. Sudan, P. Wenger, V. Hermann, R. Gallay, A. Zuttel, J. Power Sources 2003, 124, 321.

(82) M. M. Shaijumon, F. S. Ou, L. J. Ci, P. M. Ajayan, Chem. Commun. 2008, 2373.

(83) S. Talapatra, S. Kar, S. K. Pal, R. Vajtai, L. Ci, P. Victor, M. M. Shaijumon, S. Kaur, O. Nalamasu, P. M. Ajayan, Nat. Nanotechnol. 2006, 1, 112.

(84) W. Ren, H.M. Cheng, Nat. Nanotechnol. 2014, 9, 726.

(85) L. Dössel, L. Gherghel, X. Feng, K. Müllen, Angew. Chem. Int. Ed. 2011, 50, 2540.

(86) Z. Chen, W. Ren, L. Gao, B. Liu, S. Pei, H.M. Cheng, Nat. Mater. 2011, 10, 424.

(87) K.S. Novoselov, A.K. Geim, S.V. Morozov, D. Jiang, Y. Zhang, S. V. Dubonos, I. V. Grigorieva, A. A. Firsov, Science 2004, 306, 666.

(88) S. Pei, H.M. Cheng, Carbon 2012, 50, 3210.

(89) X. Yang, C. Cheng, Y. Wang, L. Qiu, D. Li, Science 2013, 341, 534.

(90) H. Li, Y. Tao, X. Zheng, J. Luo, F. Kang, H.-M. Cheng, Q.-H. Yang, Energy Environ. Sci. 2016, 9, 3135.

(91) Y. C. Si, E. T. Samulski, Chem. Mater. 2008, 20, 6792.

(92) L. Buglione, A. Bonanni, A. Ambrosi, M. Pumera, ChemPlusChem 2012, 77, 71.

(93) J. Yan, W. Sun, T. Wei, Q. Zhang, Z. Fan, F. Wei, J. Mater. Chem. 2012, 22, 11494.

(94) W. Lv, F. Sun, D.-M. Tang, H.-T. Fang, C. Liu, Q.-H. Yang, H.-M. Cheng, J. Mater. Chem. 2011, 21, 9014.

(95) Q. Qu, S. Yang, X. Feng, Adv. Mater. 2011, 23, 5574.

(96) H. Wang, H. S. Casalongue, Y. Liang, H. Dai, J. Am. Chem. Soc. 2010, 132, 7472.

(97) X. Yang, J. Zhu, L. Qiu, D. Li, Adv. Mater. 2011, 23, 2833.

(98) D. W. Wang, F. Li, J. P. Zhao, W. C. Ren, Z. G. Chen, J. Tan, Z. S. Wu, I. Gentle, G. Q. Lu, H. M. Cheng, ACS Nano 2009, 3, 1745.

(99) J. Yan, T. Wei, B. Shao, Z. J. Fan, W. Z. Qian, M. L. Zhang, F. Wei, Carbon 2010, 48, 487.

(100) Z. Lei, N. Christov, X. S. Zhao, Energy Environ. Sci. 2011, 4, 1866.

(101) Z. Fan, J. Yan, L. Zhi, Q. Zhang, T. Wei, J. Feng, M. Zhang, W. Qian, F. Wei, Adv. Mater. 2010, 22, 3723.

(102) M.-Q. Zhao, Q. Zhang, J.-Q. Huang, G.-L. Tian, T.-C. Chen, W.-Z. Qian, F. Wei, Carbon 2013, 54, 403.

(103) B. G. Choi, M. Yang, W. H. Hong, J. W. Choi, Y. S. Huh, ACS Nano 2012, 6, 4020.

(104) C. G. Liu, Z. N. Yu, D. Neff, A. Zhamu, B. Z. Jang, Nano Lett. 2010, 10, 4863.

(105) Z. Wen, X. Wang, S. Mao, Z. Bo, H. Kim, S. Cui, G. Lu, X. Feng, J. Chen, Adv. Mater. 2012, 24, 5610.

(106) L. L. Zhang, X. Zhao, M. D. Stoller, Y. Zhu, H. Ji, S. Murali, Y. Wu, S. Perales, B. Clevenger, R. S. Ruoff, Nano Lett. 2012, 12, 1806.

(107) Y. Zhu, S. Murali, M. D. Stoller, K. J. Ganesh, W. Cai, P. J. Ferreira, A. Pirkle, R. M. Wallace, K. A. Cychosz, M. Thommes, D. Su, E. A. Stach, R. S. Ruoff, Science 2011, 332, 1537.

(108) G. Wang, L. Zhang, J. Zhang, Chem. Soc. Rev. 2012, 41, 797.

(109) I. H. Kim, K. B. Kim, J. Electrochem. Soc. 2006, 153, A383.

(110) Q. X. Jia, S. G. Song, X. D. Wu, J. H. Cho, S. R. Foltyn, A. T. Findikoglu and J. L. Smith, Appl. Phys. Lett. 1996, 68, 1069.

(111) J. P. Zheng, P. J. Cygan, T. R. Jow, J. Electrochem. Soc. 1995, 142, 2699.

(112) N. Wu, S. Kuo, M. Lee, J. Power Sources 2002, 104, 62.

(113) S. Ferro, A. De Battisti, J. Phys. Chem. B, 2002, 106, 2249.

(114) C.-C. Hu, K.-H. Chang, M.-C. Lin, Y.-T. Wu, Nano Lett. 2006, 6, 2690.

(115) W. Sugimoto, S. Makino, R. Mukai, Y. Tatsumi, K. Fukuda, Y. Takasu, Y. Yamauchi, J. Power Sources 2012, 204, 244.

(116) V. D. Patake, S. M. Pawar, V. R. Shinde, T. P. Gujar, C. D. Lokhande, Curr. Appl. Phys. 2010, 10, 99.

(117) J. W. Long, K. E. Swider, C. I. Merzbacher, D. R. Rolison, Langmuir 1999, 15, 780.

(118) Z. Chen, V. Augustyn, J. Wen, Y. W. Zhang, M. Q. Shen, B. Dunn, Y. F. Lu, Adv. Mater. 2011, 23, 791.

(119) J. Yan, T. Wei, W. Qiao, B. Shao, Q. Zhao, L. Zhang, Z. Fan, Electrochim. Acta 2010, 55, 6973.

(120) B. Wang, J. S. Chen, Z. Wang, S. Madhavi, X. W. Lou, Adv. Energy Mater. 2012, 2, 1188.

(121) J. Yan, Z. J. Fan, T. Wei, Z. W. Qie, S. S. Wang, M. L. Zhang, Mater. Sci. Eng. B 2008, 151, 174.

(122) M. Toupin, T. Brousse, D. Bélanger, Chem. Mater. 2004, 16, 3184.

(123) O. Ghodbane, J.-L. Pascal, F. Favier, ACS Appl. Mater. Interfaces 2009, 1, 1130.

(124) B. G. Choi, M. Yang, W. H. Hong, J. W. Choi, Y. S. Huh, ACS Nano 2012, 6, 4020.

(125) G. Yu, L. Hu, N. Liu, H. Wang, M. Vosgueritchian, Y. Yang, Y. Cui, Z. Bao, Nano Lett. 2011, 11, 4438.

(126) X. Lang, A. Hirata, T. Fujita, M. Chen, Nat. Nanotechnol. 2011, 6, 232.

(127) J. P. Liu, J. Jiang, C. W. Cheng, H. X. Li, J. X. Zhang, H. Gong, H. J. Fan, Adv. Mater. 2011, 23, 2076.

(128) Y Shi, L Peng, Y Ding, Y Zhao, G Yu, Chem. Soc. Rev. 2015, 44, 6684.

(129) H. Jiang, J. Ma, C. Li, J. Mater. Chem. 2012, 22, 16939.

(130) M. Xue, F. Li, J. Zhu, H. Song, M. Zhang, T. Cao, Adv. Funct. Mater. 2012, 22, 1284.

(131) C. Zhong, Y. Deng, W. Hu, J. Qiao, L. Zhang, J. Zhang, Chem. Soc. Rev. 2015,44, 7484.

(132) M. Galinski, A. Lewandowski, I. Stepniak, Electrochim. Acta 2006, 51, 5567–5580.

(133) K. Fic, G. Lota, M. Meller, E. Frackowiak, Energy Environ. Sci. 2012, 5, 5842–5850.

(134) A. Yu, V. Chabot, J. Zhang, Electrochemical Supercapacitors for Energy Storage and Delivery: Fundamentals and Applications, CRC Press, 2013.

(135) J. K. McDonough, A. I. Frolov, V. Presser, J. Niu, C. H. Miller, T. Ubieto, M. V. Fedorov, Y. Gogotsi, Carbon 2012, 50, 3298.

(136) C. M. Yang, Y. J. Kim, M. Endo, H. Kanoh, M. Yudasaka, S. Iijima, K. Kaneko, J. Am. Chem. Soc. 2007, 129, 20.

(137) D. E. Jiang, J. Z. Wu, J. Phys. Chem. Lett. 2013, 4, 1260–1267.

(138) A. Takana, T. Iiyama, T. Ohba, S. Ozeki, K. Urita, T. Fujimori, H. Kanoh, K. Kaneko, J. Am. Chem. Soc. 2010, 132, 2112.

(139) D. E. Jiang, Z. Jin, D. Henderson, J. Wu, J. Phys. Chem. Lett. 2012, 3, 1727.

(140) L. Yang, B. H. Fishbine, A. Migliori, L. R. Pratt, J. Am. Chem. Soc. 2009, 131, 12373.

(141) F. Blanc, M. Leskes, C. P. Grey, Acc. Chem. Res. 2013, 46, 1952.

(142) H. Wang, T.K. J. Koster, N. M. Trease, J. Segalini, P. L. Taberna, P. Simon, Y. Gogotsi, C. P. Grey, J. Am. Chem. Soc. 2011, 133, 19270.

(143) M. Deschamps, E. Gilbert, P. Azais, E. Raymundo-Pinero, M. R. Ammar, P. Simon, D. Massiot, F. Béguin, Nat. Mater. 2013, 12, 351.

(144) H. Wang, A. C. Forse, J. M. Griffin, N.M. Trease, L. Trognko, P. L. Taberna, P. Simon, C. P. Grey, J. Am. Chem. Soc. 2013, 135, 18968.

(145) M. D. Levi, G. Salitra, N. Levy, D. Aurbach, J. Maier, Nat. Mater. 2009, 8, 872.

(146) S. Boukhalfa, D. Gordon, L. L. He, Y. B. Melnichenko, N. Nitta, A. Magasinski, G. Yushin, ACS Nano 2014, 8, 2495.

(147) F. W. Richey, B. Dyatkin, Y. Gogotsi, Y. A. Elabd, J. Am. Chem. Soc. 2013, 135, 12818.

(148) A. C. Forse, J. M. Griffin, H. Wang, N. M. Trease, V. Presser, Y. Gogotsi, P. Simon, C. P. Grey, Phys. Chem. Chem. Phys. 2013, 15, 7722.

(149) A. C. Forse, C. Merlet, J. M. Griffin, C. P. Grey, J. Am. Chem. Soc. 2016, 138, 5731.

(150) L. Q. Fan, J. Zhong, J. H. Wu, J. M. Lin, Y. F. Huang, J. Mater. Chem. A 2014, 2, 9011.

(151) P. Kurzweil, M. Chwistek, J. Power Sources 2008, 176, 555.

(152) K. Naoi, S. Ishimoto, J. I. Miyamoto, W. Naoi, Energy Environ. Sci. 2012, 5, 9363.

(153) Y. A. Shuichi Ishimoto, M. Shinya, K. Naoia, J. Electrochem. Soc. 2009, 156, A563.

(154) L. J. Hardwick, M. Hahn, P. Ruch, M. Holzapfel, W. Scheifele, H. Buqa, F. Krumeich, P. Novák, R. Kötz, Electrochim. Acta 2006, 52, 675.

(155) B. W. Ricketts, C. Ton-That, J. Power Sources 2000, 89, 64.

(156) Q. Zhang, J. Rong, D. Ma, B. Wei, Energy Environ. Sci. 2011, 4, 2152.

(157) A. Laheaar, H. Kurig, A. Janes, E. Lust, Electrochim. Acta 2009, 54, 4587.

(158) Q. Li, X. X. Zuo, J. S. Liu, X. Xiao, D. Shu, J. M. Nan, Electrochim. Acta 2011, 58, 330.

(159) R. Vali, A. Laheaar, A. Janes, E. Lust, Electrochim. Acta 2014, 121, 294.

(160) R. Chandrasekaran, M. Koh, A. Yamauchi, M. Ishikawa, J. Power Sources 2010, 195, 662.

(161) R. D. Rogers, G. A. Voth, Acc. Chem. Res. 2007, 40, 1077.

(162) M. Armand, F. Endres, D. R. MacFarlane, H. Ohno, B. Scrosati, Nat. Mater. 2009, 8, 621.

(163) P. Wasserscheid, T. Welton, Ionic liquids in synthesis, Wiley-VCH Verlag GmbH & Co. KGaA, 2002.

(164) A. Lewandowski, M. Galinski, J. Power Sources 2007,173, 822.

(165) J. G. Huddleston, A. E. Visser, W.M. Reichert, H. D. Willauer, G. A. Broker, R. D. Rogers, Green Chem. 2001, 3, 156.

(166) Y. Chen, X. Zhang, D. Zhang, P. Yu, Y. Ma, Carbon, 2011, 49, 573–580. C. Merlet, B. Rotenberg, P. A. Madden, P. L. Taberna, P. Simon, Y. Gogotsi, M. Salanne, Nat. Mater. 2012, 11, 306.

(167) G. Feng, J. Huang, B. G. Sumpter, V. Meunier, R. Qiao, Phys. Chem. Chem. Phys. 2011, 13, 14723.

(168) M. V. Fedorov, A. A. Kornyshev, Chem. Rev. 2014, 114, 2978.

(169) M. Kunze, E. Paillard, S. Jeong, G. B. Appetecchi, M. Schönhoff, M. Winter, S. Passerini, J. Phys. Chem. C 2011, 115, 19431.

(170) M. Kunze, S. Jeong, E. Paillard, M. Schönhoff, M. Winter, S. Passerini, Adv. Energy Mater. 2011, 1, 274.

(171) M. Shi, S. Kou, X. Yan, ChemSusChem 2014, 7, 3053.

(172) M. P. S. Mousavi, B. E. Wilson, S. Kashefolgheta, E. L. Anderson, S. He, P. Bühlmann, A., Stein ACS Appl. Mater. Interfaces 2016, 8, 3396.

(173) L. G. Bettini, M. Galluzzi, A. Podesta, P. Milani, P. Piseri, Carbon 2013, 59, 212.

(174) M. Lazzari, F. Soavi and M. Mastragostino, J. Power Sources 2008, 178, 490.

(175) H. Kurig, M. Vestli, K. Tõnurist, A. Jänes, E. Lust, J. Electrochem. Soc. 2012, 159, A944.

(176) T. Sato, G. Masuda, K. Takagi, Electrochim. Acta 2004, 49, 3603–3611.

(177) Y.-J. Kim, Y. Matsuzawa, S. Ozaki, K. C. Park, C. Kim, M. Endo, H. Yoshida, G. Masuda, T. Sato, M. S. Dresselhaus, J. Electrochem. Soc. 2005, 152, A710.

(178) M. Anouti, L. Timperman, M. El Hilali, A. Boisset, H. Galiano, J. Phys. Chem. C 2012, 116, 9412.

(179) S. Pohlmann, T. Olyschlager, P. Goodrich, J. Alvarez Vicente, J. Jacquemin, A. Balducci, J. Power Sources 2015,273, 931.

(180) C. Wolff, S. Jeong, E. Paillard, A. Balducci, S. Passerini J. Power Sources 2015, 293, 65.

(181) K. R. Seddon, A. Stark, M. J. Torres, Pure Appl. Chem. 2000, 72, 2275.

(182) G. H. Lane, Electrochim. Acta 2012, 83, 513.

(183) T. Tooming, T. Thomberg, L. Siinor, K. Tonurist, A. Janes, E. Lust, J. Electrochem. Soc. 2014, 161, A222.

(184) W. Y. Tsai, R. Lin, S. Murali, L. Li Zhang, J. K. McDonough, R. S. Ruoff, P. L. Taberna, Y. Gogotsi, P. Simon, Nano Energy 2013, 2, 403.

(185) R. Y. Lin, P. L. Taberna, S. Fantini, V. Presser, C. R. Perez, F. Malbosc, N. L. Rupesinghe, K. B. K. Teo, Y. Gogotsi, P. Simon, J. Phys. Chem. Lett. 2011, 2, 2396.

(186) S. Li, G. Feng, P. F. Fulvio, P. C. Hillesheim, C. Liao, S. Dai, P. T. Cummings, J. Phys. Chem. Lett. 2012, 3, 2465.

(187) L. Zhang, Z. H. Liu, H. Lv, X. Tang, K. Ooi, J. Phys. Chem. C 2007, 111, 8418.

(188) A. B. McEwen, S. F. McDevitt, V. R. Koch, J. Electrochem. Soc. 1997, 144, L84.

(189) A. Orita, K. Kamijima, M. Yoshida, J. Power Sources 2010, 195, 7471.

(190) R. Lin, P. Huang, J. Segalini, C. Largeot, P. L. Taberna, J. Chmiola, Y. Gogotsi, P. Simon, Electrochim. Acta 2009, 54, 7025.

(191) F. J. Liu, J. Power Sources 2008, 182, 383.

(192) T. Shinomiya, V. Gupta, N. Miura, Electrochim. Acta 2006, 51, 4412.

(193) S. Roldán, C. Blanco, M. Granda, R. Menéndez, R. Santamaría, Angew. Chem. Int. Ed. 2011, 50, 1699.

(194) E. Frackowiak, K. Fic, M. Meller, G. Lota, ChemSusChem 2012, 5, 1181.

(195) M. S. Wu, Y. A. Huang, C. H. Yang, J. J. Jow, Int. J. Hydrogen Energy 2007, 32, 4153.

(196) K. W. Nam, E. S. Lee, J. H. Kim, Y. H. Lee, K. B. Kim, J. Electrochem. Soc. 2005, 152, A2129.

(197) L. Cao, M. Lin, H. L. Li, J. Electrochem. Soc. 2005, 152, A806.

(198) X. Zhang, W. Shi, J. Zhu, W. Zhao, J. Ma, S. Mhaisalkar, T. L. Maria, Y. Yang, H. Zhang, H. H. Hng, Q. Yan, Nano Res. 2010, 3, 643.

(199) Y. Su, F. Wu, L. Bao, Z. Yang, New Carbon Mater. 2007, 22, 53.

(200) B. Gélinas, J. C. Forgie, D. Rochefort, J. Electrochem. Soc. 2014, 161, 161.

(201) B. Gélinas, D. Rochefort, Electrochim. Acta 2015, 162, 36.

(202) J. Han, B. Gélinas, D. Rochefort, Electrochem. Commun. 2016, 66, 42.

(203) E. Mourad, L. Coustan, S. A. Freunberger, A. Mehdi, A. Vioux, F. Favier, O. Fontaine Electrochim. Acta 2016, 206, 513.

(204) E. Mourad, L. Coustan, P. Lannelongue, D. Zigah, A. Mehdi, A. Vioux, S. A. Freunberger, F. Favier, O. Fontaine Nat. Mater. 2017, 16, 446.

(205) J. Zhou, Y. Yin, A. N. Mansour, X. Zhou, Electrochem. Solid-State Lett. 2011, 14, A25.

(206) Y. Yin, J. Zhou, A. N. Mansour, X. Zhou, J. Power Sources 2011, 196, 5997.

(207) G. Ma, J. Li, K. Sun, H. Peng, J. Mu, Z. Lei, J. Power Sources 2014, 256, 281.

(208) S. T. Senthilkumar, R. K. Selvan, J. S. Melo, C. Sanjeeviraja, ACS Appl. Mater. Interfaces 2013, 5, 10541.

(209) S. T. Senthilkumar, R. K. Selvan, N. Ponpandian, J. S. Melo, RSC Adv. 2012, 2, 8937.

(210) G. F. Ma, E. K. Feng, K. J. Sun, H. Peng, J. J. Li, Z. Q. Lei, Electrochim. Acta 2014, 135, 461.

(211) F. D. Yu, M. L. Huang, J. H. Wu, Z. Y. Qiu, L. Q. Fan, J. M. Lin, Y. B. Lin, J. Appl. Polym. Sci. 2014, 131, 39784.

(212) A. N. Mansour, J. J. Zhou, X. Y. Zhou, J. Power Sources 2014, 245, 270.

(213) J. Zhou, J. Cai, S. Cai, X. Zhou, A. N. Mansour, J. Power Sources 2011, 196, 10479.

(214) S. Murali, N. Quarles, L. Zhang, J. R. Potts, Z. Tan, Y. Lu, Y. Zhu, R. S. Ruoff, Nano Energy 2013, 2, 764.

(215) P. Simon, Y. Gogotsi, Acc. Chem. Res. 46, 5, 1094.

Chapter 2 Materials and methods

2.1 Materials

2.1.1 Synthesis and characterization of the redox-active ionic liquids

The reagents used were ferrocene, chlorosulfonic acid, phosphorus trichloride, anhydrous sodium carbonate and 1-ethyl-3-methylimidazolium bromide which were purchased from Sigma-Aldrich. Trifluoromethanesulfonamide was purchased from Synquest Laboratories. These were used without further purification. The water used in the procedures was purified with a Milli-Q system to a resistivity of 18.2 MΩ·cm (25 °C).

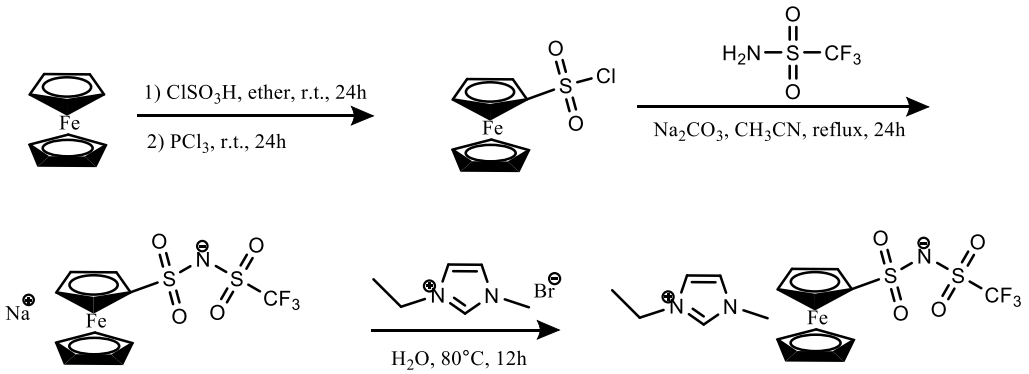

Figure 2-1. Synthesis of EMIm FcNTf.

Preparation of ferrocenesulfonyl chloride: Ferrocenesulfonyl chloride was synthesized according to a literature procedure[1]. Under inert atmosphere, chlorosulfonic acid was dropped slowly into a stirred suspension of ferrocene in anhydrous ether in an ice bath. The solution was stirred for 24 h at room temperature after dropping and produced a dark blue reaction solution. Phosphorus trichloride was then introduced and the reaction mixture was stirred for 24 h at room temperature. The solvent was evaporated under reduced pressure. The residual solid was extracted with boiling petroleum ether (b.p. 60-90 °C) and subsequently

recrystallized in petroleum ether (b.p. 30-60 °C), giving orange-red needle-like crystals with the yield of 56 %. ^{1}H NMR (DMSO-d_6, 300 MHz): δ (ppm) = 4.99 (s, 2H), 4.81 (s, 2H), 4.46 (s, 5H).

Preparation of sodium ferrocenylsulfonyl(trifluoromethylsulfonyl)imide (Na FcNTf): Trifluoromethanesulfonamide was dissolved in acetonitrile and anhydrous sodium carbonate was added. The solution was stirred for 10 minutes at room temperature. Ferrocenesulfonyl chloride was then added slowly and the resulting solution was stirred and heated at reflux temperature (90 °C) for 24 hours. The obtained brown solution was filtered before the precipitate was washed with acetonitrile. The solvent of the solution was removed under reduced pressure and produced a brown product. A mixture of THF/hexane was used for recrystallization, obtaining a light brown powder. Yield: 67 %. ^{1}H NMR (DMSO-d_6, 300 MHz): δ (ppm) = 4.53 (t, 2H), 4.28 (s, 7H).

Preparation of 1-ethyl-3-methylimidazolium ferrocenylsulfonyl (trifluoromethylsulfonyl) imide (EMIm FcNTf): Na FcNTf was dissolved in a minimal volume of water. A solution of 1-ethyl-3-methylimidazolium bromide in a minimum of water was then added slowly drop by drop. The combined solution was heated to 80 °C over 12 hours. After reaction, the excess water was carefully removed and the ionic liquid was dissolved in dichloromethane. The brown solution was washed with water three times. The organic phase was dried with magnesium sulfate, then filtered and dried under reduced pressure. Yield: 82 %.

The synthesized redox-active IL EMIm FcNTf was characterized by ^{1}H, ^{13}C and ^{19}F NMR spectroscopy on Bruker Avance 400 MHz and 300 MHz spectrometers, electrospray ionization mass spectrometry and elemental analysis. Mass spectra were recorded on a Waters 3100 mass spectrometer and elemental analysis was performed with a Fisons Instruments EA 1108 elemental analyser. The thermal properties of the synthesized redox-actie IL EMIm FcNTf were characterized by the differential scanning calorimetry (DSC) and thermal gravimetric analysis (TGA). DSC was carried out using a TA Instruments TA Q1000 under a nitrogen atmosphere. The scans were recorded between -80 to 80 °C for 2 cycles with a ramp of 1 °C per minute and with isothermal of 20 minutes between the cooling and heating. TGA

was conducted with a TA Instruments TGA 2950 under a nitrogen atmosphere, scanning from 30 to 600 °C at a heating rate of 10 °C min^{-1}.

2.1.2 Preparation of the carbon electrodes

Carbon electrodes were fabricated from a slurry consisting of 95 wt % YP-50F activated carbon powder (Kuraray Chemical, Japan) and 5 wt % polytetrafluoroethylene (PTFE) binder (Sigma-Aldrich, 60 wt % dispersion in water) in ethanol according to a literature[6] with slight modification. The slurry was stirred for at least 2 h until a homogeneous consistency was obtained before heating up to 90 °C under stirring. The resulting paste was kneaded thoroughly and rolled to form a free-standing film with a final thickness of approximately 0.2 mm. 6 mm diameter disc-shaped electrodes were then cut and dried under vacuum at 120 °C for at least 24 h. For electrochemical dilatometry experiments, the prepared electrodes were placed on a stainless steel grid (Alfa Aesar, 80 mesh, 0.127 mm) used as a current collector and were pressed for 60 s at a pressure of 2 MPa before assembled into the electrochemical dilatometer cell.

2.2 Electrochemical dilatometry for the study of supercapacitors

2.2.1 Construction of the electrochemical dilatometer

The dilatometer consists of two electrodes separated by a stiff glass frit fixed in position. A thin aluminum membrane is positioned on top of the upper working electrode (WE). The configuration of the dilatometer is illustrated in Figure 2-2. The metal membrane has a manifold function. It serves as the current collector as well as the electrolyte sealing, and it transmits any height change of the WE via the moveable plunger to the displacement transducer. This working principle allows determining the height change of the working electrode without any interference from that of the counter electrode (CE). A high-resolution displacement transducer detects dimensional changes of the WE down to 100 nanometers during one experiment lasting between a few minutes to many days.

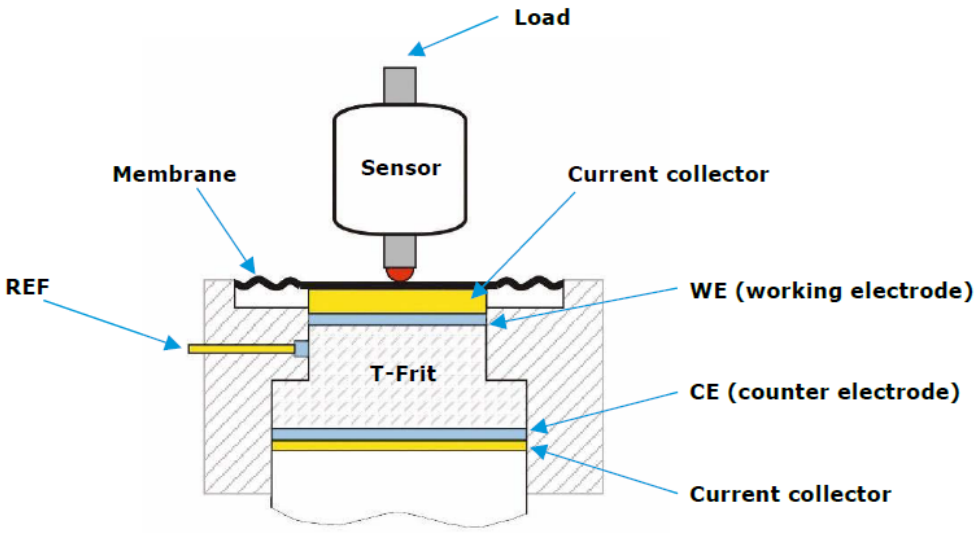

Figure 2-2. Dilatometer in the full cell configuration.

2.2.2 Electrochemical dilatometry measurement

An ECD-3 electrochemical dilatometer from EL-Cell (Germany) was used to measure the charge-induced dimensional change of electrodes. The cell with 50 wt % [EMIm][FcNTf] in ACN as the electrolyte and a fixed stiff glass frit as the separator was assembled in an argon glovebox. Galvanostatic charge-discharge experiments at current density of 0.025 $mA \cdot mg^{-1}$ between 0 and 2 V were carried out using a VMP3 potentiostat from BioLogic and displacement signals from the electrochemical dilatometer were simultaneously recorded with EC-Link Software. The relative height change is normalized by the electrode thickness which is measured prior to the experiment. For example, the displacement of the positive electrode at 2 V is 0.545 µm and the thickness of the electrode is 122 µm. As a result, the percentage of the height change is 0.44 % at this voltage as seen in the dilatometry data plot.

2.3 Solid-state NMR spectroscopy for the study of supercapacitors

2.3.1 Magic-angle spinning (MAS)

Nuclear spins are subject to a variety of magnetic interactions with the local electron distribution and other nearby nuclear spins. In general, nuclear spin interactions are anisotropic with respect to the applied magnetic field direction, and for complex and disordered materials such as SC electrodes, this leads to a broadening of the resonances in the NMR spectrum, and a loss of resolution. To mitigate this problem, magic-angle spinning (MAS) can be employed, whereby the sample is rapidly spun around an axis at the "magic" angle of 54.736° to the applied magnetic field.[2] Provided that the rotation is sufficiently rapid, the resulting modulation of the NMR signal enables removal of the anisotropic interactions such as the chemical shift anisotropy, dipolar coupling and isotropic magnetic susceptibility effects. For spin I= 1/2 nuclei, MAS commonly results in the observation of "isotropic" spectra, containing sharp resonances at the isotropic chemical shift, surrounded by spinning sidebands which are equally spaced at integer multiples of the rotation frequency from the isotropic resonance. In many cases, it is desirable to perform NMR experiments at a MAS rate that is larger than the magnitude of the anisotropic interaction so that the signal intensity is "focused" into a single isotropic resonance, thereby maximising sensitivity. However, in practice MAS experiments on SC electrodes are performed at relatively low MAS rates (a few kHz) in order to minimise leakage of the liquid electrolyte from the sample due to centrifugal forces, and consequent damage to the NMR equipment. For NMR studies of SC electrolyte species, the mobility of the electrolyte species is often sufficient to partially average the anisotropic interactions that are present, and a good resolution can be obtained in the absence of MAS (i.e., in "static" NMR measurements). However, for electrolytes with reduced mobility (e.g., ionic liquids which have higher viscosities), the molecular motion at ambient temperatures is not sufficient to yield well-resolved spectra and MAS is usually necessary in order to obtain detailed information.

2.3.2 ^{19}F nucleus NMR study

^{19}F is a highly sensitive nucleus with a 100 % natural abundance making it highly favourable for NMR studies of SCs. ^{19}F has a large chemical shift range (～200 ppm) meaning that different chemical species are well resolved and easily distinguished. Furthermore, in many electrolyte systems ^{19}F is present in a high molar ratio (e.g., in BF_4^- or CF_3 groups), which also increases the sensitivity. The use of PTFE or PVDF polymer binders in SC electrodes can lead to broad background signals in the NMR spectrum; however, these usually have much shorter relaxation times than the electrolyte species, and the background signals can be effectively removed using spin-echo or common background suppression NMR pulse sequences.[2]

2.3.3 Identifying adsorbed species in microporous carbon

For the study of SCs, NMR spectroscopy has the capability to distinguish electrolyte species adsorbed inside the carbon micropores (referred to as 'in-pore') from those in larger voids and spaces between carbon particles (referred to as 'ex-pore'), as shown in Figure 2-3a and b.[2] In general, the resonance of in-pore species is shifted to low frequency by several ppm as compared to the free species. For example, Figure 2-3c shows the ^{19}F MAS NMR spectrum of a piece of commercial activated carbon (YP-50F) film soaked with 1-methyl-1-propylpyrrolidinium bis(trifluoromethanesulfonyl)imide (Pyr_{13}TFSI) ionic liquid.[3] Two spectral features are clearly visible for the TFSI anions, with the broad feature at −84.9 ppm assigned to in-pore adsorbed anions and the narrow feature at −78.3 ppm assigned to ex-pore nonadsorbed anions. The origin of the NMR frequency shift for in-pore species stems from the "ring current" effect that is due to the presence of delocalized electrons in the sp^2-hybridized carbon surface.[4] An application of the external magnetic field B_0 induces electron circulation within the delocalised π-orbitals, leading to a secondary local magnetic field above the carbon surface that opposes the main field (as shown in Figure 2-3d). Nuclear species located near the delocalized electron system will accordingly undergo a locally altered magnetic field, giving rise to a resonance frequency shift in the NMR spectrum. Ring current-induced local magnetic fields can be diamagnetic or paramagnetic depending on the electronic structure of the

delocalized electron system. Since microporous carbons essentially consist of six-membered rings with paired electrons, the ring current-induced local magnetic field is generally diamagnetic, namely, species near the carbon surface are shielded and shifted to lower frequency in the NMR spectrum. Therefore, the ring current effect is a very useful tool for the study of adsorbed species in SC electrodes. The adsorbed species within micropores could be resolved from free species in the bulk electrolyte that reside outside of the micropores or between carbon particles. The shift in NMR frequency of the in-pore species nuclei is typically –5 and –10 ppm. In particular, the intensities of in-pore resonances can be used to provide quantitative information on the number of species adsorbed inside the micropores.[2] Moreover, provided that the adsorbed species has no direct chemical interaction with the carbon surface, the ring current effect is nucleus independent, i.e., the chemical shift of any nucleus will be shifted by a fixed value that depends only on its location to the carbon surface. Thus, it is also possible to study separately different species present near the carbon surface (i.e., cations, anions and solvent molecules), which is very challenging by other experimental means.

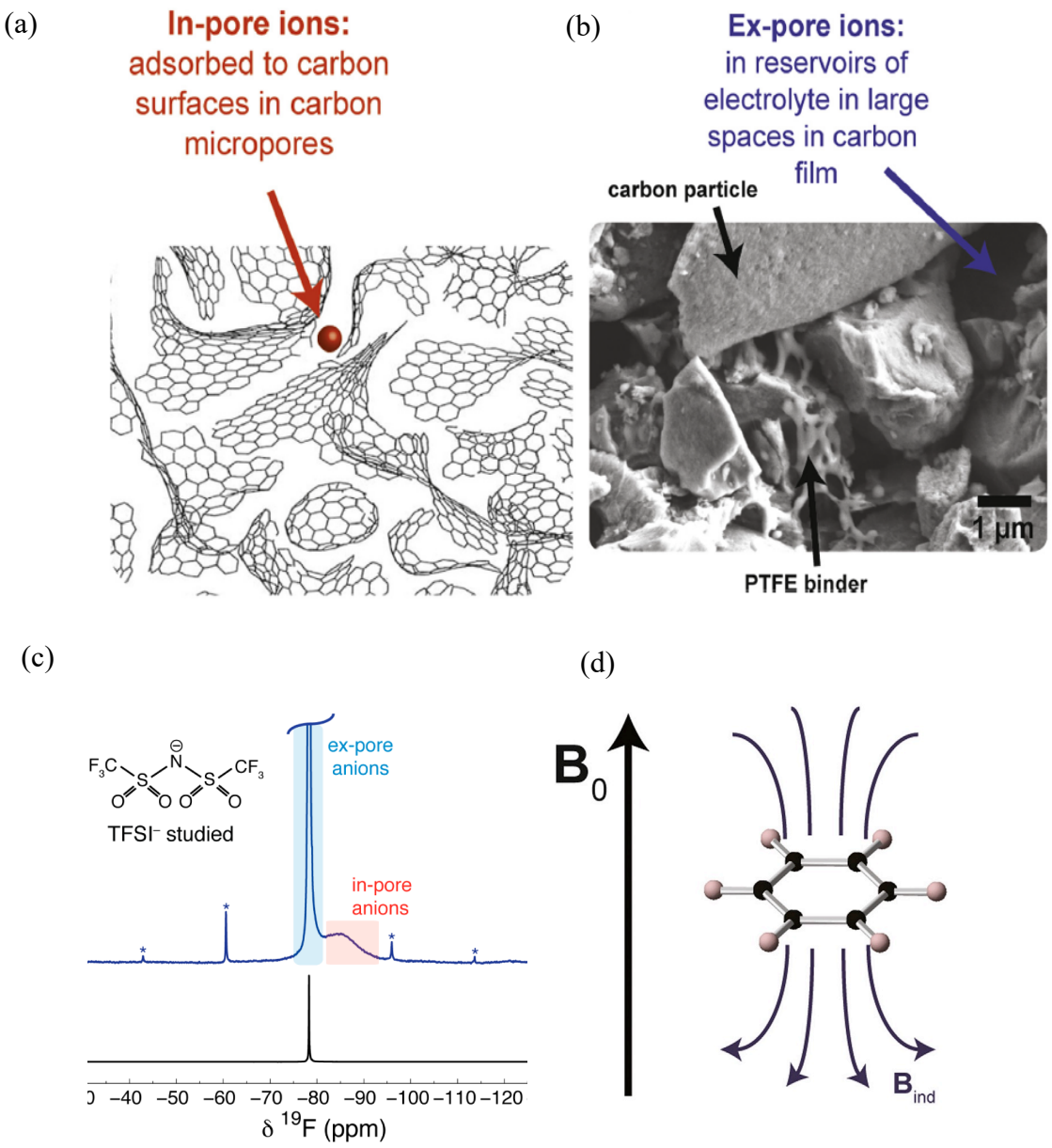

Figure 2-3. (a) A cartoon showing in-pore ions located close to carbon surfaces in carbon micropores. (b) SEM image showing voids and large spaces between carbon particles where ex-pore ions reside. Reprinted from Ref. 2. (c) ^{19}F MAS NMR (7.1 T) spectra of YP-50F carbon film soaked with $Pyr_{13}TFSI$ ionic liquid. Reprinted from Ref. 3. (d) Schematic illustration of the ring current-induced magnetic field, B_{ind}, associated with delocalized π-electrons in a six-membered carbon ring within an applied magnetic field B_0. Reprinted from Ref. 2.

2.3.4 Insight into the supercapacitor charging mechanisms

Since the integrated intensities of the in-pore resonances provide quantitative information on the number of in-pore species in the SC electrodes, NMR measurements on charged SC electrodes can offer a unique insight into the fundamental mechanisms of SCs, such as the changes of the in-pore ion populations for balancing the electronic charge that is developed on the electrode surface. The traditional assumption is that counter-ions are absorbed into the micropores to balance the electronic charge that accumulates on the electrode surface. However, the charge storage process is in fact more complex and a number of different mechanisms are possible.[5] Particularly, the NMR adsorption studies described above clearly show that a significant number of ions are already present inside micropores in uncharged electrodes, indicating that there are a number of possible mechanisms that can lead to the accumulation of ionic charge inside the micropores, as illustrated in Figure 2-4. Specifically, (1) counter-ions can be adsorbed into the carbon micropores, resulting in an overall increase in the in-pore ion population. (referred to as counter-ion adsorption) (2) It is possible that counter-ion adsorption is accompanied with co-ion desorption (referred to ion exchange) and the total population of in-pore ions does not change. (3) A further possible mechanism is that co-ions are desorbed and expelled from the micropores, leaving a surplus of in-pore counter-ions (referred to as co-ion adsorption). In this case, the total in-pore ion population is reduced. In principle, it is possible that combinations of these charging mechanisms take place, or different charging mechanisms occur in different electrodes.

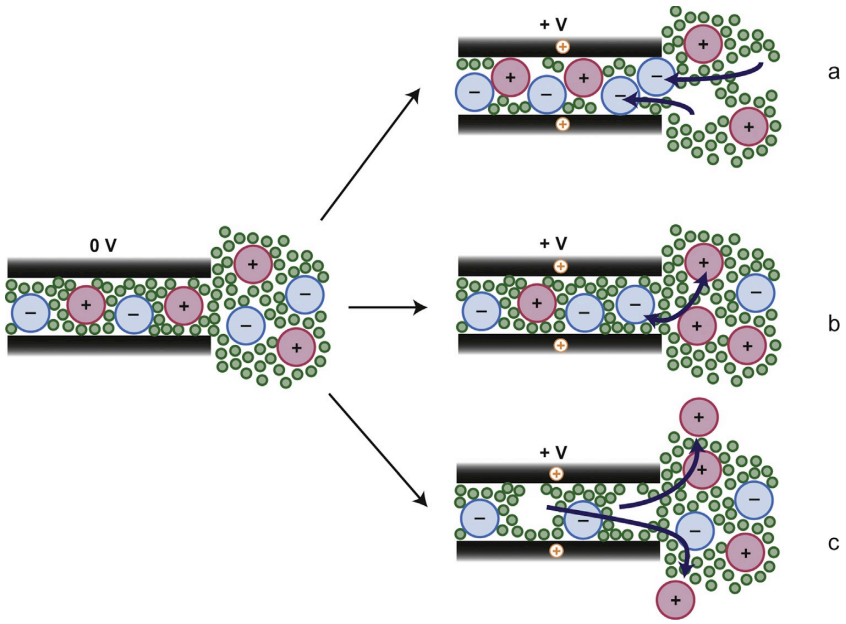

Figure 2-4. Schematic illustrations of possible charge storage mechanisms within a micropore that contains anions and cations prior to charging. If the electrode surface is positively polarized, an equal negative ionic charge can arise through either (a) adsorption of ex-pore anions into the micropores, (b) exchange of ex-pore cations for in-pore anions or (c) the expulsion of cations from the micropores. Reprinted from Ref. 5.

The different possible charging mechanisms can be distinguished through quantitative analysis of the in-pore resonance intensities. An increase in the in-pore resonance intensity during charging indicates that the studied ions are adsorbed into the micropores, whereas a decrease indicates ion expulsion. A constant in-pore resonance intensity during charging means that the population of the in-pore ions remains constant, implying that the population of the other type of ionic species must be changing in order to balance the charge on the electrode surface. By studying both ions simultaneously it is possible to construct a full picture of the charging mechanism and to determine the total ionic charge inside the micropores.

To probe the charging mechanism, NMR experiments must be performed on charged electrodes. One way to do this is by ex situ NMR, where SC test cells are charged to a specified voltage, and then disassembled to obtain the electrode for the studies. The advantage of ex situ NMR is that the electrode can be studied by conventional MAS techniques, which

provide high resolution and enable complex experiments, such as correlation and exchange experiments. The other way is by in situ NMR experiments, whereby a specially designed SC test cell is placed inside the coil of a static NMR probe and connected to an external electrochemical cycler. In situ NMR has the advantage that the SC can be studied directly under a range of charging conditions with no risk of discharge or loss of solvent during cell disassembly. In principle, in situ techniques should provide a more accurate picture since potentially short-lived and/or dynamic states within the electrode can be studied without disturbing them during cell disassembly. However, since in situ NMR experiments are necessarily performed under static conditions, it is not applicable for the study of SCs with ionic liquid systems because of their high viscosity.

References

(1) B. Gélinas, D. Rochefort, Electrochim. Acta 2015, 162, 36.

(2) J. M. Griffin, A. C. Forse, C. P. Grey, Solid State Nucl. Magn. Reson. 2016, 74-75, 16.

(3) A. C. Forse, J. M. Griffin, C. Merlet, P. M. Bayley, H. Wang, P. Simon, C. P. Grey, J. Am. Chem. Soc. 2015, 137, 7231.

(4) P. Lazzeretti, Prog. Nucl. Magn. Reson. Spectrosc. 2000, 36, 1.

(5) J. M. Griffin, A. C. Forse, H. Wang, N. M. Trease, P. L. Taberna, P. Simon, C. P. Grey, Faraday Discuss. 2014, 176, 49.

(6) H. Wang, T. K. Koster, N. M. Trease, J. Segalini, P. L.Taberna, P. Simon, Y.Gogotsi, C. P. Grey, J. Am. Chem. Soc. 2011, 133, 19270.

Chapter 3 Solid-state NMR and electrochemical dilatometry study of charge storage in supercapacitor with redox-active ionic liquid electrolyte

This chapter presents the results of solid-state NMR and electrochemical dilatometry study of charge storage in supercapacitor with redox-active ionic liquid electrolyte

This chapter was written in the form of a scientific article that was submitted to the journal

Energy Storage Materials
(Reference Number: ENSM_2018_1164_R2)

It is reproduced here in full, including the Supporting Information section, as it was at the time of submission.

Solid-state NMR and Electrochemical Dilatometry Study of Charge Storage in Supercapacitor with Redox Ionic Liquid Electrolyte

*Yanyu Wang, Cédric Malveau and Dominic Rochefort**

Département de Chimie, Université de Montréal, CP6128 Succ. Centre-Ville, Montréal, Québec, Canada H3C 3J7

Contact email: dominic.rochefort@umontreal.ca

3.1 Abstract

Redox-active electrolyte supercapacitors have been proposed to increase the capacitance and energy density of electrochemical double-layer capacitors (EDLCs) by adding a faradaic contribution to the charging mechanism. While charge storage in EDLCs has been studied extensively, the implications of having a redox-active molecule participating in charge storage are still not entirely understood. Important questions about the ability of the redox center to penetrate in the carbon micropores, on the faradaic efficiency of these centers and on the self-discharge of redox-active electrolyte supercapacitors are still open. Solid-state NMR (SS-NMR) is a powerful technique to quantify ions inside the pores of activated carbon and has been used to study the charging mechanisms in EDLCs. In this work, we demonstrate for the first time its usefulness to investigate the charge storage in an activated carbon supercapacitor based on a redox-active electrolyte. The electroactive molecule is an ionic liquid in which a triflimide anion analogue is modified with ferrocene, allowing the use of ^{19}F NMR for its quantification in the pore and chronocoulometry to determine the charge associated with the oxidation of ferrocene. We show that the charging process of such a system involves a voltage-dependant mechanism. Charge storage on the positive electrode occurs via co-ion desorption in the low voltage range and subsequently from a combination of the faradaic reaction and counter-ion adsorption at high voltage. At the negative electrode, charging occurs exclusively by counter-ion adsorption over the studied voltage range. In-situ electrochemical dilatometry measurements, done in complement to SS-NMR, further confirm the proposed mechanism. The approach described here provides a more detailed picture of the charging mechanism of redox-active electrolyte supercapacitors than electrochemical measurements alone.

3.2 Introduction

Electrochemical capacitors, also known as supercapacitors, have received considerable interest as a charge storage devices due to their distinct advantages such as high power density and long life cycle.[1,2] The storage of electrical energy in electrochemical double-layer capacitors (EDLCs) relies on the formation of an electrochemical double layer (EDL) at the interface between the electrode and electrolyte. Porous carbons, such as activated carbons, are widely used for supercapacitor electrode materials owing to their high surface area and conductivity.[3] The desolvation of electrolyte ions and the relationship between the carbon pore size and the desolvated ion size have been shown to play important roles on the capacitance.[4-7]

The energy stored in supercapacitors is related to the cell capacitance as well as the operating voltage. Room temperature ionic liquids (ILs) are studied as alternatives to organic electrolytes due to their wider electrochemical potential window of operation. This feature is highly desirable in supercapacitors due to the square dependence of the energy density on the voltage.[8-10] ILs have additional favorable properties including low vapor pressure, non-flammability and good thermal stability.[11] Another strategy to enhance energy density is via the introduction of a redox-active additive to the electrolyte.[12-21] The use of electroactive species such as iodide, hydroquinone, methylene blue or indole-based conjugated macromolecules have been reported for this purpose.[13-17] Most of the redox-active electrolyte supercapacitors are based on aqueous solutions due to the higher solubility of redox species in water than in organic solvents. Aqueous electrolytes, however, have the downside of being limited to moderate operation voltages. Redox-active ionic liquids (RILs) can overcome the solubility and electrochemical stability limitations of organic and aqueous electrolytes. These electroactive phases are obtained by attaching a redox-active moiety to one or both of the ions of ionic liquids[22-26], and electrochemical characterizations show their potential use in electrochemical devices including supercapacitors. Our group has reported on a supercapacitor using a redox-active electrolyte made from ionic liquids functionalized with electroactive ferrocene.[27] Compared with pure ferrocene dissolved in organic solvent, the concentration of the redox-active moiety in ferrocene-functionalized ionic liquid is significantly enhanced up to 2.4 M. The operating voltage for the supercapacitor based on this redox ionic liquid reached 2.5 V and an energy density of 13.3 $Wh \cdot kg^{-1}$ was achieved, which is approximately twice than

that with the unmodified ionic liquid (purely EDL charging). More recently, Mourad et al. presented a biredox ionic liquid that is an ionic liquid functionalized with redox-active species on both cation and anion, for application in supercapacitors.[28] They demonstrated that the capacitance has a two-fold improvement and sustains 2,000 cycles without deterioration. These examples clearly demonstrate that the redox-active electrolytes in supercapacitors offer increased energy thanks to the faradaic charging arising from the redox-active species.

A number of theoretical and experimental methods have been developed to study charge storage mechanisms in EDLCs. Molecular dynamics simulations can describe various adsorption modes for ions at the microscopic scale using specific model and can be used to explore new route to improve energy storage efficiency.[29-32] In situ experimental methodologies based on electrochemical quartz crystal microbalance (EQCM)[33-34] and infrared spectroscopy (IR)[35] have been used to address questions concerning details of ion behaviour in real devices. EQCM is capable of measuring mass variation of electrodes during charging and discharging process. In situ IR method allows the movement of cations and anions of electrolyte in or from carbon micropores to be tracked upon charging. However, a key limitation of EQCM and IR methods is that the in-pore ions cannot be directly detected. Nuclear magnetic resonance (NMR) spectroscopy, including in situ[36-42] and ex situ[43-45] approaches, stand out as a particularly powerful tool to study the molecular mechanisms of charge storage by identifying and quantifying ions adsorbed within carbon micropores. This originates from the shift of the resonance frequency of nuclei strongly interacting with the local electronic density of activated carbon; the ring current effect.[46] Both in situ and ex situ NMR studies of supercapacitors with organic electrolytes or ionic liquids have shown that the electrolyte ions are spontaneously adsorbed into the carbon micropores in the absence of an applied voltage and that the ion population within the micropores changes as a voltage is applied. Importantly, the charge storage mechanism can vary significantly when different electrolytes or even identical electrolyte with different concentrations are used. Three possible pathways for charge storage mechanisms in supercapacitors are proposed based on NMR studies of supercapacitors with porous carbon electrodes and organic electrolytes.[38, 47-48] One possible mechanism is adsorption of counter-ions, resulting in an overall increase in the population of in-pore ions with a charge opposite to that of the carbon electrode. Alternatively, charging can be driven by the desorption of co-ions, resulting in a surplus of the in-pore

counter-ions and a reduction of the total in-pore ion population. Finally, it is possible that the counter-ion adsorption is accompanied by simultaneous co-ion desorption (referred to ion-exchange) and the total in-pore ion population remains constant.

Dimensional changes of the carbon electrodes of supercapacitors may play an important role in the overall energy balance of the charging process.[50] In situ electrochemical dilatometry has been widely used as a reliable tool to monitor the charge-induced dimensional changes of various carbons such as activated carbon, carbide-derived carbon, carbon nanotubes or graphene in supercapacitors.[49-56] The expansion of the carbon electrodes is related to both the carbon pore size distribution and electrolyte. Studies have shown than that the activated carbon electrodes exhibit a reversible expansion up to a few percent of the initial thickness upon charging.[54] The macroscopic expansion of electrode observed by dilatometry could be correlated to a microscopic change in terms of ionic migration. The combination of NMR and electrochemical dilatometry provides a more complete picture of the charging mechanism of supercapacitors.

In this work, the charge storage in a redox-active electrolyte supercapacitor using activated carbon (YP-50F) electrodes and an electroactive ionic liquid electrolyte was studied by ex situ ^{19}F MAS NMR and in situ electrochemical dilatometry. The ionic liquid 1-ethyl-3-methylimidazolium ferrocenylsulfonyl-(trifluoromethylsulfonyl)-imide (EMIm FcNTf) was selected due to its high concentration of redox centers, miscibility with many organic solvents and electrochemical stability. The ferrocene redox center linked to the FcNTf anion allows monitoring both the anion inclusion in the carbon from the ^{19}F signal and the amount of faradaic charge by chronocoulometry from a single charging step. First, we look at the spontaneous adsorption of FcNTf in the micropores of the activated carbon in the absence of potential to evaluate the impact of the larger ion size. Then we present the results of the ion quantification in the pores as a function of the voltage applied to a symmetrical supercapacitor cell to provide insights into the charge storage mechanism. We will show how the faradaic contribution of charge storage arising from the oxidation of ferrocene can be determined by subtraction of the EDL ionic charge calculated with the in-pore ion population measured by NMR from the total electronic charge. Then, we complementarily measure the electrode volume change during the charging process using electrochemical dilatometry. The results gathered reveal important information about the difference in charging between EDLCs and

redox-active electrolyte supercapacitors, allowing us to propose a charge storage mechanism for this system.

3.3 Materials and Methods

3.3.1 Carbon Electrode Fabrication

Carbon electrodes were fabricated from a slurry consisting of 95 wt % YP-50F activated carbon powder (Kuraray Chemical, Japan) and 5 wt % polytetrafluoroethylene (PTFE) binder (Sigma-Aldrich, 60 wt % dispersion in water) in ethanol. The slurry was stirred for at least 2 h until a homogeneous consistency was obtained before heating up to 90 °C under stirring. The resulting paste was kneaded thoroughly and rolled to form a free-standing film with a final thickness of approximately 0.2 mm. 6 mm diameter disc-shaped electrodes were then cut and dried under vacuum at 120 °C for at least 24 h. For electrochemical dilatometry experiments, the prepared electrodes were placed on a stainless steel grid (Alfa Aesar, 80 mesh, 0.127 mm) used as a current collector and were pressed for 60 s at a pressure of 2 MPa before assembled into the electrochemical dilatometer cell.

3.3.2 Redox-active Ionic Liquid and Electrolytes

The synthesis of redox ionic liquids EMIm FcNTf was done according to previous studies[24] and the synthesized compounds were characterized by ^{1}H, ^{13}C and ^{19}F NMR spectroscopy on Bruker Avance 400 MHz and 300 MHz spectrometers, electrospray ionization mass spectrometry and elemental analysis. Mass spectra were recorded on a Waters 3100 mass spectrometer and elemental analysis was performed with a Fisons Instruments EA 1108 elemental analyser. Thermal analyses, including differential scanning calorimetry (DSC) and thermal gravimetric analysis (TGA) were performed on TA Instruments TA Q1000 and TGA 2950, respectively. The results of all characterizations are presented in the Supporting Information. The electrolytes for supercapacitor are different concentration solutions (80 wt %, 50 wt % and 30 wt %) of redox ionic liquid EMIm FcNTf in acetonitrile (Sigma Aldrich, 99.8 % anhydrous), referred to as EMIm FcNTf/ACN.

3.3.3 Cell Preparation

All supercapacitor cells were prepared adapting a two-electrode Swagelok cell configuration. Symmetric cells were assembled inside an argon glovebox, with four stacked thin paper disks as the separator. Carbon electrodes were soaked in the prepared electrolytes overnight before assembled into the cell. The mass of both electrodes is in the range of 5.8 to 6.6 mg and the mass discrepancy between two electrodes in each cell is lower than 0.1 mg.

3.3.4 SS-NMR Experimental Details

All SS-NMR experiments were performed with a Bruker Avance II 400 spectrometer operating at a magnetic field strength of 9.4 T, corresponding to a ^{19}F Larmor frequency of 376.3 MHz and equipped with a 4.0 mm double-resonance MAS probe. All ^{19}F NMR spectra were acquired at 8 kHz MAS. The PTFE binder and probe background signals were removed using presaturation (set on a spinning sideband free of any other signals[57]) and background suppression pulse sequences, respectively. A radiofrequency strength of 50 kHz and a recycle delay of 3 s were used to collect a total of 256 scans for each NMR experiment. Spectral deconvolutions were conducted using the SOLA package in Topspin software and two single peaks were used to fit in-pore and ex-pore resonances. Spinning sidebands were taken into account using a chemical shift anisotropy model in the SOLA package in order to obtain better accuracy of resonance intensities.

All electrochemical experiments were carried out with a BioLogic VMP3 Potentiostat. Prior to applying a fixed voltage for the NMR measurements, supercapacitor cells were initially cycled by galvanostatic charge–discharge (GCD) experiments for 5 cycles at a current density of 0.05 $mA \cdot mg^{-1}$ between 0 and 2 V. Different constant voltages of 0, 0.5, 1.0, 1.5 and 2.0 V were sequentially applied to the cells for 1 h. After disconnected from potentiostat, the cells were disassembled quickly and any excess electrolyte on the external of the electrodes was carefully removed by touching the surface of the electrodes with a small piece of tissue paper. Both the positive and negative carbon electrodes were then weighed before individually packing into 4 mm outer diameter zirconia MAS rotors for NMR measurements.

3.3.5 In Situ Electrochemical Dilatometry Experiments

An ECD-3 electrochemical dilatometer from EL-Cell (Germany) was used to measure the charge-induced dimensional change of the electrodes. The cell with 50 wt % EMIm FcNTf in ACN as electrolyte and a fixed stiff glass frit as separator was assembled in an argon glovebox. Galvanostatic charge-discharge cycles at a current density of 0.025 $mA \cdot mg^{-1}$ between 0 and 2 V were carried out using the same potentiostat and displacement signal from the electrochemical dilatometer was simultaneously recorded with EC-Link Software. The relative height change was normalized by the electrode thickness, measured prior to the experiment.

3.4 Results and Discussion

3.4.1 Static & MAS NMR Spectra of Soaked Electrodes

The Kuraray YP-50F activated carbon was selected for its porosity that is suitable to accommodate the ions of the ionic liquid used in this study. N_2 adsorption isotherms and pore size distribution calculations for the YP-50F show a first pore population at ca. 0.7 nm accounting for nearly 50 % of the total pore volume (see Fig. 1 of reference 58 for PSD). The molecular volume of the FcNTf anion is larger than that of the unmodified NTf_2 (2.71 vs. 1.48 $Å^3$)[59] and a lower occupancy of the porosity by the former is expected. It will be however shown later that a correlation exists between the in-pore signal intensity and the FcNTf concentration, confirming that the modified anion can populate the YP-50F porosity. ^{19}F MAS (8 kHz) and static spectra of the YP-50F activated carbon electrodes soaked with an electrolyte composed of 50 wt % of the electroactive ionic liquid EMIm FcNTf in ACN are shown in Figure 3-1. In the MAS spectrum, two featured resonances for the FcNTf anions are clearly observed. The sharp “ex-pore” resonance corresponding to the ions residing in the bulk of the electrolyte (i.e., outside the micropores or between the carbon particles) is observed at -77.9 ppm, while the broad “in-pore” resonance assigned to the ions located inside the carbon microporesis is observed at -85.1 ppm. The in-pore resonance is shifted to lower frequency by a value of 7.2 ppm relative to ex-pore resonance, due to the change of local magnetic environment within the micropores arising from the ring current effects.[48] A smaller difference

in the chemical shifts between the in-pore and ex-pore was observed for the unmodified EMIm NTf_2 ionic liquid (6.3 ppm).[44] The difference between these ionic liquids suggests that the local magnetic environment felt by the F atom on the in-pore anions is slightly affected by the presence of ferrocene as π-π interactions are possible between the activated carbon and the FcNTf anion. The observation of a distinct in-pore resonance in the spectrum of Figure 3-1 indicates that the redox-active anion from the ionic liquid EMIm FcNTf spontaneously populates the carbon micropores even in the absence of an applied potential and despite the larger anion radius. Static NMR measurement for the same carbon electrode (Figure 3-1 bottom) provided an insufficient resolution to distinguish quantitatively the in-pore ions from the ex-pore ions because of the high viscosity of the ionic liquid. The shoulder on the lower frequency side for the ex-pore ions is however visible. Consequently, since the MAS is required, the measurements on this electrolyte will be done in an ex-situ mode were the electrodes are charged in Swagelok-type cells, recuperated from the cells and transferred in the NMR for measurements.

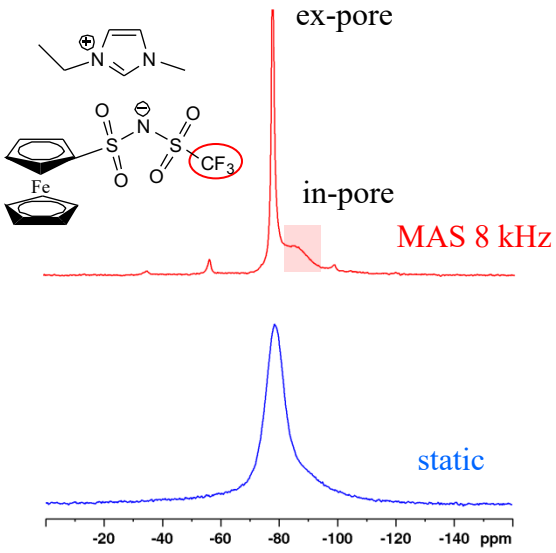

Figure 3-1. ^{19}F NMR spectra recorded at MAS (8 kHz, top) and in static mode (bottom) shows the necessity of spinning to obtain a sufficient resolution to isolate the in-pore ion contribution. The signals came only from the F atoms on the FcNTf anion. The peaks at about -35, -55 and -100 ppm are spinning sidebands. The measurements were done on the YP-50F carbon electrodes (95 wt % activated carbon and 5 wt % PTFE) soaked overnight in a solution of 50 wt % of the ionic liquid EMIm FcNTf in acetonitrile. The excess of electrolyte was removed prior to the measurements.

Electrolytes with 30, 50 and 80 wt % of the EMIm FcNTf ionic liquid in acetonitrile were prepared to study the effect of the IL concentration on the signal of the FcNTf adsorbed in the carbon micropores. Figure 3-2 shows the ^{19}F NMR spectra for each sample after soaking overnight in the electrolyte. The linewidth of the in-pore resonance drops from 4417 Hz (80 wt %, Figure 3-2c) to 4243 Hz (50 wt %, Figure 3-2b) and to 3600 Hz (30 wt %, Figure 3-2a) due to the higher mobility of ions in the less viscous electrolytes containing less ionic liquid. We also note that the difference in the ^{19}F chemical shifts between the in-pore and ex-pore resonances decreases slightly from 7.2 ppm (80 wt % and 50 wt %) to 6.6 ppm (30 wt %). It is presumed that more solvent increases the average distance between carbon and ions and correspondingly reduces the ring current effects.[44]

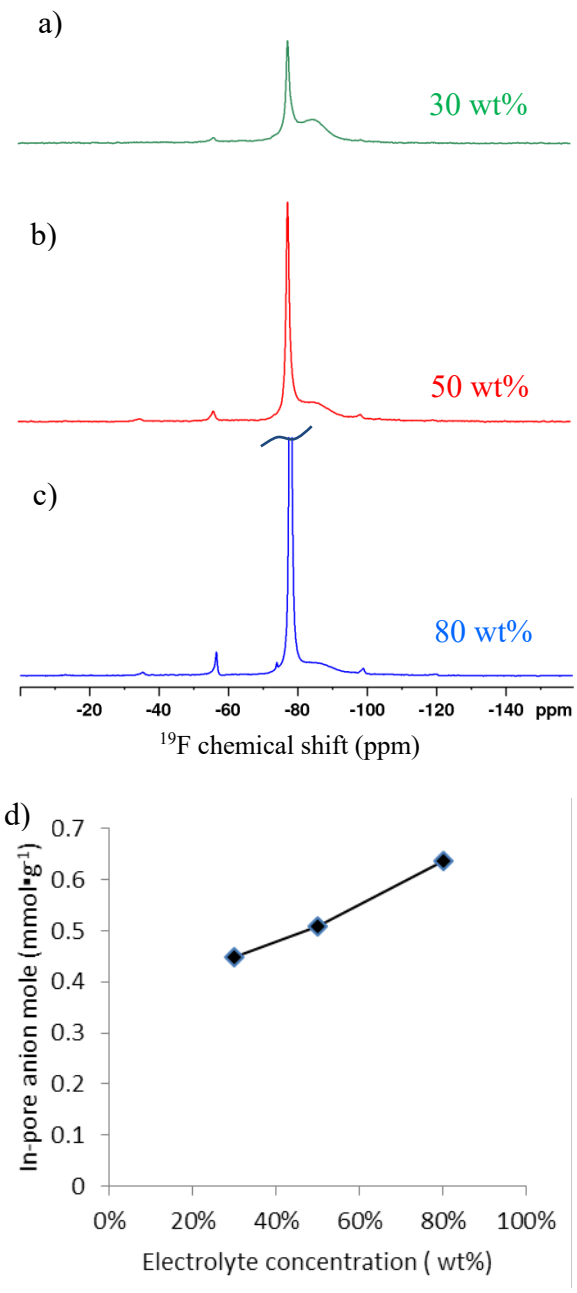

Figure 3-2. ^{19}F NMR spectra of YP-50F carbon electrodes after contacting an excess of three different EMIm FcNTf/ACN electrolytes overnight and removing the excess solution. The electrolytes contained (a) 30 wt %, (b) 50 wt % and (c) 80 wt % of the redox ionic liquid. The ex-pore peak (δ = -78 ppm) intensity reflects the increasing quantity of FcNTf in the interparticle spaces of the porous electrode. The deconvolution of the spectra was used to evaluate the relative surface area of both peaks (ex-pore and in-pore) and the concentration of the in-pore anions (presented in the d) panel).

Figure 3-2 also shows a significant impact of the ionic liquid concentration on the peak intensities. In order to quantify the amount of ions in the pore, the spectra were deconvoluted using SOLA analysis into two contributions for both ex- and in-pore resonance peaks. Knowing the total amount of the ionic liquid in the electrode (by weight), it is then possible to quantify the in-pore ion population per gram of activated carbon material. Figure 3-2d shows that the quantiy of anions in the carbon pores is strongly correlated to electrolyte concentration in electroactive ionic liquid EMIm FcNTf. This trend is consistent with results obtained for traditional (unmodified) ionic liquids such as PEt_4-BF_4/ACN electrolytes, where the in-pore ion population rises linearly with the increase in the electrolyte concentration.[41] The quantity of FcNTf anions in the carbon pores is between 0.45 and 0.64 $mmol \cdot g^{-1}$. In the case of an electrolyte composed of 65 wt % of the unmodified EMIm NTf_2 ionic liquid in ACN, 1.2 $mmol \cdot g^{-1}$ of the NTf_2 anions was determined in a similar electrode made from YP-50F carbon (from the same supplier).[44] As the radius of the anion is significantly increased by the addition of ferrocene, it is not surprising that the number of mole of in-pore FcNTf is lower than that of NTf_2. Since the peak of the in-pore resonance at 80 wt % electrolyte is quite broad and may provide a higher uncertainty in the quantification, the electrolyte containing 50 wt % EMIm FcNTf was chosen for the finer analysis of the variation of the in-pore ion population as a function of the voltage applied.

3.4.2 Ex Situ NMR Study of Charge Storage

Ex situ NMR experiments were carried out to probe the variation of the in-pore FcNTf ions during the charging process of a redox supercapacitor. A series of supercapacitor cells composed of 2 symmetrical carbon electrodes using the 50 wt % EMIm FcNTf/ACN electrolyte were charged to different voltages, ranging from 0 V to 2 V for a period of 1 hour. The cells were then dismounted and the ^{19}F NMR spectra were recorded for both the positive and negative electrodes. Figure 3-3 shows that the spectra of the electrodes poised at 0 V are similar to those recorded on the soaked (unbiased) electrodes. The chemical shifts of both peaks are found at the same position as in Figure 3-1 and 3-2 (ex-pore ions at -77.9 ppm and in-pore ions at -84.9 ppm). As the voltage is increased, a clear change in the in-pore anions

peak occurs at the positive electrode. The peak intensity gradually increases and shifts towards higher frequencies. At the negative electrode on the other hand, only the resonant frequency evolves with the voltage applied, apart from a slight increase of the in-pore peak intensity at 2.0 V. A finer analysis of the peaks was carried out and the spectral deconvolution and fitting are presented in Figure S1 of the Supporting Information.

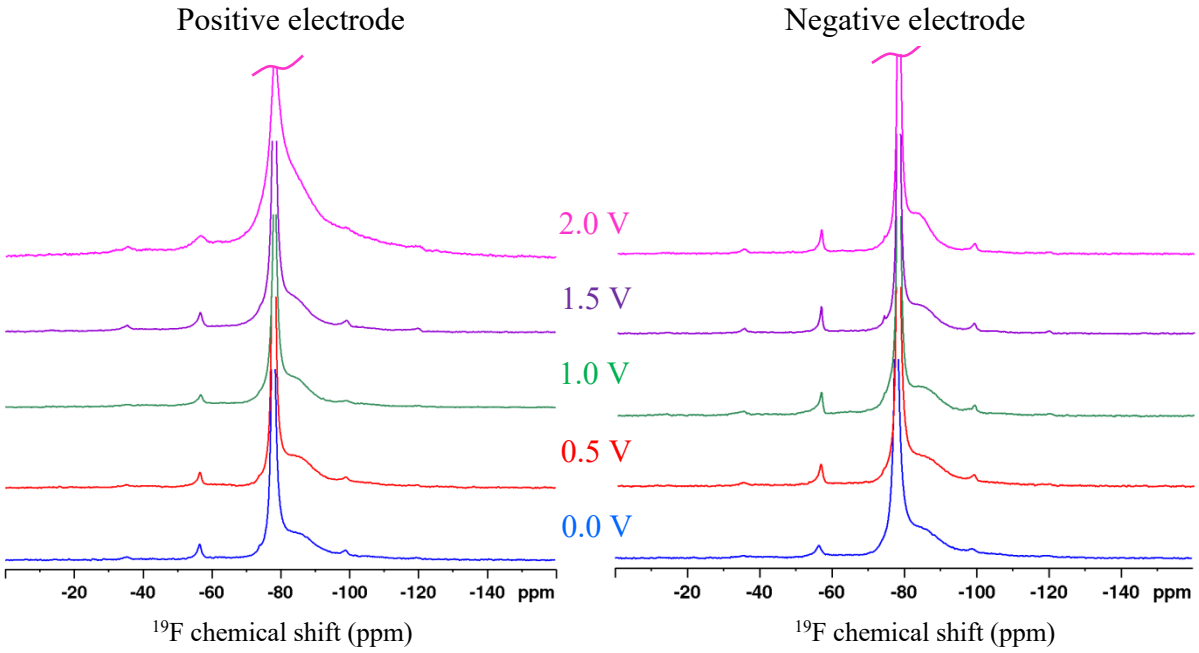

Figure 3-3. ^{19}F NMR spectra of the positive and negative YP-50F activated electrodes of a supercapacitor cell that was charged at different voltages. All cells used a 50 wt % EMIm FcNTf redox ionic liquid in acetonitrile electrolyte and were charged using a 1 h potentiostatic step at the given voltage for 1 h (after equilibrating the cell with 5 GCD cycles, see Material and methods section for conditions). An increase in the relative proportion of in-pore FcNTf anions is observed at higher voltage values only at the positive electrode, as expected for double-layer charging. The quantity of anions in the carbon of the negative electrode remained constant.

Figure 3-4 shows that the chemical shifts of the ex-pore ion peak remain unchanged with an increase in cell voltage, which is to be expected since the effect of charging the electrode is felt locally and will not extend far in the electrolyte. However, the peak for the in-

pore anions in both the positive and negative electrodes gradually moves towards higher frequencies with increasing voltagwe and stabilizes after 1.5 V. This has been observed in NMR studies of similar carbon-ionic liquid systems[36, 38, 41-42, 44] (although using unmodified ILs) and is an indication of a change in the electronic structure of the carbon surface induced by the application of a potential.[42] Several possible factors could account for the changes in the resonance frequencies of the adsorbed ions, but the most likely are the changes in the nature of the ions populating the pores or different interactions with the carbon. We notice that the magnitude of the chemical shift displacement of the in-pore peak between 0 and 2 V in our system (ca. 3 ppm) is smaller compared to an unmodified ILs.[36, 38, 41-42, 44] For example, the shift in resonance of ^{19}F peak in EMIm NTf_2 can reach almost 7 ppm between the uncharged and fully charged state of a capacitor.[44] This difference is unlikely due to the system relaxation at OCP (self-discharge) as larger shifts were reported for both ex situ and in situ measurements in the literature.

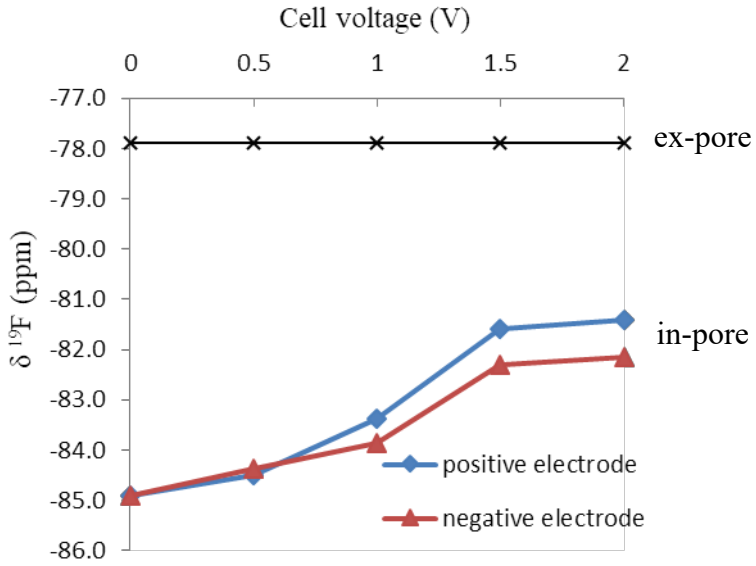

Figure 3-4. Effect of the voltage on the ^{19}F chemical shift of in-pore (red triangle and blue diamond for negative and positive electrode, respectively) and ex-pore (black cross) anions. This variation of the peak resonance suggests a modification of the immediate anion environment during the charging process, an effect commonly seen with ionic liquids in activated carbon electrodes. The chemical shift of anions outside of the pores (bulk and interparticle spacing) is not affected by the voltage. Before recording the NMR spectra, the supercapacitor cells were poised to a voltage between 0 and 2 V for a duration of 1 h.

Next we turn to the quantification of the anions inside the pores as a function of the applied voltage to gain a better understanding of the charging mechanism. The result of the integration after deconvolution of each peak is plotted in Figure 3-5. At the positive electrode (Figure 3-5a), the population of the in-pore anions remained approximately constant at the initial value measured for unbiased electrodes up to a voltage of 1.0 V. A steep increase in the population is observed at higher voltages. This increase is indicative of the insertion of FcNTf anions inside the microporous carbon structure to compensate the charge accumulating at the electrode surface at more positive voltage. This is a direct consequence of the double-layer charging mechanism and such a relationship between the charge storage and ion population of the carbon pores has been demonstrated on many occasions for unmodified ionic liquids.[36, 38] Meanwhile, at the negative electrode (Figure 3-5b) the amount of anions inside the pores remains constant over the entire voltage range. The accumulation of charge at the negative

electrode is therefore likely compensated by the adsorption of cations (counter-ion adsorption model). We attempted several approaches to follow the imidazolium cations using ^{13}C and ^{1}H but without success. Others have been able to analyse changes in the ionic liquid cation population in and out of the activated carbon microstructure using SS-NMR.[44] In our case, the additional ^{13}C and ^{1}H signals attributed to the ferrocene on FcNTf precluded the isolation of the signals from imidazolium. The FcNTf peaks were too broad and overlapped with those of imidazolium. The small increase in the anion population at 2.0 V on the negative electrode is probably caused by the co-adsorption of some anions accompanying the large amounts of cations as strong ion-ion interactions are found in ionic liquid electrolytes.[45] It should be noted that ferrocenium is paramagnetic and, as such, could interfere with the NMR signal of its surroundings and complicate the quantification of in- pore ions by reducing ^{19}F signal intensity. The total ^{19}F signal was however not significantly affected by the presence of ferrocenium and the paramagnetic effect is only marginal (Figure 3-S2).

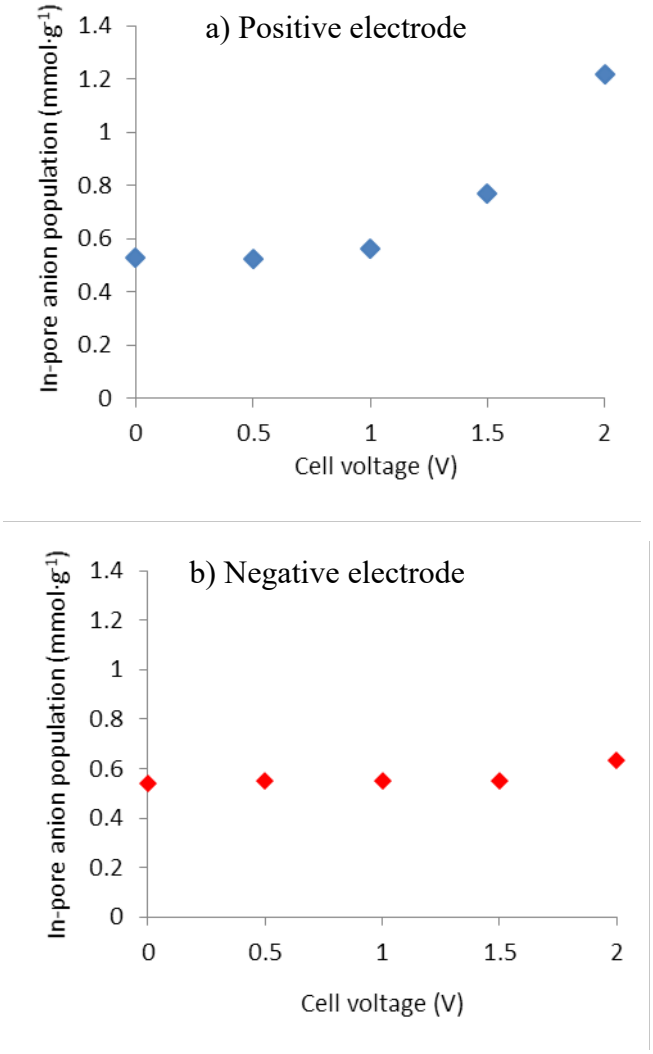

Figure 3-5. In-pore FcNTf anion population found in the positive (a) and negative electrode (b) of a supercapacitor after applying different voltage between 0.0 and 2.0 V for 1 h. Values are given as millimoles per gram of YP-50F carbon in each electrode and were calculated from the relative peak surface area after deconvolution of the NMR spectra. The increase at the positive electrode between 1.0 and 2.0 V is indicative of significant amounts of anion into pores during charging of the supercapacitor.

The interest in redox-active electrolyte supercapacitor lies in their ability to increase charge storage density via the faradaic reaction of an electroactive molecule dissolved in the electrolyte.[13-14, 27-28] The goal of the following experiment is to evaluate if the SS-NMR approach, so far applied to study purely non-faradaic charge storage, can be used to

understand the mixed (faradaic and non-faradaic) mechanisms in redox-active electrolyte supercapacitors. To do so, we intended to correlate the fraction of the charge associated with the anions populating the carbon pores, or "ionic charge", with the total charge stored during the charging step calculated by the integration of chronoamperometric curve. Because the FcNTf anions are found in the micropores in the absence of a potential bias (see Figures 3-2 and 3-5 and associated discussion), the ionic charge is calculated from the increase in the amount of anion in the positive electrode from the value of 0.53 $mmol \cdot g^{-1}$ found in Figure 3-5 which sets the 0 ionic charge value. A zero ionic charge (after applying 0.0 and 0.5 V for instance, see Figure 3-6) means that there is no net anion movement into the micropores. The total charge of 14 $C \cdot g^{-1}$ calculated from the chronoamperometric curve using 0.5 V must therefore imply another mechanism. The expulsion of cations from the pore is more likely since a cyclic voltammogram recorded with the cell before the chronoamperometric measurement does not show the oxidation of ferrocene at that potential (see Figure 3-S3 in the Supporting Information).

Further increases in voltage (≥ 1.0 V) yield an increase in both the ionic and total charges. The increase in ionic charge simply means that more anions are inserted in the carbon micropores as a result of double-layer (DL) charging and other authors reported that the total electronic charge equals the ionic charge in EDLCs.38, 41 In contrast, Figure 3-6 reveals a significant excess of charge between the total and ionic (anionic) charges. For example, at 2.0 V, the total charge calculated from the integration of the i-t curves reaches 226 C·g-1 while the amount of anions account for only 66 C·g-1. The remaining charge density can either originate from the oxidation of the ferrocene moiety on the anion (faradaic charging) or from the expulsion of EMIM cations out of the carbon micropores. For reasons explained above, we were unable to determine the population of cations in the micropore but we can however estimate the maximum charge that would be associated with their expulsion. To do so we first assume that the amounts of anions and cations in the micropores are equal at OCP after the soaking step (see Figure 3-2d). This is a reasonable assumption to maintain charge neutrality and it has been shown to be true with unmodified ionic liquids.41 Now if we suppose that all these cations (5.3 x 10-4 mole·g-1) are expelled from the micropores of the positive electrode during charging, they would contribute to the charge by 51 C·g-1. The data from Figure 3-6 shows that for potentials ≥ 1.5 V, the expulsion of cations is insufficient to account for all the

charge density and that consequently, a significant fraction of the total charge comes from faradaic charging. This explanation is further supported by the fact that the oxidation peak is found at these potential values on a cyclic voltammogram recorded with the supercapacitor cell (Figure 3-S4a in Supporting Information) and the existence of a potential plateau of the positive electrode during galvanostatic charging (Figure 3-S4b60 At this point we should note that these results, being done ex-situ, provide a snapshot of the system after equilibrating the cell at a given voltage for 1 h. While the precise impact of dismounting the cell prior to the measurement is difficult to assess, we provide the NMR spectrum recorded immediately after dismounting the cell and after 1.5 h in the NMR (Figure 3-S5). In-situ NMR will be necessary to probe the dynamics of these two modes and provide a better understanding. In-situ approach will however be possible only using a diluted solution of the electroactive FcNTf since the use of MAS is required to distinguish both in- and ex-pore signals in viscous media.

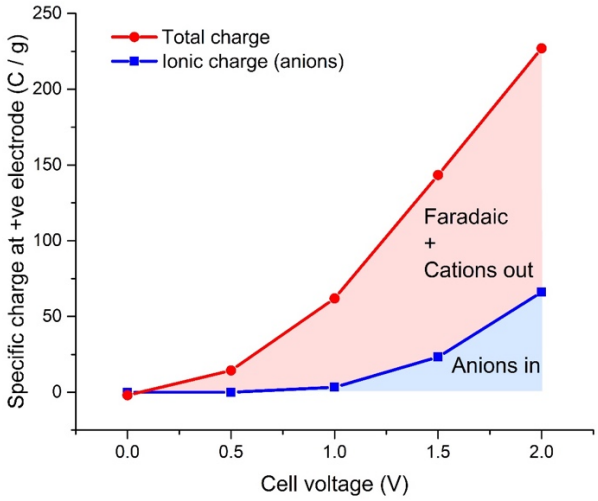

Figure 3-6. Comparison of ionic and total electronic charge stored in the supercapacitor at different voltages. The ionic charge is calculated from the increase in the quantity of in-pore FcNTf anions relative to the amount found in the carbon after soaking (unbiased electrodes, Figure 3-2d). The total charge represents the amount of coulomb that was accumulated over the potentiostatic step. For an applied voltage of 1.0 V and above, the oxidation of ferrocene to ferrocenium becomes a significant contribution to the charging mechanism.

3.4.3. In Situ Electrochemical Dilatometry Measurements of Charging Cells

To complement the results described above, electrochemical dilatometry measurements were carried out on the positive and negative electrodes with galvanostatic charge and discharge. These were done in separate experiments as the in-situ cell allow following the thickness evolution of one electrode at a time. The galvanostatic charge-discharge curves and the corresponding electrochemical dilatometry profiles for both the positive and negative electrodes are depicted in Figure 3-7a and 3-7c, respectively. Reversible electrode expansions during each charging and discharging cycle are observed on both the positive and negative electrodes. A zoom on one cycle at the positive electrode is shown in Figure 3-7b, where a slightly negative expansion (contraction) at the very beginning of the charging process is observed. Such contraction of the electrode can only be explained with an expulsion of cations, which was suggested as a possible mechanism above. Starting from around 1 V, the

positive electrode begins to swell, consecutively reaching a 0.5 % expansion. The electrode expansion is believed to be predominantly related to the accumulation of ions (or ion insertion) within micropores, which correlates well with the NMR observations described above.[55] At the negative electrode, only a pronounced expansion is observed, reaching 1.4 % of the thickness change over the full voltage range (Figure 3-7c). In comparison with positive electrode, the negative electrode expansion is larger by a factor of 2.8. This has been also observed by other authors,[49-56] which is thought to be a result of weakness in states density of π-electron system of carbon for positive polarization and enhancement for negative polarization.[56]

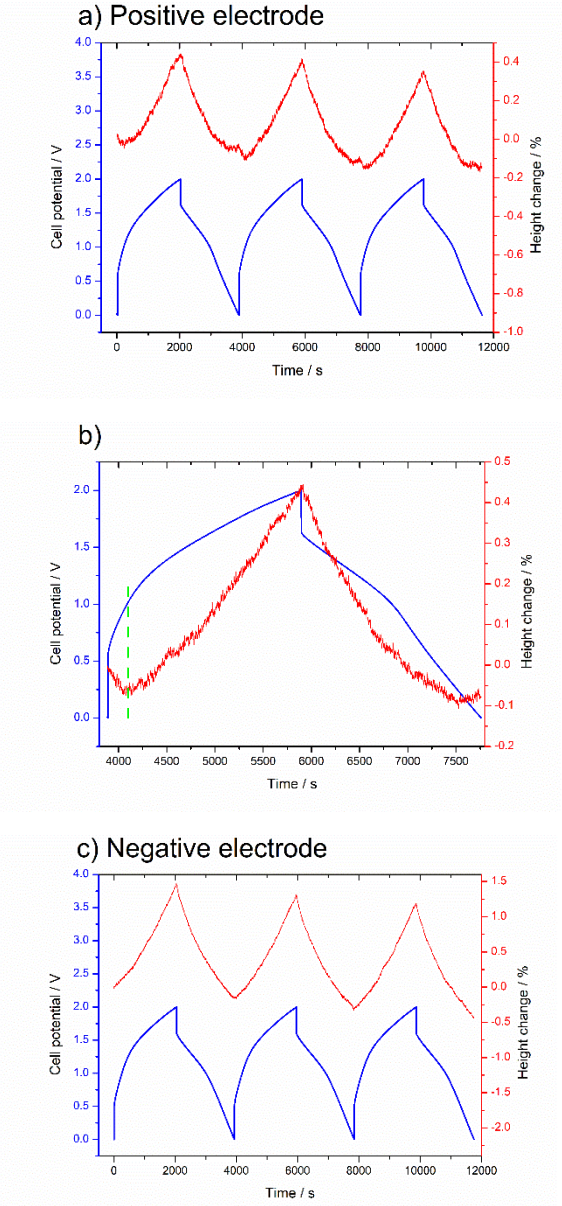

Figure 3-7. Results from the in situ electrochemical dilatometry measurements on a supercapacitors cell with 50 wt % EMIm FcNTf acetonitrile solution as electrolyte. The measurements were done at a current density of 25 mA/g on the positive (a and b) and on the negative electrode (c), separately. Panel (b) shows an enlargement of the second cycle at the positive electrode. At low voltage, a contraction of the electrode is noted which is attributed to the expulsion of cations. This small feature of the dilatometry curve was consistently observed in all measurements with the EMIm FcNTf ionic liquid (at the positive electrode only).

3.4.4 Summary of Charging Process

Based on the SS-NMR and electrochemical dilatometry results presented above, we propose a possible charging mechanism for the supercapacitor composed of YP-50F carbon electrodes with the electroactive ionic liquids EMIm FcNTf electrolyte. The mechanism (schematically described in Figure 3-8) is based on the similarities observed in previous NMR studies of EDLCs for the double-layer contribution to charge storage to which we now add the faradaic contribution. Initially, the electrolyte ions populate the micropores of carbon before any voltage is applied. As the cell is charged, cations are first expelled from the micropores on the positive electrode at low voltage with electrical double-layer charging. As voltage increases, the faradaic reaction begins at the positive electrode involving the oxidation of ferrocene to ferrocenium. The additional positive charge is compensated by further expulsion of cations and insertion of anions in the micropores. The counter-ion insertion is however more important than co-ion desorption since the electrode presents a net volume increase. When the voltage reaches 1.0 V, both the faradaic (ferrocene oxidation) and capacitive processes (ion movements to and from micropores) co-exist. On the negative electrode only the counter-ion $EMIm^+$ adsorption happens over the full range of voltage studied as supported by the electrode volume expansion observed.

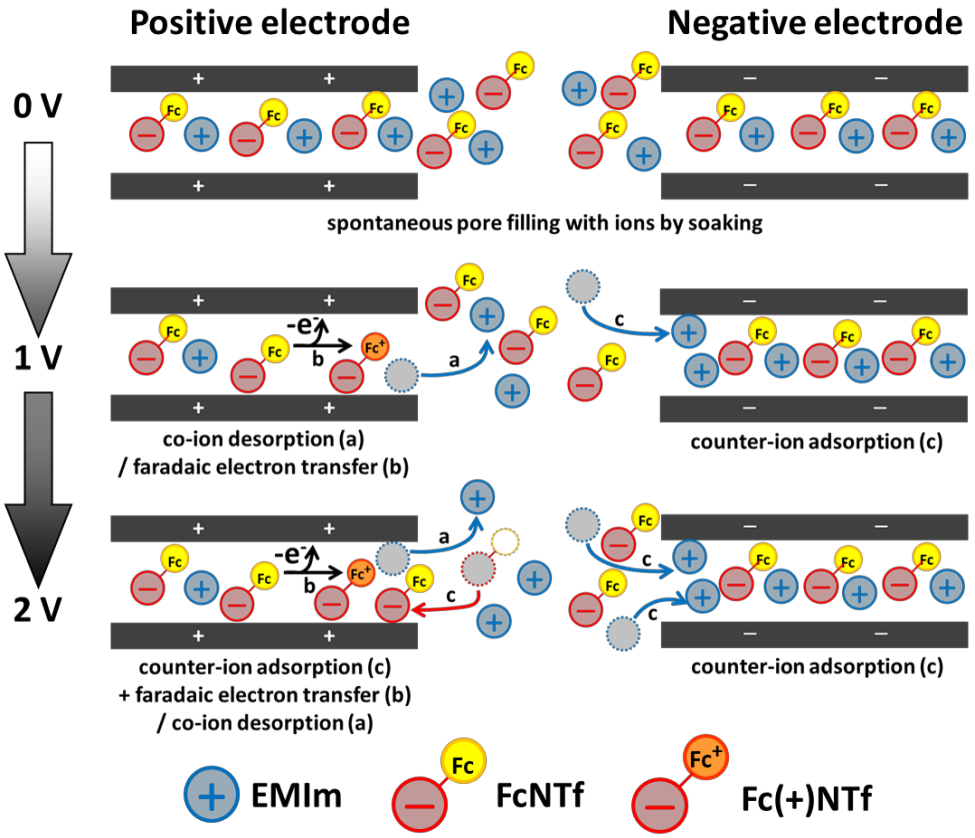

Figure 3-8. Schematic illustration of the different possible ion displacement inside and outside of the carbon micropores involved in supercapacitors based on the redox-active ionic liquid EMIm FcNTf electrolyte at different potentials. The different processes illustrated are proposed on the basis of the experimental results from NMR. The blue and red arrows indicate cations and anions (respectively) moving in or out of the micropores and the black arrows denote an electron transfer reaction. Note that solvent (acetonitrile) molecules are omitted for clarity and that electron transfer is also possible on the carbon particle surface, outside of the carbon pores (not shown).

3.5 Conclusions

Solid-state NMR spectroscopy is a powerful technique to study charge storage mechanism of double-layer capacitors at the molecular level. The technique has been applied so far to the study of activated carbon capacitors employing conventional and ionic liquid

electrolytes. Here we expanded its application to study the charging mechanisms of redox-active electrolytes capacitors, where an electroactive species is added in the electrolyte to increase energy density. To do so we employed an electroactive ionic liquid, 1-ethyl-3-methylimidazolium ferrocenylsulfonyl-(trifluoromethylsulfonyl)-imide (EMIm FcNTf), which bears the redox-active center on the anion. Changes in the population of FcNTf anions inside the pores of the activated carbon were monitored from the ^{19}F NMR signal. The results presented in this study demonstrate that the charge storage mechanism for supercapacitors based on redox electrolyte changes with the polarization of the cell. Specifically, charge storage at the positive electrode occurs via co-ion desorption (EMIm cations being expulsed from the pores) and faradaic reaction (FcNTf oxidation) at low voltage. At 1.0 V and above, counter-ion adsorption (further insertion of FcNTf anions in the micropores) contributes significantly to the charging process as evidenced by NMR. Charging at the negative electrode occurs exclusively by the counter-ion adsorption over the studied voltage range. These observations were confirmed by electrochemical dilatometry, which shows, at the positive electrode, a small contraction upon cation expulsion from the micropores at low voltage and an expansion when FcNTf anions penetrate the pores.

The faradaic contribution to the charge storage can be evaluated by a comparison between the ionic and total electronic charge, providing finer details on the mechanism than a purely electrochemical approach. Unfortunately, the presence of ferrocene broadens the ^{13}C and ^{1}H NMR spectra of the EMIm FcNTf, rendering the quantification of the imidazolium cation impossible due to the overlapping of peaks. Isotopic labeling might solve this issue. While the exact fraction of charge related to cation desorption is not determined, this process account for 25 % of the charge storage at the most. Finally, we emphasise that the approach used here could be applied to understand the origin of the important issue of self-discharge in redox-active electrolyte supercapacitors. This will require operating in an in-situ mode, an approach that will be pursued in our laboratory.

ASSOCIATED CONTENT

Supporting Information

Representative deconvolutions of NMR spectra, cyclic voltammograms of supercapacitors, and characterization and thermal analysis data of redox ionic liquid EMIm FcNTf.

AUTHOR INFORMATION

Corresponding Author

*dominic.rochefort@umontreal.ca

Notes

The authors declare no competing financial interest.

3.6 Acknowledgements

We thank Dr. Bruno Gélinas for the initial design and synthesis of redox ionic liquids based on triflimide-ferrocene. We acknowledge the financial support of the Natural Science and Engineering Council of Canada (NSERC) through the Discovery Grant Program.

References

[1] Miller, J.R.; Simon, P., Electrochemical Capacitors for Energy Management, Science 321 (2008) 651-652. https://doi.org/10.1126/science.1158736.

[2] Wang, Y.; Song, Y.; Xia, Y., Electrochemical capacitors: mechanism, materials, systems, characterization and applications, Chem. Soc. Rev. 45 (2016) 5925-5950. https://doi.org/10.1039/c5cs00580a.

[3] Simon, P.; Gogotsi, Y., Materials for electrochemical capacitors, Nat. Mater. 7 (2008) 845-854. https://doi.org/10.1038/nmat2297.

[4] Chmiola, J.; Yushin, G.; Gogotsi, Y.; Portet, C.; Simon, P.; Taberna, P.L., Anomalous Increase in Carbon Capacitance at Pore Sizes Less Than 1 Nanometer, Science 313 (2006) 1760-1763. https://doi.org/10.1126/science.1132195

[5] Largeot, C.; Portet, C.; Chmiola, J.; Taberna, P.L.; Gogotsi, Y.; Simon, P., Relation between the Ion Size and Pore Size for an Electric Double-Layer Capacitor, J. Am. Chem. Soc. 130 (2008) 2730-2731. https://doi.org/10.1021/ja7106178.

[6] Vix-Guterl, C.; Frackowiak, E.; Jurewicz, K.; Friebe, M.; Parmentier, J.; Béguin, F., Electrochemical energy storage in ordered porous carbon materials, Carbon 43 (2005) 1293-1302. https://doi.org/10.1016/j.carbon.2004.12.028.

[7] Chmiola, J.; Largeot, C.; Taberna, P.L.; Simon, P.; Gogotsi, Y., Desolvation of ions in subnanometer pores and its effect on capacitance and double-layer theory, Angew. Chem. Int. Ed. 47 (2008) 3392-3395. https://doi.org/10.1002/anie.200704894.

[8] Armand, M.; Endres, F.; MacFarlane, D.R.; Ohno, H.; Scrosati, B., Ionic-liquid materials for the electrochemical challenges of the future, Nat. Mater. 8 (2009) 621-629. https://doi.org/10.1038/nmat2448.

[9] MacFarlane, D.R.; Forsyth, M.; Howlett, P.C.; Kar, M.; Passerini, S.; Pringle, J.M.; Ohno, H.; Watanabe, M.; Yan, F.; Zheng, W.; Zhang, S.; Zhang, J., Ionic liquids and their solid-state analogues as materials for energy generation and storage, Nat. Rev. Mater. 1 (2016) 15005. https://doi.org/10.1038/natrevmats.2015.5.

[10] Zhong, C.; Deng, Y.; Hu, W.; Qiao, J.; Zhang, L.; Zhang, J., A review of electrolyte materials and compositions for electrochemical supercapacitors, Chem. Soc. Rev. 44 (2015) 7484-7539. https://doi.org/10.1039/c5cs00303b.

[11] Plechkova, N.V.; Seddon, K.R., Applications of ionic liquids in the chemical industry, Chem. Soc. Rev. 37 (2008) 123-150. https://doi.org/10.1039/b006677j.

[12] Frackowiak, E.; Fic, K.; Meller, M.; Lota, G., Electrochemistry Serving People and Nature: High-Energy Ecocapacitors based on Redox-Active Electrolytes, Chemsuschem 5 (2012) 1181-1185. https://doi.org/10.1002/cssc.201200227.

[13] Frackowiak, E.; Meller, M.; Menzel, J.; Gastol, D.; Fic, K., Redox-active electrolyte for supercapacitor application, Faraday Discuss. 172 (2014) 179-198. https://doi.org/10.1039/C4FD00052H.

[14] Roldan, S.; Blanco, C.; Granda, M.; Menendez, R.; Santamaria, R., Towards a further generation of high-energy carbon-based capacitors by using redox-active electrolytes, Angew. Chem. Int. Ed. 50 (2011) 1699-1701. https://doi.org/10.1002/anie.201006811.

[15] Roldán, S.; Granda, M.; Menéndez, R.; Santamaría, R.; Blanco, C., Supercapacitor modified with methylene blue as redox active electrolyte, Electrochim. Acta 83 (2012) 241-246. https://doi.org/10.1016/j.electacta.2012.08.026.

[16] Senthilkumar, S.T.; Selvan, R.K.; Lee, Y.S.; Melo, J.S., Electric double layer capacitor and its improved specific capacitance using redox additive electrolyte, J. Mater. Chem. A 1 (2013) 1086-1095. https://doi.org/10.1039/c2ta00210h.

[17] Xiong, T.; Lee, W.S.V.; Chen, L.; Tan, T.L.; Huang, X.; Xue, J., Indole-based conjugated macromolecules as a redox-mediated electrolyte for an ultrahigh power supercapacitor, Energy Environ. Sci. 10 (2017) 2441-2449. https://doi.org/10.1039/c7ee02584j.

[18] Gorska, B.; Frackowiak, E.; Beguin, F., Redox active electrolytes in carbon/carbon electrochemical capacitors, Curr. Opin. Electrochem. 9 (2018) 95-105. https://doi.org/https://doi.org/10.1016/j.coelec.2018.05.006.

[19] Sankar, K.V.; Seo, Y.; Lee, S.C.; Chan Jun, S., Redox Additive-Improved Electrochemically and Structurally Robust Binder-Free Nickel Pyrophosphate Nanorods as Superior Cathode for Hybrid Supercapacitors, ACS Appl. Mater. Interfaces 10 (2018) 8045-8056. https://doi.org/10.1021/acsami.7b19357.

[20] Hu, L.; Shi, C.; Guo, K.; Zhai, T.; Li, H.; Wang, Y., Electrochemical Double-Layer Capacitor Energized by Adding an Ambipolar Organic Redox Radical into the Electrolyte, Angew. Chem. Int. Ed. 57 (2018) 8214-8218. https://doi.org/doi:10.1002/anie.201804582.

[21] Jayaramulu, K.; Dubal, D.P.; Nagar, B.; Ranc, V.; Tomanec, O.; Petr, M.; Datta, K.K.R.; Zboril, R.; Gómez-Romero, P.; Fischer, R.A., Ultrathin Hierarchical Porous Carbon Nanosheets for High-Performance Supercapacitors and Redox Electrolyte Energy Storage, Adv. Mat. 30 (2018) 1705789. https://doi.org/doi:10.1002/adma.201705789.

[22] Balasubramanian, R.; Wang, W.; Murray, R.W., Redox Ionic Liquid Phases: Ferrocenated Imidazoliums, J. Am. Chem. Soc. 128 (2006) 9994-9995. https://doi.org/10.1021/ja0625327.

[23] Gélinas, B.; Forgie, J.C.; Rochefort, D., Conductivity and Electrochemistry of Ferrocenyl-Imidazolium Redox Ionic Liquids with Different Alkyl Chain Lengths, J. Electrochem. Soc. 161 (2014) H161-H165. https://doi.org/10.1149/2.017404jes.

[24] Gélinas, B.; Rochefort, D., Synthesis and characterization of an electroactive ionic liquid based on the ferrocenylsulfonyl(trifluoromethylsulfonyl)imide anion, Electrochim. Acta 162 (2015) 36-44. https://doi.org/10.1016/j.electacta.2014.11.154.

[25] Mourad, E.; Coustan, L.; Freunberger, S.A.; Mehdi, A.; Vioux, A.; Favier, F.; Fontaine, O., Biredox ionic liquids: electrochemical investigation and impact of ion size on electron transfer, Electrochim. Acta 206 (2016) 513-523. https://doi.org/10.1016/j.electacta.2016.02.211.

[26] Chen, X.; Xu, D.; Qiu, L.; Li, S.; Zhang, W.; Yan, F., Imidazolium functionalized TEMPO/iodide hybrid redox couple for highly efficient dye-sensitized solar cells, J. Mater. Chem. A 1 (2013) 8759-8765. https://doi.org/10.1039/c3ta11521f.

[27] Xie, H.J.; Gélinas, B.; Rochefort, D., Redox-active electrolyte supercapacitors using electroactive ionic liquids, Electrochem. Comm. 66 (2016) 42-45. https://doi.org/10.1016/j.elecom.2016.02.019.

[28] Mourad, E.; Coustan, L.; Lannelongue, P.; Zigah, D.; Mehdi, A.; Vioux, A.; Freunberger, S.A.; Favier, F.; Fontaine, O., Biredox ionic liquids with solid-like redox density in the liquid state for high-energy supercapacitors, Nat. Mater. 16 (2017) 446-453. https://doi.org/10.1038/nmat4808.

[29] Burt, R.; Birkett, G.; Zhao, X.S., A review of molecular modelling of electric double layer capacitors, Phys. Chem. Chem. Phys. 16 (2014) 6519-6538. https://doi.org/10.1039/c3cp55186e.

[30] Merlet, C.; Rotenberg, B.; Madden, P.A.; Taberna, P.L.; Simon, P.; Gogotsi, Y.; Salanne, M., On the molecular origin of supercapacitance in nanoporous carbon electrodes, Nat. Mater. 11 (2012) 306-310. https://doi.org/10.1038/nmat3260.

[31] Merlet, C.; Pean, C.; Rotenberg, B.; Madden, P.A.; Daffos, B.; Taberna, P.L.; Simon, P.; Salanne, M., Highly confined ions store charge more efficiently in supercapacitors, Nat. Commun. 4 (2013) 2701. https://doi.org/10.1038/ncomms3701.

[32] Kondrat, S.; Wu, P.; Qiao, R.; Kornyshev, A.A., Accelerating charging dynamics in subnanometre pores, Nat. Mater. 13 (2014) 387-393. https://doi.org/10.1038/nmat3916.

[33] Levi, M.D.; Salitra, G.; Levy, N.; Aurbach, D.; Maier, J., Application of a quartz-crystal microbalance to measure ionic fluxes in microporous carbons for energy storage, Nat. Mater. 8 (2009) 872-875. https://doi.org/10.1038/nmat2559.

[34] Tsai, W.Y.; Taberna, P.L.; Simon, P., Electrochemical quartz crystal microbalance (EQCM) study of ion dynamics in nanoporous carbons, J. Am. Chem. Soc. 136 (2014) 8722-8728. https://doi.org/10.1021/ja503449w.

[35] Richey, F.W.; Dyatkin, B.; Gogotsi, Y.; Elabd, Y.A., Ion dynamics in porous carbon electrodes in supercapacitors using in situ infrared spectroelectrochemistry, J. Am. Chem. Soc. 135 (2013) 12818-12826. https://doi.org/10.1021/ja406120e.

[36] Deschamps, M.; Gilbert, E.; Azais, P.; Raymundo-Pinero, E.; Ammar, M.R.; Simon, P.; Massiot, D.; Beguin, F., Exploring electrolyte organization in supercapacitor electrodes with solid-state NMR, Nat. Mater. 12 (2013) 351-358. https://doi.org/10.1038/nmat3567.

[37] Forse, Alexander C.; Griffin, John M.; Merlet, C.; Carretero-Gonzalez, J.; Raji, A.-Rahman O.; Trease, Nicole M.; Grey, Clare P., Direct observation of ion dynamics in supercapacitor electrodes using in situ diffusion NMR spectroscopy, Nat. Energy 2 (2017) 16216. https://doi.org/10.1038/nenergy.2016.216.

[38] Griffin, J.M.; Forse, A.C.; Wang, H.; Trease, N.M.; Taberna, P.L.; Simon, P.; Grey, C.P., Ion counting in supercapacitor electrodes using NMR spectroscopy, Faraday Discuss. 176 (2014) 49-68. https://doi.org/10.1039/c4fd00138a.

[39] Luo, Z.X.; Xing, Y.Z.; Ling, Y.C.; Kleinhammes, A.; Wu, Y., Electroneutrality breakdown and specific ion effects in nanoconfined aqueous electrolytes observed by NMR, Nat. Commun. 6 (2015) 6358. https://doi.org/10.1038/ncomms7358.

[40] Luo, Z.X.; Xing, Y.Z.; Liu, S.; Ling, Y.C.; Kleinhammes, A.; Wu, Y., Dehydration of Ions in Voltage-Gated Carbon Nanopores Observed by in Situ NMR, J. Phys. Chem. Lett. 6 (2015) 5022-5026. https://doi.org/10.1021/acs.jpclett.5b02208.

[41] Griffin, J.M.; Forse, A.C.; Tsai, W.Y.; Taberna, P.L.; Simon, P.; Grey, C.P., In situ NMR and electrochemical quartz crystal microbalance techniques reveal the structure of the electrical double layer in supercapacitors, Nat. Mater. 14 (2015) 812-819. https://doi.org/10.1038/nmat4318.

[42] Wang, H.; Forse, A.C.; Griffin, J.M.; Trease, N.M.; Trognko, L.; Taberna, P.L.; Simon, P.; Grey, C.P., In situ NMR spectroscopy of supercapacitors: insight into the charge storage mechanism, J. Am. Chem. Soc. 135 (2013) 18968-18980. https://doi.org/10.1021/ja410287s.

[43] Wang, H.; Koster, T.K.; Trease, N.M.; Segalini, J.; Taberna, P.L.; Simon, P.; Gogotsi, Y.; Grey, C.P., Real-time NMR studies of electrochemical double-layer capacitors, J. Am. Chem. Soc. 133 (2011) 19270-19273. https://doi.org/10.1021/ja2072115.

[44] Forse, A.C.; Griffin, J.M.; Merlet, C.; Bayley, P.M.; Wang, H.; Simon, P.; Grey, C.P., NMR Study of Ion Dynamics and Charge Storage in Ionic Liquid Supercapacitors, J. Am. Chem. Soc. 137 (2015) 7231-7242. https://doi.org/10.1021/jacs.5b03958.

[45] Li, K.; Bo, Z.; Yan, J.; Cen, K., Solid-state NMR Study of Ion Adsorption and Charge Storage in Graphene Film Supercapacitor Electrodes, Sci. Rep. 6 (2016) 39689. https://doi.org/10.1038/srep39689.

[46] Forse, A.C.; Griffin, J.M.; Presser, V.; Gogotsi, Y.; Grey, C.P., Ring Current Effects: Factors Affecting the NMR Chemical Shift of Molecules Adsorbed on Porous Carbons, J. Phys. Chem. C 118 (2014) 7508-7514. https://doi.org/10.1021/jp502387x.

[47] Forse, A.C.; Merlet, C.; Griffin, J.M.; Grey, C.P., New Perspectives on the Charging Mechanisms of Supercapacitors, J. Am. Chem. Soc. 138 (2016) 5731-5744. https://doi.org/10.1021/jacs.6b02115.

[48] Griffin, J.M.; Forse, A.C.; Grey, C.P., Solid-state NMR studies of supercapacitors, Solid State Nucl. Magn. Reson. 74-75 (2016) 16-35. https://doi.org/10.1016/j.ssnmr.2016.03.003.

[49] Jäckel, N.; Patrick Emge, S.; Krüner, B.; Roling, B.; Presser, V., Quantitative Information about Electrosorption of Ionic Liquids in Carbon Nanopores from Electrochemical Dilatometry and Quartz Crystal Microbalance Measurements, J. Phys. Chem. C 121 (2017) 19120-19128. https://doi.org/10.1021/acs.jpcc.7b06915.

[50] Koczwara, C.; Rumswinkel, S.; Prehal, C.; Jackel, N.; Elsasser, M.S.; Amenitsch, H.; Presser, V.; Husing, N.; Paris, O., In Situ Measurement of Electrosorption-Induced Deformation Reveals the Importance of Micropores in Hierarchical Carbons, ACS Appl. Mater. Interfaces 9 (2017) 23319-23324. https://doi.org/10.1021/acsami.7b07058.

[51] Kaasik, F.; Tamm, T.; Hantel, M.M.; Perre, E.; Aabloo, A.; Lust, E.; Bazant, M.Z.; Presser, V., Anisometric charge dependent swelling of porous carbon in an ionic liquid, Electrochem. Comm. 34 (2013) 196-199. https://doi.org/10.1016/j.elecom.2013.06.011.

[52] Hantel, M.M.; Presser, V.; Kötz, R.; Gogotsi, Y., In situ electrochemical dilatometry of carbide-derived carbons, Electrochem. Comm. 13 (2011) 1221-1224. https://doi.org/10.1016/j.elecom.2011.08.039.

[53] Hantel, M.M.; Presser, V.; McDonough, J.K.; Feng, G.; Cummings, P.T.; Gogotsi, Y.; Kötz, R., In Situ Electrochemical Dilatometry of Onion-Like Carbon and Carbon Black, J. Electrochem. Soc. 159 (2012) A1897-A1903. https://doi.org/10.1149/2.006212jes.

[54] Hahn, M.; Barbieri, O.; Campana, F.P.; Kötz, R.; Gallay, R., Carbon based double layer capacitors with aprotic electrolyte solutions: the possible role of intercalation/insertion processes, Applied Physics A 82 (2006) 633-638. https://doi.org/10.1007/s00339-005-3403-1.

[55] Ruch, P.W.; Kötz, R.; Wokaun, A., Electrochemical characterization of single-walled carbon nanotubes for electrochemical double layer capacitors using non-aqueous electrolyte, Electrochim. Acta 54 (2009) 4451-4458. https://doi.org/10.1016/j.electacta.2009.03.022.

[56] Hantel, M.M.; Weingarth, D.; Kötz, R., Parameters determining dimensional changes of porous carbons during capacitive charging, Carbon 69 (2014) 275-286. https://doi.org/10.1016/j.carbon.2013.12.026.

[57] Caravatti, P.; Bodenhausen, G.; Ernst, R.R., Selective pulse experiments in high-resolution solid state NMR, J. Magn. Reson. 55 (1983) 88-103. https://doi.org/https://doi.org/10.1016/0022-2364(83)90279-2.

[58] Piwek, J.; Platek, A.; Fic, K.; Frackowiak, E., Carbon-based electrochemical capacitors with acetate aqueous electrolytes, Electrochim. Acta 215 (2016) 179-186. https://doi.org/https://doi.org/10.1016/j.electacta.2016.08.061.

[59] Molinspiration Cheminformatics 2019. https://www.molinspiration.com/cgi-bin/properties.

[60] Akinwolemiwa, B.; Peng, C.; Chen, G.Z., Redox Electrolytes in Supercapacitors, J. Electrochem. Soc. 162 (2015) A5054-A5059. https://doi.org/10.1149/2.0111505jes.

3.7 Supporting information

List of content:

- Examples of deconvoluted ^{19}F NMR spectra
- Cyclic voltammogram of the supercapacitor cell
- Three-electrode cell GCD
- Chemical and physico-chemical characterization of the EMIM FcNTf ionic liquid

3.7.1 Deconvolution of ex situ NMR spectra

Spectral deconvolutions were implemented using the SOLA package in Topspin software. A single peak was used to fit the ex-pore and in-pore resonance, respectively. Representative deconvolutions ofex situ NMR spectra are shown in Figure 3-S1.

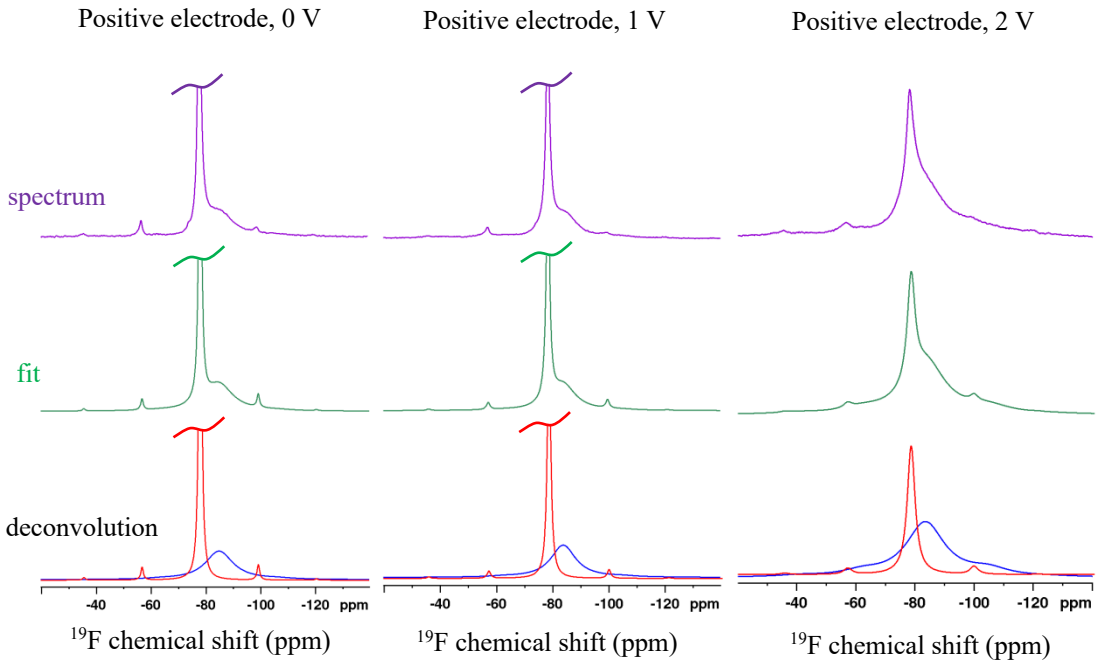

Figure 3-S1. Spectral deconvolutions of *ex situ* ^{19}FNMR data.

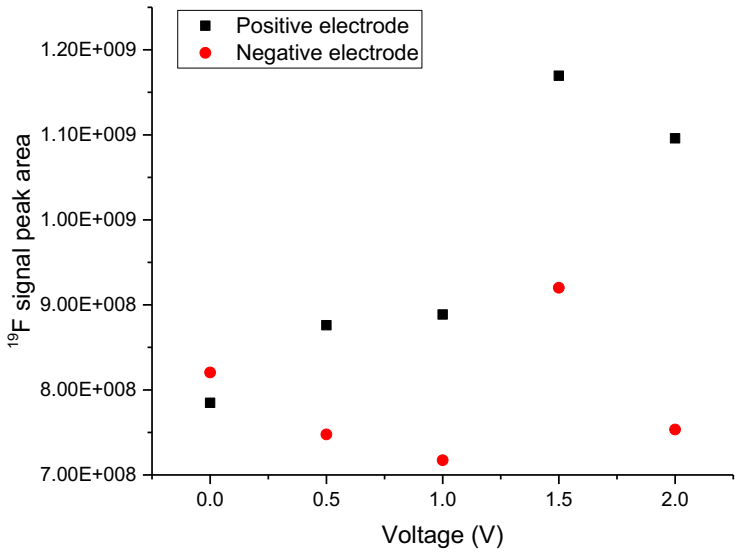

Figure 3-S2. Total 19F signal calculated from the sum of the peak surface area for ex-pore and in-pore contributions after applying different voltage between 0.0 and 2.0 V for 1 h.

3.7.2 Cyclic voltammogram of supercapacitor with 50 % EMIm FcNTf in ACN

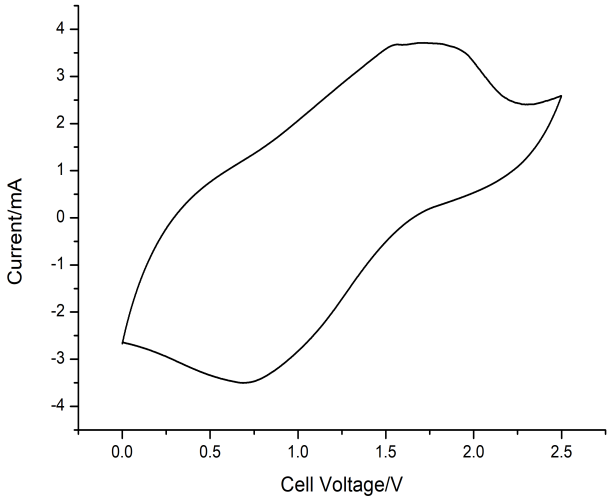

Figure 3-S3. Cyclic voltammogram recorded with two-electrode Swagelok cell with 50% EMIm FcNTf in ACN at a scan rate of 10 mV·s-1 at 25 °C.

a)

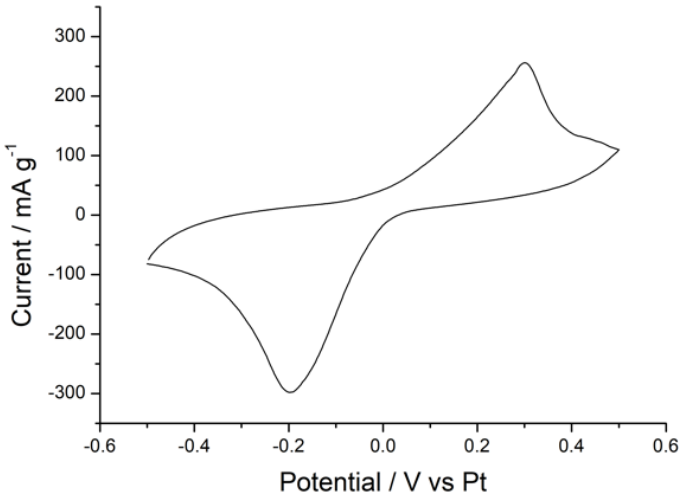

b)

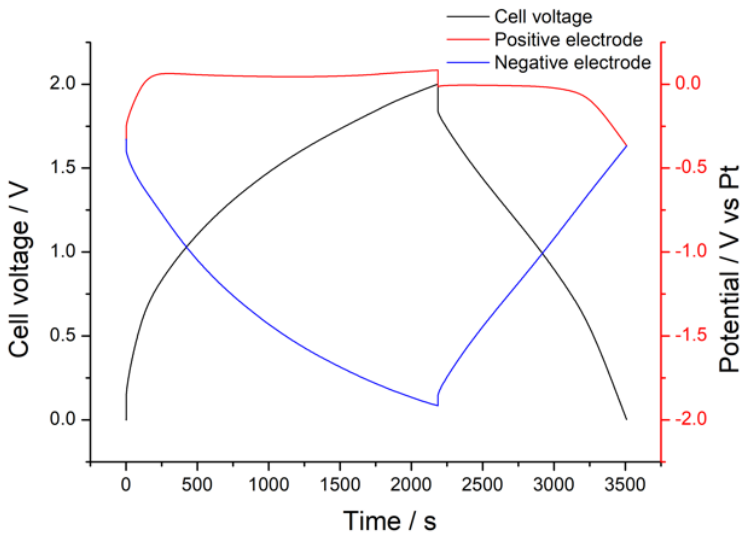

Figure 3-S4. a) Cyclic voltammogram recorded with three-electrode Swagelok cell with 50 % EMIm FcNTf in ACN at a scan rate of 1 $mV \cdot s^{-1}$ at 25 °C. b) Galvanostatic charge-discharge profiles recorded with three-electrode Swagelok cell with 50 % EMIm FcNTf in ACN at a current density of 50 $mA \cdot g^{-1}$ at 25 °C.

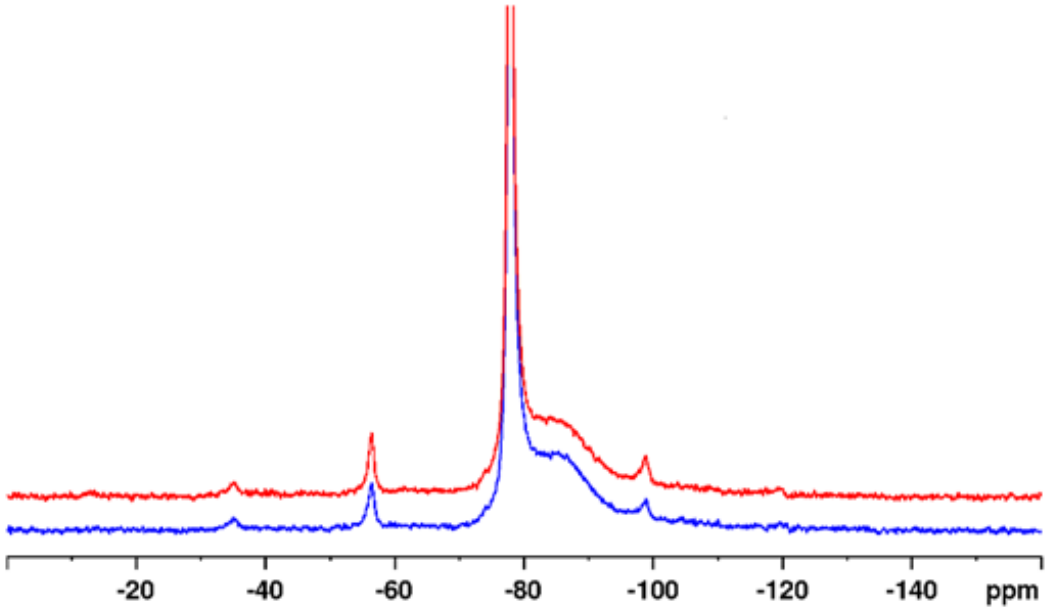

Figure 3-S5. Comparison of the NMR spectra (19F signal) recorded immediately on the positive electrode carbon material after dismounting the cell (0 h) and after leaving the active material for 1.5 h in the NMR.

3.7.3 Details of the NMR Characterization of EMIm FcNTf Ionic Liquid

^{1}H NMR (DMSO-d_6, 400 MHz): δ (ppm) = 9.11 (s, 1H, Im^+), 7.74 (d, 2H, Im^+), 4.54 (t, 2H, Cp-SO_2Cl), 4.30 (s, 7H, Cp), 4.18 (m, 2H, CH_2Im^+), 3.85 (s, 3H, CH_3Im^+), 1.42 (t, 3H, CH_3).

^{13}C NMR (DMSO-d_6, 125 MHz): δ (ppm) = 136.68 (Im^+), 124.04 (Im^+), 122.43 (Im^+), 122.74 (-CF_3), 118.43 (-CF_3), 94.57 (Cp-SO_2Cl), 70.41 (Cp), 69.17 (Cp), 68.59 (Cp), 44.58 (CH_3Im^+), 36.16 (CH_2Im^+), 15.56 (CH_3).

^{19}F NMR (DMSO-d_6, 282 MHz): δ (ppm) = -79.07 (-CF_3).

MS (ESI) m/z: $[M^*]^+$, calcd. for $C_6H_{11}N_2^+$: 111.14, found: 111.17; $[M^*]^-$, calcd. for $C_{11}H_9F_3NO_4S_2Fe^-$: 395.93, found 395.95.

Elemental analysis: calcd. for $C_{17}H_{20}F_3N_3O_4S_2Fe$: C 40.25, H 3.97, N 8.28, S 12.64, found: C 40.48, H 3.93, N 8.09, S 12.41

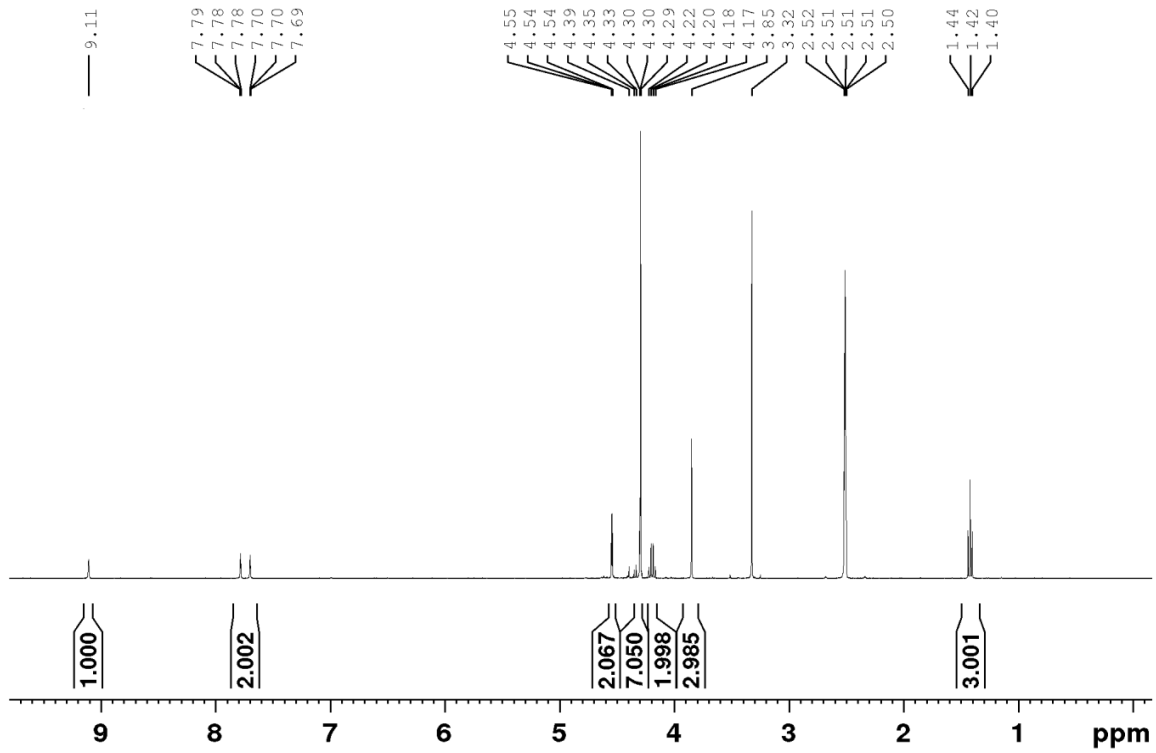

Figure 3-S6. ^{1}H NMR of of EMIm FcNTf.

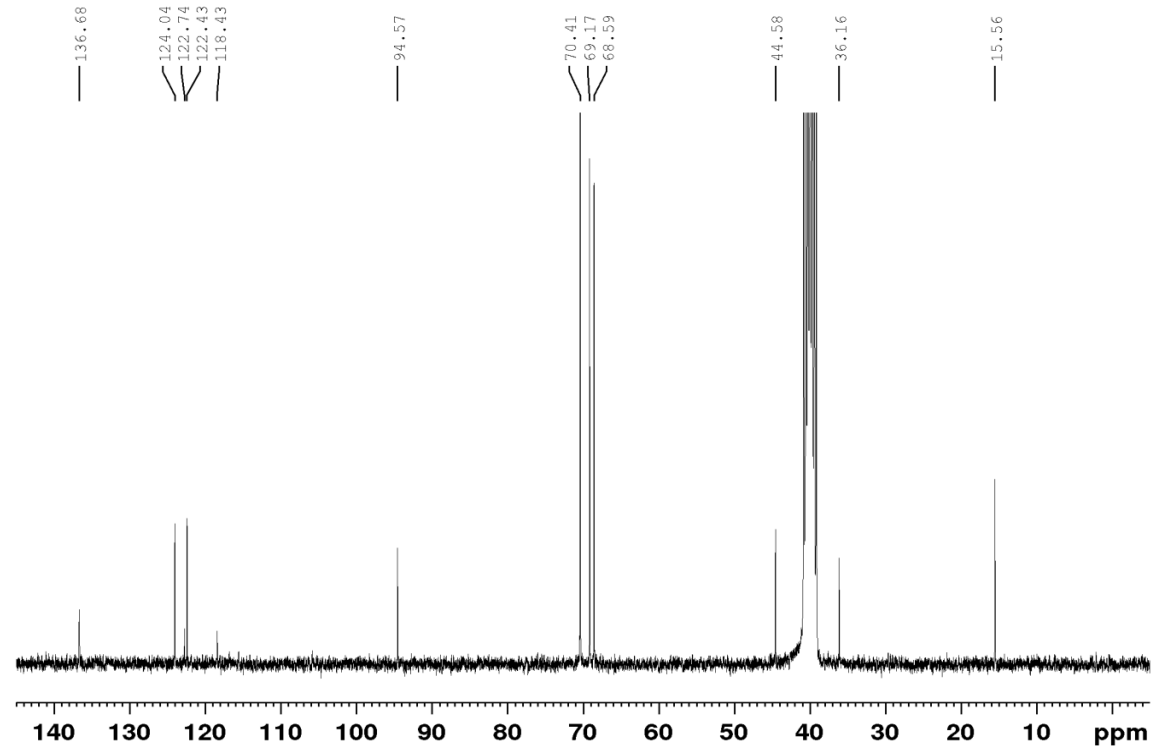

Figure 3-S7. ^{13}C NMR of EMIm FcNTf.

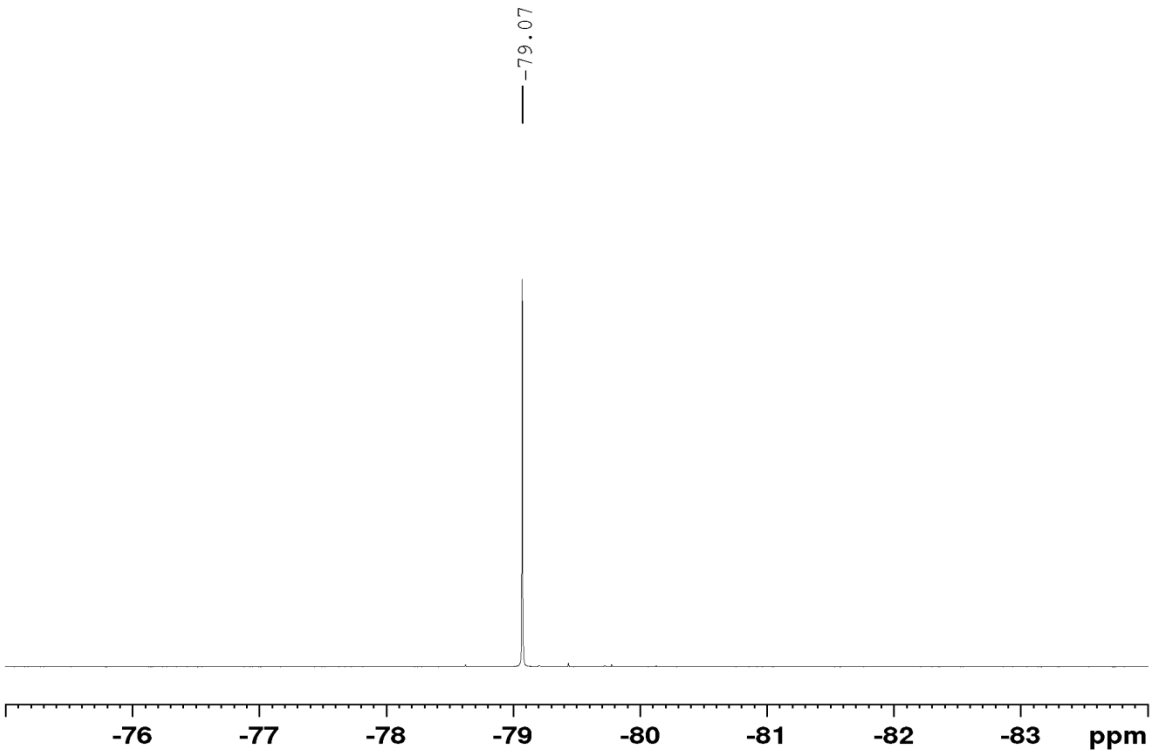

Figure 3-S8. ^{19}F NMR of EMIm FcNTf.

3.7.4 Thermal analysis of EMIm FcNTf

Differential scanning calorimetry (DSC) was carried out using a TA Instruments TA Q1000 under a nitrogen atmosphere. The scans were recorded between -80 and 80 °C for 2 cycles with a ramp of 1 °C per minute and with isothermal of 20 minutes between the cooling and heating. DSC profile showed very broad melting due to the very slow dynamics of phase transitions for the IL. The first cycle showed melting point at 65 °C and glass-transition temperature at -32 °C, while the second cycle showed no melting and glass transition because of kinetics slower than the heating and cooling scan rate. The process was kinetically sluggish due to the asymmetrical anion and high viscosity.

Thermal gravimetric analysis (TGA) was conducted with a TA Instruments TGA 2950 under a nitrogen atmosphere, scanning from 30 to 600 °C at a heating rate of 10 °C min^{-1}. A decomposition temperature of 284 °C was determined.

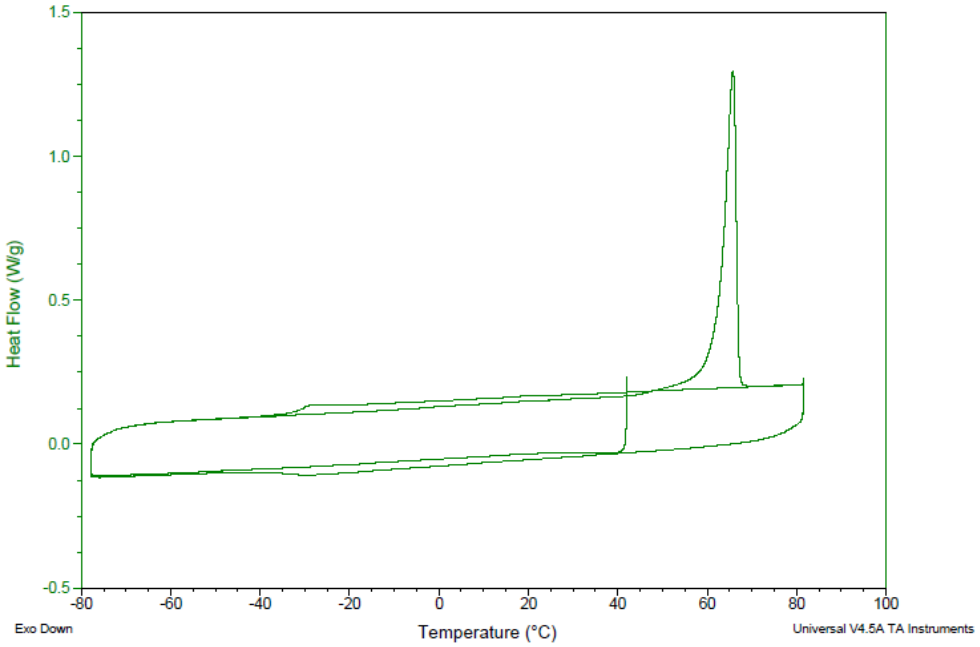

Figure 3-S9. DSC profile of EMIm FcNTf.

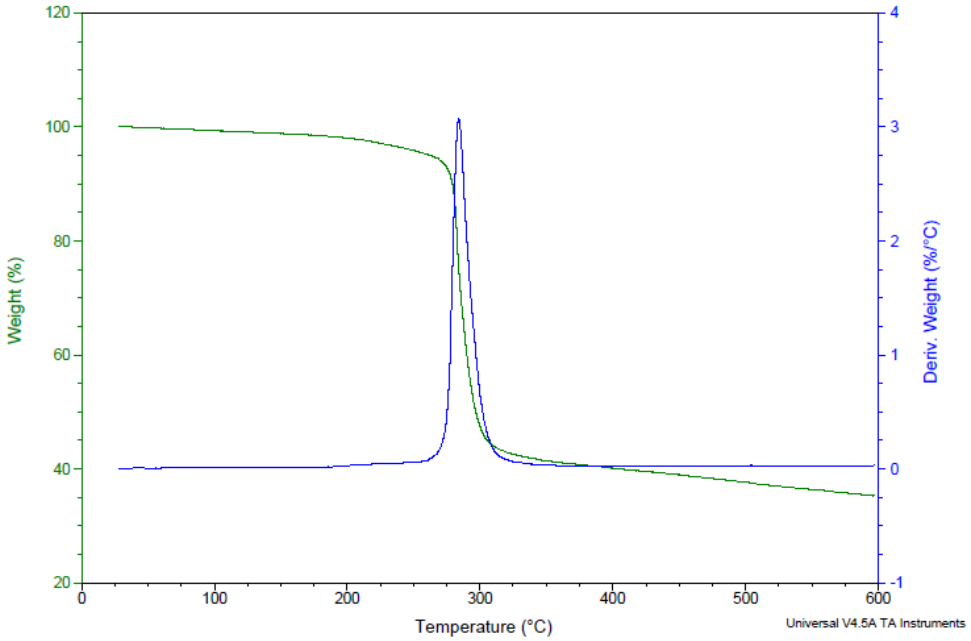

Figure 3-S10. TGA profile of EMIm FcNTf.

Chapter 4 Conclusions

Supercapacitors using redox-active electrolytes exhibit an increase in the value of energy density in comparison with those of non-redox systems. The fundamental study of the charge storage mechanism in SCs with redox-active electrolytes is crucial for understanding the intrinsic electrochemistry of redox-active SCs and benefits the developments and applications of SCs with redox-active electrolytes. Therefore, I used solid-state NMR spectroscopy and electrochemical dilatometry to explore the charge storage mechanism in the SCs using redox-active ionic liquid electrolytes.

The results demonstrate that the charge storage mechanism for SCs involving a redox ionic liquid electrolyte differs between the positive and negative electrodes, and the charging process has distinct mechanisms at different voltage stages, namely, charge storage on positive electrode occurs via co-ion desorption at low voltage range and subsequently counter-ion adsorption at high voltage range, whereas charging on negative electrode occurs exclusively by counter-ion adsorption over the studied voltage range. The charge storage in SCs with redox species is different from those with non-redox electrolyte, providing new insight on the fundamental theories of SCs. NMR spectroscopy results providing useful information on the charge storage mechanism at the molecular level, along with electrochemical dilatometry measurements on the macroscopic scale give a full detailed picture for the charge storage mechanism in SCs with redox-active electrolyte. In addition, the faradaic contribution is also an important aspect for SCs with redox-active species. Herein, by comparison between ionic charge and total electronic charge that are calculated from NMR results and electrochemical chronoamperometry, respectively, the faradaic contribution in SCs with redox-active electrolyte has been quantified, which offers a direct evidence for the enhancement in the energy storage in SCs involving redox species and enables a better understanding in faradaic process for the charge storage in redox-active SCs.

This study is unprecedented in the investigation of charge storage for redox-active SCs. Redox-active SCs employing redox-active species for electrolytes include redox aqueous electrolytes, redox organic electrolytes and redox ionic liquid electrolytes. The charge storage mechanism would be different when different electrolyte or even the same electrolyte with different concentrations is used. In addition, the carbon materials for SCs electrode also play a

significant role in the charge storage process because of the distinction in the structure of carbon materials. Therefore, it is necessary to study more redox-active SC systems with different electrolytes or electrode materials in order to obtain a thorough understanding of the charge storage mechanism for redox-active SCs. The method developed in this study opens the way for the study of charging storage mechanism in SCs with redox-active species and is applicable for the study of SCs with other redox-active systems. More importantly, ex situ NMR spectroscopy involves practical challenges, such as discharging of supercapacitors, evaporation of solvent during cell disassembly, which potentially alters the local environments of ions within the carbon micropores. In situ NMR spectroscopy has the advantage that the supercapacitor can be directly studied with no risk of discharge or loss of solvent during cell disassembly and in principle it provides more accurate information for the charge storage in SCs. Therefore, in situ NMR spectroscopy method for the study of charge storage in SCs is necessary for the next steps.